Karlsruher Institut für Technologie

Analysis of the Cryptochrome-like Photolyase CryA and its Impact on Stress Adaptation in *Aspergillus nidulans*

Zur Erlangung des akademischen Grades eines

DOKTORS DER NATURWISSENSCHAFTEN

(Dr. rer. nat.)

von der KIT-Fakultät für Chemie und Biowissenschaften

des Karlsruher Instituts für Technologie (KIT)

genehmigte

DISSERTATION

von

M. Sc. Alexander Ulrich Lukas Landmark

Dekan: Prof. Dr. Martin Bastmeyer

Referent: Prof. Dr. Reinhard Fischer

Koreferent: Prof. Dr. Nicholas Foulkes

Tag der mündlichen Prüfung: 16.04.2026

Gewidmet meiner Oma Gertrud

Damit en Enkel au endlich en Titel hat

Eidesstattliche Erklärung

Die Arbeiten im Rahmen dieser Dissertation wurden von Januar 2023 bis März 2026 am Institut für Angewandte Biowissenschaften des Karlsruher Institut für Technologie (KIT) durchgeführt. Die Arbeiten wurden von Prof. Dr. Reinhard Fischer betreut.

Ich erkläre hiermit, dass ich die vorliegende Arbeit eigenständig und ausschließlich unter Verwendung der angegebenen Hilfsmittel verfasst habe. Sämtliche Stellen, die dem Wortlaut oder dem Sinn nach aus fremden Quellen entnommen wurden, sind durch entsprechende Quellenangaben eindeutig gekennzeichnet. Die Regeln zur Sicherung guter wissenschaftlicher Praxis des Karlsruher Instituts für Technologie (KIT) in der gültigen Fassung vom 26.06.2017 wurden von mir eingehalten. Die elektronische und die schriftliche Fassung der Arbeit sind identisch. Die ordnungsgemäße Angabe und Archivierung der Primärdaten gemäß § 3 Abs. 1 der Regeln zur Sicherung guter wissenschaftlicher Praxis des KIT ist am Institut gewährleistet.

Datum, Ort

Alexander Landmark

List of publications

Landmark, A., Rudolf, T., Hundshammer, K., Böhm, J., Leister, K., Erhardt, S., Fischer, R. (2026). The photolyase/cryptochrome of *Aspergillus nidulans* senses oxidative stress and shuttles from nuclei to mitochondria. *Nat. Commun.* **17**(1):1483.

Leister, K., Don, Y., Landmark, A., Ma, Y., Schreckenberger, B., Yu, Z., Lu, L. & Fischer, R. (2025). Distinct roles of phytochromes A and B in *Aspergillus fumigatus* in environmental sensing and pathogenicity. *mBio* **16**(11):e0220425.

Table of Contents

Zusammenfassung

Die präzise Wahrnehmung äußerer Umwelteinflüsse ist für alle Organismen von grundlegender Bedeutung, da sie eine gezielte Reaktion auf potenzielle Bedrohungen ermöglicht. Für pilzliche Organismen, die nicht in der Lage sind, Gefahren räumlich auszuweichen, ist ein ausgefeiltes Sensorsystem unerlässlich, um geeignete Anpassungsreaktionen einzuleiten. Im Laufe der Evolution haben sich spezialisierte Photorezeptoren entwickelt, die spezifische Lichtwellenlängen detektieren und entsprechende physiologische Prozesse aktivieren können. Eine bedeutende Gruppe solcher Lichtrezeptoren ist die Cryptochrom/Photolyase-Familie, deren Mitglieder in Tieren und Pflanzen bereits umfassend charakterisiert wurden. In pilzlichen Organismen hingegen ist das Verständnis dieser Blaulichtrezeptoren nach wie vor lückenhaft. Der Modellorganismus *Aspergillus nidulans* kodiert mit der CPD-I-Photolyase CryA ein einzelnes Mitglied dieser Familie. CryA fand vor allem wegen seiner dualen Funktion Beachtung: Einerseits ist CryA in der Lage, UV-induzierte DNA-Schäden zu reparieren, andererseits reguliert CryA als ein Cryptochrom-ähnliches Protein die Entwicklung von *A. nidulans*.

In der vorliegenden Arbeit wird zuerst die Rolle von CryA in der Lichtwahrnehmung näher untersucht. Bioinformatische Analysen bestätigen, dass CryA eine kanonische CPD I Photolyase ist, die FAD und 5,10-MTHF als Chromophore nutzt und eine N-terminale Extension aufweist. Letzterem kommt im weiteren Verlauf der Arbeit eine zentrale funktionelle Bedeutung zu. Mutationen in *cryA* verursachen erhebliche Entwicklungsstörungen in *A. nidulans*, die sich auf Wachstum, Sekundärmetabolismus und sexuelle Reproduktion auswirken. Da diese Prozesse normalerweise unter der Kontrolle des Rotlichtrezeptors FphA stehen, wurden Interaktionsstudien durchgeführt. Diese zeigen, dass CryA im Zellkern direkt mit FphA interagiert und dort dessen Histonmodifizierungsaktivität hemmt. Da die Expression von *cryA* licht- und FphA-abhängig ist, deuten diese Ergebnisse darauf hin, dass CryA nach dem Prinzip eines negativen Rückkopplungsmechanismus die frühe Lichtantwort in *A. nidulans* hemmt.

Im zweiten Teil der Arbeit wird die Funktion von CryA in der oxidativen Stressantwort untersucht. Die Expression von *cryA* wird durch reaktive Sauerstoffspezies induziert und steht unter der Kontrolle des bZIP-Transkriptionsfaktors AtfA. Die Deletion von *cryA* führt zu einer erhöhten Resistenz

gegenüber verschiedenen oxidativen Stressoren in *A. nidulans*, insbesondere gegenüber H_2O_2. Expressionsanalysen zeigen, dass zentrale Antioxidantien in der Deletionsstamm differentiell reguliert sind, was die verbesserte Überlebensfähigkeit unter oxidativem Stress erklärt. CryA interagiert mit AtfA im Zellkern und scheint, analog zur Lichtantwort, die oxidative Stressantwort über einen negativen Rückkopplungsmechanismus zu modulieren. Besonders bemerkenswert ist dabei, dass die Behandlung mit H_2O_2 einen raschen intrazellulären Transport von CryA aus dem Zellkern zu den Mitochondrien auslöst. Diese Translokation ist von spezifischen Aminosäuresequenzen sowie der N-terminalen Extension abhängig und wird durch ein konserviertes Cystein in dieser Extension gesteuert. Fehlt entweder die N-terminale Extension oder dieses Cystein, unterbleibt sowohl die nukleäre Retention als auch der induzierte Transport zu den Mitochondrien. Dieses Ergebnis spiegelt sich auch auf transkriptioneller Ebene wider: Antioxidantien sind sowohl in der vollständigen Deletionsmutante als auch in der Cysteinmutante stärker hochreguliert als im Wildtyp. Im Gegensatz dazu führt die konstitutive Lokalisierung einer CryA-Variante ausschließlich an den Mitochondrien zu einer erhöhten Empfindlichkeit gegenüber H_2O_2. Diese Ergebnisse legen nahe, dass CryA weit mehr als ein Repressor der frühen Lichtantwort ist: Es fungiert zugleich als molekularer Sensor für oxidative Signale und beeinflusst die zelluläre Stressantwort in Abhängigkeit von seiner subzellulären Lokalisation.

Abstract

The precise perception of external environmental influences is of fundamental importance for all organisms, as it enables a targeted response to potential threats. For fungal organisms, which are unable to spatially avoid dangers, a sophisticated sensor system is essential for initiating appropriate adaptive responses. Over the course of evolution, specialized photoreceptors have developed that can detect specific wavelengths of light and activate corresponding physiological processes. An important group of such light receptors is the cryptochrome/photolyase family, whose members have already been extensively characterized in animals and plants. In fungal organisms, however, our understanding of these blue light receptors remains incomplete. The model organism *A. nidulans* encodes a single member of this family, the CPD I photolyase CryA. CryA was described before primarily because of its dual function: on the one hand, CryA is able to repair UV-induced DNA damage, and on the other hand, CryA regulates the development of *A. nidulans* as a cryptochrome-like protein.

This study first examines the role of CryA in light perception in more detail. Bioinformatic analyses confirm that CryA is a canonical CPD I photolyase that uses FAD and 5,10-MTHF as chromophores and has an N-terminal extension. The latter plays a central functional role in the further course of the study. Mutations in *cryA* cause significant developmental disorders in *A. nidulans*, affecting growth, secondary metabolism, and sexual reproduction. Since these processes are normally controlled by the red-light receptor FphA, interaction studies were conducted. These show that CryA interacts directly with FphA in the cell nucleus, where it inhibits its histone modification activity. Since the expression of *cryA* is light- and FphA-dependent, these results suggest that CryA inhibits the early light response in *A. nidulans* according to the principle of a negative feedback mechanism.

The second part of the thesis investigates the function of CryA in the oxidative stress response. The expression of *cryA* is induced by reactive oxygen species and is controlled by the bZIP transcription factor AtfA. Deletion of *cryA* leads to increased resistance to various oxidative stressors in *A. nidulans*, particularly H_2O_2. Expression analyses show that central antioxidants are differentially regulated in the deletion strain, which explains the improved survivability under oxidative stress. CryA interacts with AtfA in the cell nucleus and, analogous to the light response, appears to modulate

the oxidative stress response via a negative feedback mechanism. It is particularly noteworthy that treatment with H_2O_2 triggers rapid intracellular transport of CryA from the nucleus to the mitochondria. This translocation is dependent on specific amino acid sequences and the N-terminal extension and is controlled by a conserved cysteine in this extension. Removal of the N-terminal extension completely abolishes nuclear retention while the deletion of the cysteine hinders the transport from the nucleus to the mitochondria. This result is also reflected at the transcriptional level: antioxidants are more strongly upregulated in both the complete deletion mutant and the cysteine mutant than in the wild type. In contrast, the constitutive localization of a CryA variant exclusively to the mitochondria leads to increased sensitivity to H_2O_2. These results suggest that CryA is much more than a repressor of the early light response: it also functions as a molecular sensor for oxidative signals and influences the cellular stress response depending on its subcellular localization.

1. Introduction

The ability to perceive and adapt to environmental fluctuations is a fundamental requirement for the survival of all living organisms. Environmental stress, ranging from osmotic shock and temperature variability to oxidative stress and irradiation, threatens cellular homeostasis and genomic integrity. Understanding the molecular mechanisms that substantiate the stress response is therefore not only biologically significant but also holds critical relevance for biotechnology, agriculture, and medicine. In pathogenic fungi, stress adaptation correlates directly with virulence and drug resistance, while in industrial biotechnology, it dictates the efficiency of secondary metabolite production (Gerke & Braus, 2014; Beekman & Ene, 2020; Eagan & Keller, 2025; Rana & Thakur, 2025).

Fungal model organisms serve as invaluable prototypes for deciphering complex signaling networks in eukaryotes. Unlike simpler yeasts, filamentous fungi exhibit complex multicellular developmental programs that are tightly coordinated with environmental sensing. Studies have elucidated the convergence of general sensory inputs, such as light and temperature, with specialized stress signaling networks, including the high-osmolarity glycerol (HOG) and cell wall integrity (CWI) pathways. In fungi, this integration is partly facilitated by photoreceptors containing light-sensitive pigments, which detect the visible spectrum to trigger downstream light-dependent biological processes (Yu *et al.*, 2016; Yu & Fischer, 2019; Yaakoub *et al.*, 2022; Corrochano *et al.*, 2025).

Beyond their canonical function in circadian regulation and photomorphogenesis, fungal photoreceptors are increasingly recognized as integral components of the general stress response network. In nature, light exposure is frequently a proxy for concurrent environmental threats, including temperature fluctuations, desiccation, and oxidative stress. Consequently, photoreceptors do not operate in isolation; they exhibit extensive cross-talk with stress-activated signaling pathways and other transcription factors, effectively coupling light perception with cellular defense mechanisms. This integration allows fungi to anticipate and prepare for abiotic challenges, modulating the expression of antioxidant enzymes and stress-response proteins before damage occurs (Brandt *et al.*, 2008; Lokhandwala *et al.*, 2015; Zhu & Idnurm, 2018; Schuhmacher *et al.*, 2024; Leister *et al.*, 2025).

1.1 The filamentous fungus *Aspergillus nidulans*

For over seven decades, the filamentous ascomycete *A. nidulans* has been a model for the study of eukaryotic cell biology, genetics, and metabolic regulation. Originally established in the early 1950s by Guido Pontecorvo as a system for studying genetic recombination, its applications have expanded far beyond classical genetics. Today, *A. nidulans* is a prominent model for understanding how multicellular fungi integrate environmental signals, such as light, temperature, and osmotic pressure, to regulate complex life cycles, adaptation to harsh conditions, and secondary metabolism (Pontecorvo *et al.*, 1953; Pinheiro *et al.*, 2023).

The fact that *A. nidulans* requires simple nutrition, combined with low pathogenicity and a fast reproductive cycle, makes it an ideal laboratory organism. In addition, it is used in the production of natural and heterologous enzymes, such as xylanases for sugar production and echinocandin B as precursor for important antifungal compounds (Vazquez & Sobel, 2006; Kumar, 2020; Pinheiro *et al.*, 2023). Unlike the single-celled yeast *Saccharomyces cerevisiae*, *A. nidulans* exhibits sophisticated multicellular morphology, alternating between vegetative hyphal growth and two distinct reproductive states: asexual conidiation and sexual development. The formation of sexual fruiting bodies, known as cleistothecia, is a hallmark of this species **(Fig. 1a)**. Because *A. nidulans* is homothallic (self-fertile), researchers can easily manipulate its sexual cycle to study the inheritance of specific traits and the regulation of developmental changes (Seo *et al.*, 2004; Blumenstein *et al.*, 2005; Bayram *et al.*, 2010).

A central aspect of its role in sensory research is the discovery of the Velvet complex, a global regulatory hub composed of proteins such as velvet A (VeA), velvet-like protein B (VelB), and the methyltransferase loss of aflatoxin regulator expression A (LaeA) (Käfer, 1965; Bayram *et al.*, 2008b). The Velvet complex acts as a molecular bridge, linking light perception to the production of secondary metabolites and reproductive choices. In the dark, VeA translocates into the nucleus to promote sexual development and toxin production. This process is inhibited by red light through the red-light sensitive photoreceptor fungal phytochrome A (FphA) **(Fig. 1b)** (Blumenstein *et al.*, 2005; Bayram *et al.*, 2010). This sophisticated integration of photobiology and metabolism makes *A. nidulans* an ideal model organism for studying how environmental stimuli are perceived and responded to on a molecular level.

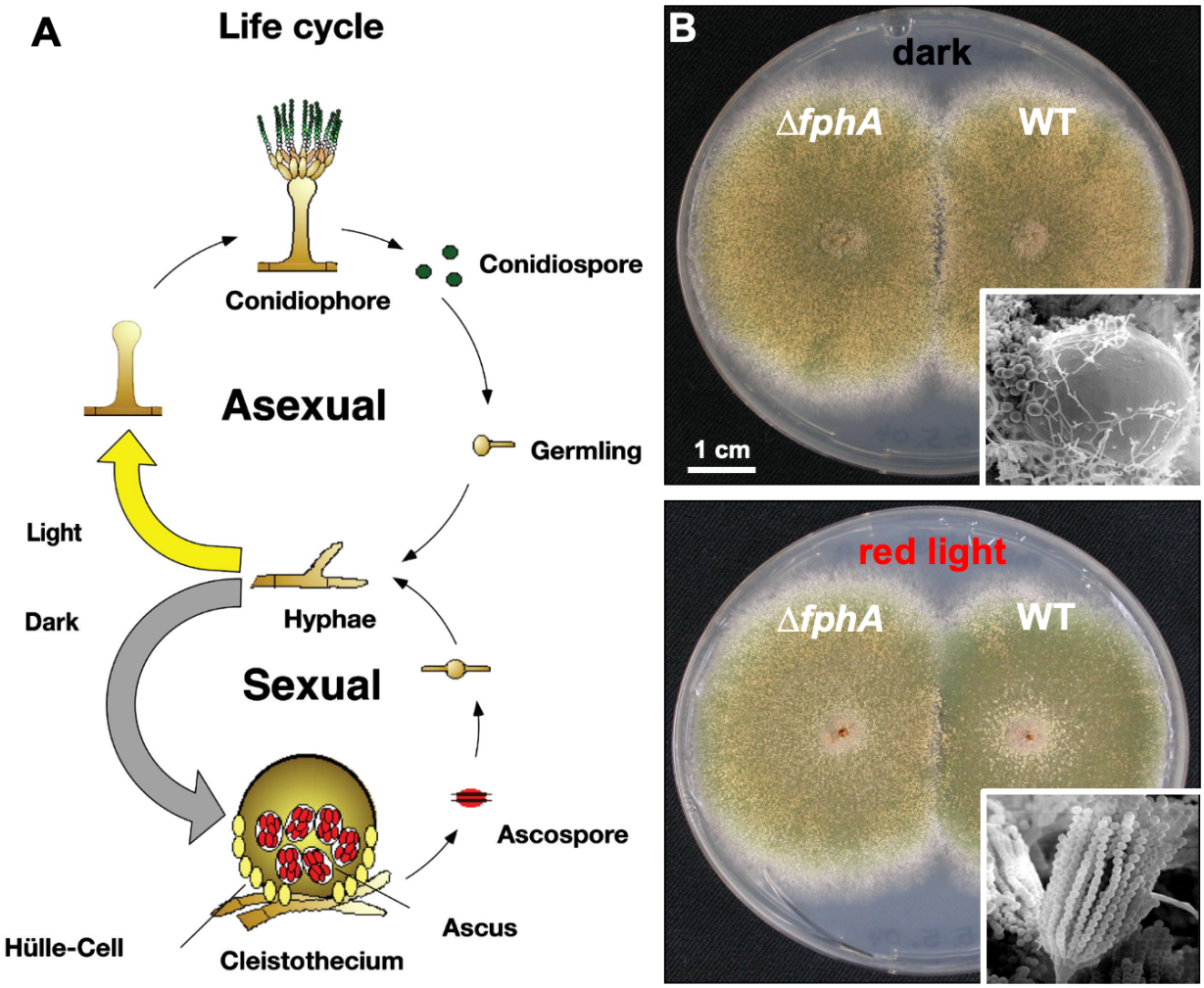

Figure 1*:* Light serves as a crucial regulator of developmental differentiation in *A. nidulans*. (A) In the absence of specific environmental cues, the fungus maintains vegetative growth through hyphal extension. However, under dark conditions, the developmental program shifts toward sexual reproduction, characterized by the differentiation of Hülle cells and the formation of cleistothecia (fruiting bodies). Conversely, the perception of light triggers a transition to asexual development, leading to the dominance of conidiophores and a characteristic green pigmentation. **(B)** Comparison of the wild type (WT) with a Δ*fphA* knockout strain. In the dark, both strains form yellowish cleistothecia, but only the WT responds to red light by shifting to conidiation. The Δ*fphA* mutant continues to produce cleistothecia even under red light, highlighting the necessity of FphA in transducing the signal for asexual development (modified after (Blumenstein *et al.*, 2005; Bayram *et al.*, 2010).

1.2 Stress perception in *A. nidulans*

The fungal mode of action to perceive environmental stimuli is crucial for survival and adaptation and therefore many physiological mechanisms are regulated by stress. Since fungi are sessile organisms, they lack the ability to move to more advantageous conditions; hence, they need a flexible and adaptative system which reacts immediately upon impending abiotic stress (Purschwitz *et al.*, 2006; Fischer *et al.*, 2016; Schumacher, 2017). Such a systemic response developed most likely from ancestral prokaryotic two-component systems (TCS), and the effective establishment and diversification of mitogen-activated protein kinase (MAPK) cascades (Papon &

Stock, 2019; Yu & Fischer, 2019; Bayram & Bayram, 2023). Compared to the one-step transduction TCS in prokaryotic organisms, fungi employ several multi-step phosphate-based mechanisms. They are evolutionarily conserved between many different species, especially for filamentous fungi and yeasts, but homologs are also found in mammals and plants (Krysan & Colcombet, 2018; Du *et al.*, 2025). Typically, a fungal TCS consists of three core signal transducers: a membrane-associated sensor with histidine kinase activity (HK), a corresponding response regulator (RR) as phosphate acceptor, and an additional histidine-containing phosphotransmitter (HPt). Consequently, these components trigger downstream MAPK pathways, transmitting the signal into the nucleus, activating gene expression. Additionally, G-protein coupled receptors (GPCRs) and small GTPases sense specific stimuli and trigger corresponding pathways (Ninfa & Magasanik, 1986; Bahn *et al.*, 2006; Azuma *et al.*, 2007; Fujioka *et al.*, 2007; Bayram *et al.*, 2012).

There are three primary MAPK cascades in *A. nidulans* for stress perception. Among these, the HOG pathway represents the most extensively characterized regulatory system, serving as a critical convergence point for diverse environmental stimuli. It is specifically tuned to integrate signals from hyperosmotic conditions, oxidative stress, and nutrient deprivation, while also acting as the primary transducer for red-light perception via the phytochrome system (Hagiwara *et al.*, 2009a; Lara-Rojas *et al.*, 2011; Yu *et al.*, 2016; Baltussen *et al.*, 2020; Yaakoub *et al.*, 2022).

Mechanical stress on the fungal cell wall, originating from thermal fluctuations, osmotic pressure, or exposure to cell wall-targeting fungicides, is primarily integrated via the CWI pathway. This signaling cascade remodels the cell wall structure by upregulating the biosynthetic machinery for chitin and β-glucans, thereby maintaining structural stability under adverse conditions. Furthermore, the CWI pathway acts in close coordination with the HOG pathway to ensure a holistic response to multifaceted environmental threats (Fuchs & Mylonakis, 2009; Binder *et al.*, 2010; Futagami & Goto, 2012; Laz *et al.*, 2020; Liao *et al.*, 2021; Doan *et al.*, 2025).

The third core MAPK cascade in *A. nidulans* is the pheromone-responsive developmental pathway, which governs the critical transition between asexual and sexual reproduction. Although it is not a primary transducer of acute environmental stress, this pathway serves as a vital sensor of global environmental fitness and dictates the switch between different life cycles in response to current environmental conditions. This cascade also converges with the HOG pathway on the regulation of

the sexual transcription factor VeA. In this context, under conditions of high osmotic or oxidative stress, the fungus can prioritize cellular homeostasis associated with asexual over VeA driven sexual development. This interplay ensures that the transition to sexual reproduction is initiated only when environmental conditions are favorable for long-term fitness (Lara-Rojas *et al.*, 2011; Frawley *et al.*, 2018; Garrido-Bazán *et al.*, 2018).

Depending on the incoming stress-signal different HKs are activated and translate the signal downstream via an HPt to the response regulator. For the HOG-pathway several histidine kinases are activated through incoming stress. The most important kinases are NikA (Nitrogen independent kinase A), which controls turgor pressure and is sensitive to intracellular ROS levels, and the aforementioned phytochrome FphA, crucial for the perception of light fluctuations (Hagiwara *et al.*, 2009a; Hagiwara *et al.*, 2009b; Yu & Fischer, 2019). Furthermore, kinases like the protein histidine kinases A and B (PhkA/PhkB) function as inhibitors under sufficient nutrient availability, while the hybrid kinase TcsB (Two component system B) together with FphA acts as functional thermal sensor (Hagiwara *et al.*, 2016; Yu *et al.*, 2019).

When environmental stress is perceived, the associated sensory histidine kinases are inhibited, triggering the dephosphorylation of the central HPt protein, YpdA (Yeast phosphodistribution protein A). As the central phosphorelay hub, YpdA integrates multiple environmental signals into a singular output signal. Its dephosphorylation relieves the inhibition of the response regulator SskA (Suppressor of sensor kinase A), which in turn initiates downstream MAPK proteins. This cascade involves the MAPK kinase kinase SskB (Suppressor of sensor kinase B), followed by the MAPK kinase PbsB (Polyblastic suppressor of SltB). The signaling culminates in the phosphorylation and nuclear translocation of the terminal MAPK, SakA (Stress-activated kinase A). Once in the nucleus, SakA primarily activates the bZIP transcription factor AtfA (ATF/CREB transcription factor A) to promote the General Stress Response (GSR). This transcriptional reprogramming includes the induction of chaperones and heat shock proteins, the upregulation of antioxidant defenses such as catalases and superoxide dismutases, and the biosynthesis of protective osmolytes such as glycerol and trehalose. Furthermore, AtfA modulates light-responsive developmental systems by activating conidiation factors and transcription factors essential for asexual differentiation (Vargas-Pérez *et al.*, 2007; Lara-Rojas *et al.*, 2011; Hagiwara *et al.*, 2016; Idnurm & Bahn, 2016) **(Fig. 2)**.

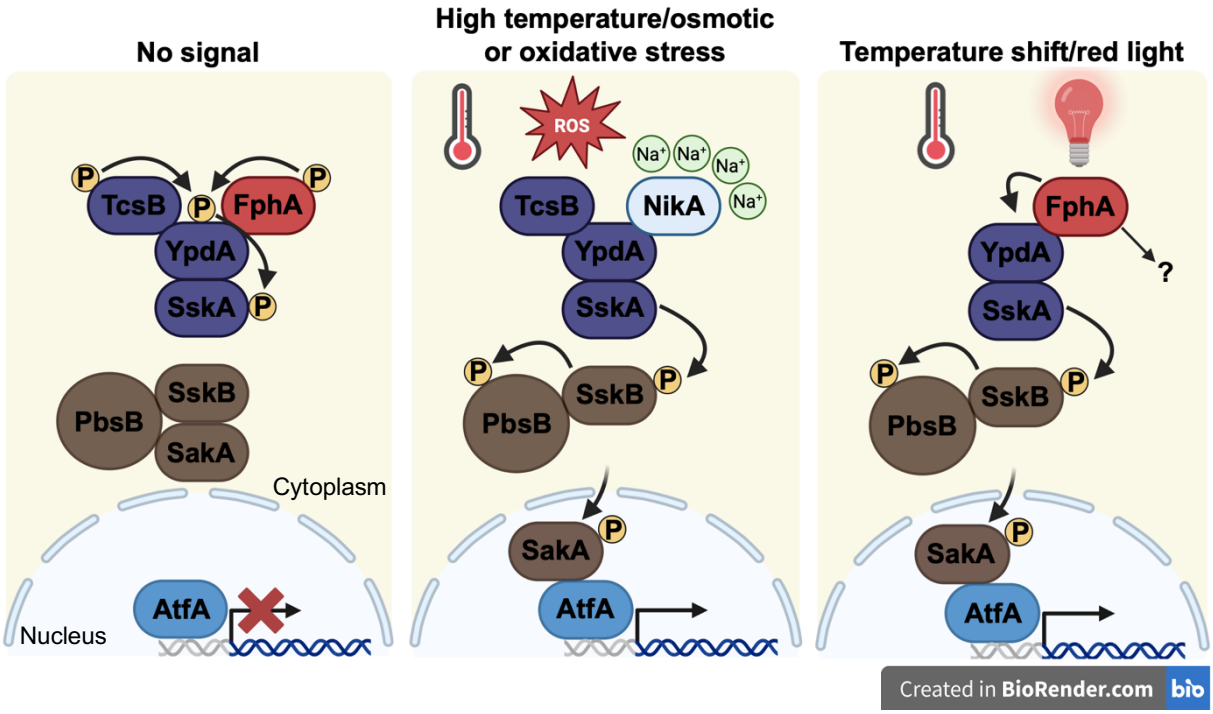

Figure *2:* Model of the MAPK HOG pathway in *A. nidulans*. Under homeostatic conditions like darkness, isotonicity, and normothermia, sensor histidine kinases are constitutively active. These HKs maintain a phosphate flux toward the intermediate phosphotransfer protein YpdA, which in turn phosphorylates the response regulator SskA, thereby repressing downstream MAPK signaling. Conversely, environmental changes such as thermal shifts, red light, or oxidative and osmotic stress trigger the dephosphorylation of these sensors (including TcsB, FphA, and NikA, respectively). This initiates a kinase cascade culminating in the nuclear translocation of the terminal MAPK, SakA. Upon nuclear entry, SakA interacts with the bZIP transcription factor AtfA to coordinate the stress-response program, including the induction of molecular chaperones, the initiation of asexual conidiation, and the biosynthesis of protective osmolytes and antioxidants. Generated in BioRender and modified after (Idnurm & Bahn, 2016; Takala *et al.*, 2020).

Although not fully characterized in *A. nidulans*, evidence from related species demonstrates that the HOG pathway interacts with CWI and pheromone signaling, resulting in either competitive or amplified responses. This integration serves to fine-tune the fungal stress response and inhibit conflicting developmental programs, thereby preventing metabolic waste and improving overall fitness (Fuchs & Mylonakis, 2009; Garrido-Bazán *et al.*, 2018; Frawley *et al.*, 2020; Carrasco-Navarro & Aguirre, 2021; Doan *et al.*, 2025).

Interestingly, AtfA resides permanently in the nucleus and is bound to the promoter of stress genes, even under non-stress conditions (Miskei *et al.*, 2025). Transcriptional activity of AtfA depends on the physical interaction and phosphorylation through SakA (Carrasco-Navarro & Aguirre, 2021). If the nuclear localization of SakA is prevented, gene expression is significantly lowered under stress conditions. Additionally, without AtfA present in the nucleus, SakA appears to not accumulate in the nucleus (Lara-Rojas *et al.*, 2011). The phosphorylation of SakA in *Aspergillus fumigatus* is regulated by the phosphatase 2C homolog B (PtcB), and *ptcB* deletion mutants revealed that this enzymatic action is crucial for the deactivation of the HOG-

pathway (Winkelströter *et al.*, 2015). In *Saccharomyces cerevisiae*, the SakA homologue Hog1 activates two phosphatases (Phosphatase protein 2/3) at the posttranscriptional level, leading in a negative feedback loop (NFL)-like manner to the dephosphorylation of Hog1, thereby modulating the nuclear retention and stopping the GSR (Wurgler-Murphy *et al.*, 1997; Mattison & Ota, 2000). Although *A. nidulans* possesses homologues of the relevant phosphatases, the mechanism governing the inactivation of the HOG pathway, specifically AtfA, remains uncharacterized (Carrasco-Navarro & Aguirre, 2021). Consequently, it is unclear whether the downregulation of SakA and AtfA is driven by dephosphorylation events or by competitive protein-protein interactions with unidentified partners (Yu & Fischer, 2019).

1.3 Oxidative stress response in *A. nidulans*

Key molecules, such as nucleic acids, proteins, and lipids, are regulated by chemical modifications, leading to major changes in biological processes (Yaakoub *et al.*, 2022). Redox reactions involving reactive oxygen species (ROS) are one of the main type of reactions and are crucial in all living cells. Most of these molecules accumulate endogenously as consequence of the metabolism (Breitenbach *et al.*, 2015). Such oxygen species are comprised of radical and non-radical molecules, including superoxide anions ($O_2^{\cdot -}$), hydrogen peroxide (H_2O_2), and the highly reactive hydroxyl radical ($^{\cdot}OH$). Although ROS are quite detrimental to the cell in elevated concentrations, some of these molecules are actively used as signaling substances and in metabolic reactions. Additionally, they serve important roles in interactions between pathogenic fungi with plants and in the degradation of dead biomass (Breitenbach *et al.*, 2015; Mattila *et al.*, 2022). In eukaryotes, the intracellular production of ROS is compartmentalized to maintain a stable distribution of oxidizing and reducing metabolites, resulting in a redox potential of –310 mV (Breitenbach *et al.*, 2015). The respiratory chain, localized in the mitochondria, together with NADPH (Nicotinamide Adenine Dinucleotide Phosphate) oxidase (NOX) enzymes, embedded in the membrane, are mainly responsible for ROS production (Laurindo *et al.*, 2014; Yaakoub *et al.*, 2022) **(Fig. 3)**. In addition, the oxidation of fatty acids in the peroxisomes and maturation of proteins at the endoplasmic reticulum generate intracellular ROS (Schrader & Fahimi, 2006; Laurindo *et al.*, 2014).

Aside from these endogenous machineries, there are several exogenous factors, which induce the formation of ROS, such as high temperatures, heavy metals,

strong radiation with UV and blue light, and biotic agents (El-Esawi *et al.*, 2017; Zhang *et al.*, 2017; Oiki *et al.*, 2022; Yaakoub *et al.*, 2022; Li *et al.*, 2024). The use of ROS-inducing xenobiotics, specifically the redox-cycling agents menadione and paraquat alongside exogenous H_2O_2, provide a foundation for investigating how oxidative shifts influence cellular behavior. In *Aspergillus* species, these stimuli are not merely cytotoxic; they serve as morphogenetic signals that modulate key life-cycle transitions (Oiki *et al.*, 2022; Li *et al.*, 2024). Elevated ROS levels are essential for promoting asexual differentiation and conidiation, and they similarly regulate biofilm architecture in yeast (Cáp *et al.*, 2012). Furthermore, for phytopathogenic fungi, the integration of these oxidative signals is critical for activating virulence programs, enabling the pathogen to sense and counter the host's oxidative defenses (Segal & Wilson, 2018; Zhang *et al.*, 2020).

To maintain redox homeostasis, *A. nidulans* utilizes a sophisticated network of antioxidants specialized to its various developmental stages. These enzymatic systems provide a multi-layered defense that neutralizes external ROS while precisely regulating internal redox levels to prevent cellular damage. This defense mechanism is primarily anchored by the sequential action of superoxide dismutases (SODs) and catalases. The process initiates with the dismutation of the superoxide anion into hydrogen peroxide, a reaction mediated by distinct SOD isoforms such as the mitochondrial Superoxide dismutase A (SodA) and cytosolic SodB (Yaakoub *et al.*, 2022). Subsequently, the accumulated H_2O_2 is neutralized by a family of catalases, whose expression is precisely regulated to ensure protection across the fungal life cycle. Specifically, the highly stable Catalase A (CatA) accumulates in conidia to confer resistance against stress during dormancy, whereas the inducible catalase CatB functions as the primary scavenger in vegetative hyphae (Navarro *et al.*, 1996; Kawasaki *et al.*, 1997; Kawasaki & Aguirre, 2001). Catalase C is constitutively expressed and localizes to peroxisomes, possibly connected to the oxidation of fatty acids (Kawasaki & Aguirre, 2001; Schrader & Fahimi, 2006). The fourth catalase, CatD, is induced in late stationary phases in vegetative hyphae and responds to glucose starvation and high temperatures (Kawasaki & Aguirre, 2001). This enzymatic barrier is further reinforced by the peroxiredoxin and glutathione-dependent systems, encoded by genes such as *prxA* (peroxiredoxins), *glrA* (glutathione reductase), and t*rxA* (thioredoxin), which maintain the thiol-disulfide equilibrium essential for protein function (Sato *et al.*, 2009; Loor *et al.*, 2010; Liu *et al.*, 2025).

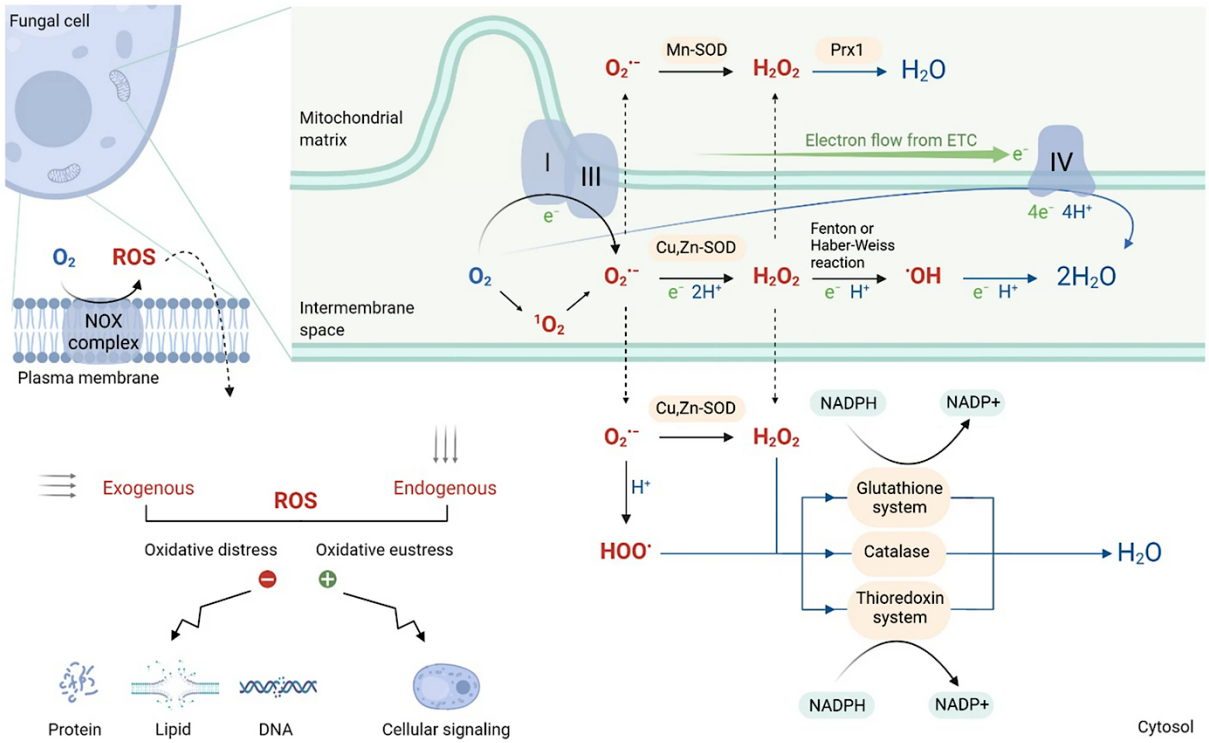

Figure 3: Compartments of reactive oxygen species metabolism and the correspondent fungal responses. Intracellular ROS in fungi are primarily produced in the mitochondria followed by the NOX complex embedded in the plasma membrane. NOX enzymes catalyze oxygen to hydrogen peroxide which can diffuse back in the cell. Additionally, the respiratory chain produces H_2O_2 and $O_2^{\cdot-}$ as a byproduct of the reduction of oxygen to molecular water. $O_2^{\cdot-}$ serves as a precursor of H_2O_2 through the activity of the superoxide dismutase, can be protonated to the hydroperoxyl radical ($HOO^{\cdot}$), or is catalyzed via the Fenton or Haber-Weiss reaction to the hydroxyl radical ($^{\cdot}OH$). The mitochondrial SOD enzyme and the antioxidant peroxiredoxin reduces the oxygen radicals to water and are therefore important for the mitochondrial redox homeostasis. ROS can also diffuse out of the mitochondria and serve together with exogenous sources as an important cellular signal in nontoxic concentrations (oxidative eustress). In high concentrations (oxidative distress) ROS damage macromolecules, such as proteins, lipids and nucleic acids. To prevent toxic concentrations of ROS, the fungal cell employs several antioxidant systems, including catalases, the glutathione and thioredoxin reductases, and cytosolic superoxide dismutases. These enzymes utilize NADPH to neutralize ROS by reducing it to water, thereby stabilizing the cytosolic redox potential (Yaakoub *et al.*, 2022).

To modulate the cellular response under oxidative stress, *A. nidulans* employs a dual-layered regulatory system that integrates the High Osmolarity Glycerol signaling pathway and SakA with the redox-sensing bZIP transcription factor Nuclear ap-1-like (NapA) (Carrasco-Navarro & Aguirre, 2021; Yaakoub *et al.*, 2022). This coordinated response allows the fungus to transition from growth-oriented metabolism to a specialized stress program when challenged by exogenous ROS. As mentioned earlier, the SakA-mediated pathway functions as a canonical mitogen-activated protein kinase (MAPK) cascade, where oxidative signals trigger the phosphorylation and subsequent nuclear translocation of the SakA kinase (Garrido-Bazán *et al.*, 2018). Once localized to the nucleus, SakA interacts with the bZIP transcription factor AtfA to drive the expression of stress-tolerance genes, most notably the conidial catalase *catA* and the thioredoxin system, which are essential for preserving the viability of dormant

spores and mediating the transition between vegetative growth and asexual development (Navarro *et al.*, 1996; Kawasaki *et al.*, 1997; Miskei *et al.*, 2025).

In parallel to the MAPK-mediated response, NapA, the fungal ortholog of the well characterized yeast Yap1, functions as the primary molecular sensor of the intracellular H_2O_2 concentrations (Liu *et al.*, 2025). Unlike the kinase-driven activation of AtfA, NapA is regulated by the direct oxidation of its cysteine residues, which induces a conformational change that prevents its nuclear export (Mendoza-Martínez *et al.*, 2017; Liu *et al.*, 2025). The resulting nuclear accumulation of NapA facilitates the rapid upregulation of antioxidant genes, including the hyphal catalase *catB*, the thioredoxin system *trxA* together with the thioredoxin reductase *trrA*, and the peroxiredoxin *prxA* (Yaakoub et al., 2022; Liu et al., 2025).

This response is further refined by the integration of the Skn7-like response regulator SrrA (Stress response regulator A). SrrA is phosphorylated through YpdA and is necessary together with NapA for *catB* induction in response to H_2O_2 and menadione (Vargas-Pérez *et al.*, 2007; Mendoza-Martínez *et al.*, 2017). These synergistic pathways ensures that while NapA together with SrrA handles the immediate detoxification of critical intracellular levels of ROS in active hyphae, the SakA-AtfA interaction integrates these signals into a broader developmental by activating the general stress response (Vargas-Pérez *et al.*, 2007; Lara-Rojas *et al.*, 2011; Hagiwara *et al.*, 2016; Mendoza-Martínez *et al.*, 2017; Garrido-Bazán *et al.*, 2018; Carrasco-Navarro & Aguirre, 2021). Together, these pathways form a robust regulatory network that ensures *A. nidulans* can maintain redox homeostasis across diverse environmental niches and complex life cycles (Yaakoub *et al.*, 2022) **(Fig. 4)**.

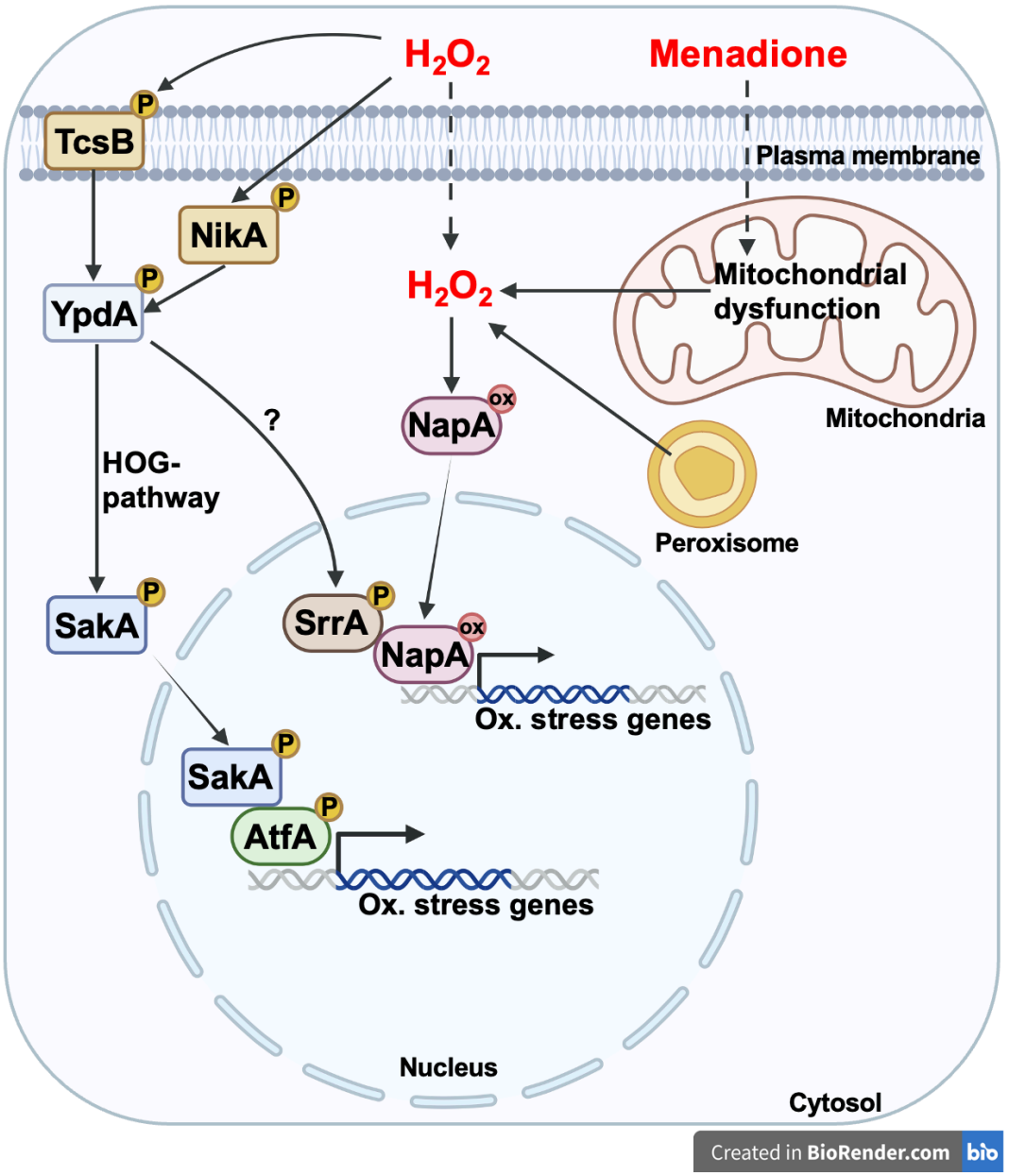

Figure 4: Oxidative stress pathways in *A. nidulans*. Histidine kinases, such as NikA and TcsB, detect hydrogen peroxide, leading to the autophosphorylation of the sensor. This event triggers an interaction with the response regulator YpdA, which is in turn phosphorylated and activated. Through the MAPK cascade, the signal is transferred to the terminal MAPK SakA. This promotes nuclear localization and interaction with the bZIP transcription factor AtfA, which activates the expression of antioxidants, such as catalases, and the thioredoxin system. In addition to diffusing through the plasma membrane into the cell, H_2O_2 is also a byproduct of fatty acid oxidation in peroxisomes. Furthermore, xenobiotics such as menadione lead to mitochondrial dysfunction and high intracellular ROS concentrations. To counteract this change in redox homeostasis, the bZIP transcription factor NapA, which is localized in the cytosol, is oxidized by H_2O_2, triggering a conformational shift and nuclear import. Additionally, YpdA, independently of the HOG pathway, stimulates the phosphorylation of SrrA, which interacts with NapA to promote, alongside AtfA, the oxidative stress response. Generated in BioRender and modified after (Yaakoub *et al.*, 2022).

1.4 Fungal photoreceptors

Sunlight is a ubiquitous and rhythmic environmental factor to which life on Earth has adapted throughout the course of evolution. Varying in intensity, wavelength, and angle of incidence depending on the time of day and season, sunlight provides critical data regarding ambient temperature and temporal context, thereby demanding a high

degree of phenotypic adaptation from organisms (Yu & Fischer, 2019). While photoautotrophs such as plants and green algae must optimize light capture for energy generation through photosynthesis, heterotrophic organisms also rely on light as a vital informational cue (Bayram & Bayram, 2023). Beyond its energetic potential, light functions as a primary "zeitgeber," synchronizing the organism's endogenous biological clock, the circadian rhythm, with the external day-night cycle (Walker *et al.*, 2020; Sanchez *et al.*, 2022). This circadian system is a time-keeping mechanism found across all domains of life, evolved to anticipate environmental transitions rather than merely reacting to them.

The circadian clock has three main characteristics which are identical for all species; it is an endogenous process, the rhythm is entrainable through environmental stimuli, and the system appears to be temperature compensated (Sanchez *et al.*, 2022). In humans, the circadian clock controls hormonal regulation, sleep-wake cycles, and metabolic homeostasis, while in plants, the integration of light signaling with inputs such as temperature and nutrient availability modulates complex developmental pathways (McClung, 2006; Walker *et al.*, 2020; Wang *et al.*, 2024). Central to this molecular system is the transcriptional-translational feedback loop (TTFL). In mammals, the core of this feedback loop is composed of the two positive regulatory factors CLOCK and BMAL (brain and muscle ARNT-like). These proteins form heterodimers that drive the transcriptional expression of Period (PER1-3) and Cryptochrome (CRY1-2) genes. Functioning as negative elements, the resulting PER and CRY proteins heterodimerize and inhibit the activity of the CLOCK/BMAL complex. This interaction suppresses their own transcription, effectively resetting the oscillator and generating a rhythmic cycle (Trott & Menet, 2018; Sanchez *et al.*, 2022).

In the fungal kingdom, the molecular basis of circadian rhythms has been most extensively characterized in the filamentous fungus *Neurospora crassa* (Baker et al., 2012). The fungus exhibits a robust circadian rhythm characterized by the periodic transition to the asexual production of macroconidia. This developmental shift involves the formation of aerial hyphae and the accumulation of bright orange carotenoid pigments. These morphological changes follow a period of approximately 22.5 hours, occurring predominantly during the subjective day (dawn to dusk) (Baker *et al.*, 2012). Central to this system is the frequency (*frq*) locus, which acts as the negative element in the TTFL. The expression of *frq* is driven by the White-Collar Complex (WCC), a heterodimeric transcription factor composed of the light-sensitive White-Collar 1 (WC-

1) and the structurally analogous WC-2 (Baker *et al.*, 2012). Although WC-2 lacks a flavin-binding pocket and is not inherently light-responsive, it remains indispensable for the stability and functionality of WC-1. Operating as a unified complex, the WCC functions as the master blue-light sensor, regulating the fungal circadian clock and developmental response to light (Linden & Macino, 1997; Ballario *et al.*, 1998; Cheng *et al.*, 2001; Froehlich *et al.*, 2003; Olmedo *et al.*, 2013). This system exemplifies how fungi utilize specific chromoproteins, designated photoreceptors, to translate photonic energy into biological signals (Bayram & Bayram, 2023; Corrochano *et al.*, 2025). Fungal photoreceptors are crucial regulators of morphogenesis; they govern the transition between vegetative growth and asexual or sexual reproduction, trigger the production of secondary metabolites, and modulate stress responses (Bayram *et al.*, 2010; Yu & Fischer, 2019). These proteins detect light via a specialized cofactor called a chromophore, which contains a conjugated π-electron system capable of absorbing specific wavelengths (Ziegler & Möglich, 2015). Based on the photochemical properties of these chromophores, fungal photoreceptors are categorized into three major classes: blue-light receptors using flavins, green-light receptors using retinal, and red-light receptors utilizing linear tetrapyrroles (Bayram *et al.*, 2010; Yu & Fischer, 2019; Bayram & Bayram, 2023) **(Fig. 5)**.

Blue-light receptors constitute the most diverse class in fungi and are subdivided based on their sensing domains. The first group includes proteins containing a Light, Oxygen, and Voltage (LOV) domain, such as the WCC or VIVID (VVD) (Schafmeier *et al.*, 2005; Gin *et al.*, 2013; Lokhandwala *et al.*, 2015). These receptors utilize flavin adenine dinucleotide (FAD) or flavin mononucleotide (FMN) as a chromophore (Schuhmacher *et al.*, 2024). In addition, both white-collar proteins harbor two Per-Arnt-Sim (PAS) domains, crucial for protein-protein interaction, and a zinc finger domain (ZFD) for DNA binding and gene regulation (Ballario *et al.*, 1996; Ballario *et al.*, 1998). The LOV domain exhibits high homology to plant phototropins, utilizing a conserved light inducible mechanism to transduce blue-light signals. This activation involves the reversible formation of a covalent thioether bond between a conserved cysteine residue in the LOV domain and the flavin ring, triggering a conformational change essential for signal transduction (Dasgupta *et al.*, 2015; Schuhmacher *et al.*, 2024). Prolonged incubation in the dark leads to the disruption of the bond, thereby inactivating the WCC (Yu & Fischer, 2019; Schuhmacher *et al.*, 2024). To modulate the positive blue light response, *N. crassa* employs a second, distinct regulatory system to

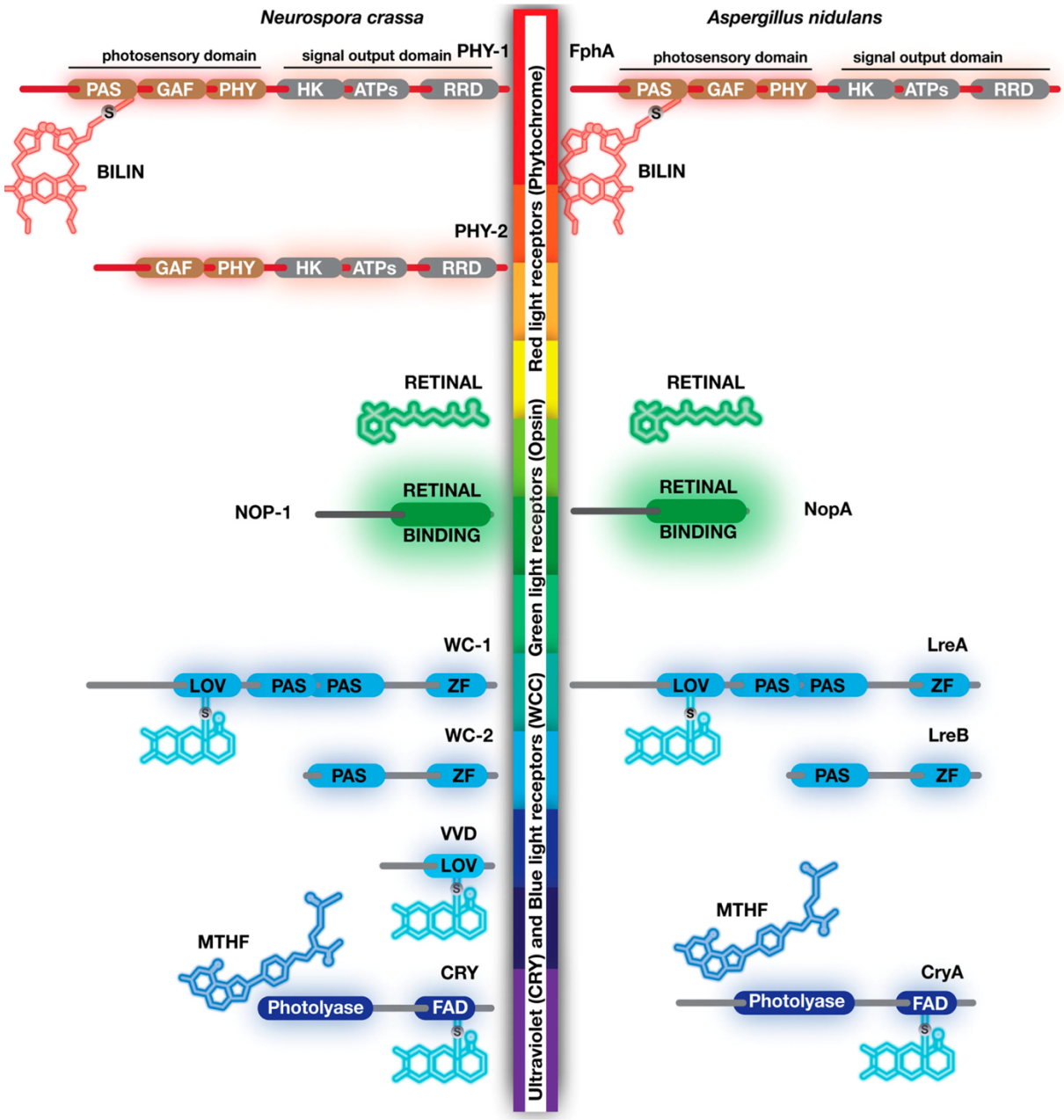

Figure 5: Common light receptors and the corresponding chromophores in the fungal model organisms *N. crassa* and *A. nidulans*. The phytochrome PHY-1 from *N. crassa* and FphA from *A. nidulans* are red-light receptors, which utilize biliverdin as chromophore to absorb the red to far-red spectrum. They possess two modules, the N-terminal chromophore binding photosensory module comprised of an N-terminal extension followed by the PAS-GAF-PHY domains, and a signal output module which is composed of a histidine kinase domain (HK), an ATPase domain (ATPs) and a response regulator domain (RRD). Absorption of red light triggers the conformational shift of the inactive P_r form to the active P_{fr} form. This activation can be reverted by prolonged darkness or absorption with far-red light. *N. crassa* harbors an additional phytochrome PHY-2 which shares high homology with PHY-1 but does not contain a PAS domain, therefore does not bind a chromophore. Membrane bound opsins such as NOP-1 (*N. crassa*) and NopA (*A. nidulans*) are associated with the green light sensitive chromophore retinal which is an aldehyde form of vitamin A. Green light induces the conversion from all-*trans* retinal to 13-*cis* retinal causing conformational changes in the opsin protein. The group of blue light receptors is composed of the LOV-domain proteins WC-1 and WC-2 in *N. crassa* (LreA and LreB in *A. nidulans*, respectively) and VVD which is not present in *A. nidulans*. In addition, both organisms contain a UVA and blue light sensitive cryptochrome (CRY in *N. crassa*, CryA in *A. nidulans*). WC-1 and VVD proteins contain a LOV domain with a conserved cysteine for binding the flavin chromophore. The two PAS domains mediate protein-protein interactions, and the zink-finger domain (ZF) is crucial for DNA binding. WC-2 does not harbor a LOV-domain for chromophore binding but shares high sequence homology with WC-1 proteins. While cryptochromes have a conserved FAD binding domain (FAD) for the main chromophore FAD, they utilize secondary antenna chromophores such as MTHF for enhanced light absorption capabilities. The respective length of each protein is correspondent to their relative amino acid sequence (Bayram & Bayram, 2023).

repress WCC activity and establish photoadaptation. While FRQ is responsible for inhibiting WCC functionality primarily during the subjective night to reset the circadian cycle, the fungus relies on the LOV-photoreceptor VVD to control sensitivity throughout the day. Upon light induction by the WCC, VVD accumulates in the nucleus where it physically interacts with the LOV domain of WC-1. This interaction competitively inhibits the formation of active WCC homodimers, thereby preventing sustained transcriptional activation and attenuating the light response (Hunt *et al.*, 2010; Gin *et al.*, 2013). This dual negative-feedback loop presents a sophisticated integration of photoreceptors, enabling the fungal cell to dynamically adapt to fluctuating light intensities and qualities within its environment (Yu & Fischer, 2019; Bayram & Bayram, 2023).

The second group comprises the Cryptochrome/Photolyase Family (CPF), which binds FAD and often a secondary antenna pigment. While photolyases utilize UV-A or blue light energy to directly repair UV-induced DNA damage, cryptochromes have evolved to function primarily in signaling, but the area of responsibility differs significantly between different species. In animals, they are primarily utilized as light independent negative regulators of the circadian rhythm, while *in planta* cryptochromes are known for their regulation of shade avoidance and controlling the flowering time (Bayram *et al.*, 2008a; Kottke *et al.*, 2017; Lopez *et al.*, 2021; Deppisch *et al.*, 2022). Although they are distributed in most fungal species, in comparison to LOV-domain blue light receptors, knowledge about fungal CPF members and their functions is still limited (Yu & Fischer, 2019; Bayram & Bayram, 2023). The final subgroup consists of proteins with Blue Light Using Flavin (BLUF) domains, which bind flavins non-covalently and restructure the hydrogen bond network upon excitation, though their specific physiological roles in fungi remain less characterized than in bacteria. These proteins are uniquely restricted to *Ustilago* species and remain functionally enigmatic to this day (Masuda *et al.*, 2004; Park & Tame, 2017; Yu & Fischer, 2019).

Complementing blue-light sensitivity, fungi possess green-light receptors known as opsins. These are seven-transmembrane helix proteins homologous to bacterial rhodopsins, utilizing all-*trans*-retinal as their chromophore via a Schiff base linkage. Green light induces photoisomerization by converting the all-*trans*-retinal to 13-*cis*-retinal (Brown, 2004; Purschwitz *et al.*, 2006; García-Martínez *et al.*, 2015). Fungal opsins are broadly classified into three subfamilies based on their photocycle kinetics and function. The *Neurospora* Rhodopsin (NR)-like opsins, such as NOP-1, harbor a

slow photocycle and function as sensory receptors to modulate ROS stress responses and conidiation (Wang *et al.*, 2018b; Rozenberg *et al.*, 2021). In contrast, the *Leptosphaeria maculans* Rhodopsin (LR)-like and Carotenoid Opsin (CarO)-like families function primarily as light-driven proton pumps with rapid photocycles, contributing to the electrochemical gradient across the membrane (García-Martínez *et al.*, 2015; Lyu *et al.*, 2016; Panzer *et al.*, 2019). However, certain members, such as SOP1 in *Sclerotinia sclerotiorum*, exhibit dual functionality, influencing virulence and stress tolerance independent of their ion-transport capabilities (Lyu *et al.*, 2016).

The final major group of light sensors consists of phytochromes, a widespread superfamily of photoreceptors that sense red and far-red light using a linear tetrapyrrole (bilin) chromophore. Originally discovered in plants, where they regulate critical developmental transitions such as germination and flowering and are involved in the circadian rhythm, phytochromes have since been identified in bacteria, cyanobacteria, and fungi, revealing an ancient evolutionary origin (Lamparter *et al.*, 1997; Lamparter *et al.*, 2002; Blumenstein *et al.*, 2005; Lopez *et al.*, 2021). The defining characteristic of this family is their inducible photoswitch; they exist in two stable, distinct spectral states that are interconvertible by light. The receptor is synthesized in the red-light-absorbing form (P_r-state), which acts as the ground state in most species. Upon absorption of a red photon (approximately 660 nm), the bilin chromophore undergoes a *cis-trans* isomerization around the C_{15}=C_{16} double bond. This conformational shift triggers the protein to adopt the far-red-absorbing active form (P_{fr}-state). Conversely, absorption of a far-red photon (approximately 730 nm), prolonged incubation in the dark or high temperature reverts the molecule to the inactive P_r-state (Song *et al.*, 2011; Yu *et al.*, 2019; Yu & Fischer, 2019). This intrinsic reversibility allows organisms to act as biological spectrometers, assessing not just the presence of light, but the quality of the ambient environment based on the changing ratio of red to far-red light (Li *et al.*, 2011). This is especially important in plants, where the nuclear import and transcriptional activity of the two phytochromes (PhyA and PhyB) is controlled by the light quality. They are critical in transmitting light as an input signal to the circadian clock of the plant, thereby promoting systemic responses such as seed germination, de-etiolation, leaf expansion, and chlorophyll production (Genoud *et al.*, 2008; Sheerin *et al.*, 2015; Tripathi *et al.*, 2019; Lopez *et al.*, 2021).

In the fungal kingdom, phytochromes act as distinct light sensors that fulfill a dual role as “bacterial” histidine kinases and eukaryotic nuclear regulators (Yu *et al.*,

2016). The fungal phytochrome FphA from *A. nidulans* retains the light inducible reversibility: the protein can absorb red light to convert into the active P_{fr}-form and far-red light or temperature shifts to revert to the inactive P_r-form. This reversibility allows the fungus to adapt to changes in light and temperature conditions and prepare for incoming environmental threats (Blumenstein *et al.*, 2005; Yu *et al.*, 2016; Yu *et al.*, 2019). Structurally, FphA is a typical hybrid histidine kinase (Azuma *et al.*, 2007). Like most phytochromes, FphA needs to be a homodimer to act as a functional photoreceptor. The protein comprises a conserved N-terminal sensory module (PAS-GAF-PHY domain) and a C-terminal output module that contains both a histidine kinase domain and a response regulator domain (Blumenstein *et al.*, 2005; Brandt *et al.*, 2008; Takala *et al.*, 2020). In addition, FphA contains a variable N-terminal extension (NTE), relevant for isomerization stability. The PAS domain contains a conserved cysteine (C195) and covalently binds the fungal chromophore, the biliverdin. The GAF domain (cGMP-specific phosphodiesterases; cyanobacterial adenylate cyclases; formate hydrogen lyase) contains an essential histidine residue (H504) that is responsible for chromophore stability and coordination. The PHY domain (phytochrome) transfers the light induced photoisomerization to the response regulator module and stabilizes the P_{fr} form (Brandt *et al.*, 2008; Fischer *et al.*, 2020).

Although there is no structural data available for fungal phytochromes, the mechanism behind the light activated conformational shift should be like plant and bacterial phytochromes on basis of sequence and domain homology. Upon light perception, chromophore isomerization in the PAS domain triggers a conformational shift at the β-sheet hairpin structure, which in turn refolds as a short α-helix (Takala *et al.*, 2020). This structural change is transferred to the output module inducing autophosphorylation of the histidine kinase domains at the residue H770. This structural modification shifts the response regulator, resulting in the exposition of the aspartic acid residue D1181. This enables FphA to accept a phosphoryl group from the phosphotransfer protein YpdA, thereby activating the downstream kinase cascade of the HOG pathway (Azuma *et al.*, 2007; Brandt *et al.*, 2008; Yu *et al.*, 2016; Takala *et al.*, 2020) **(Fig. 6)**.

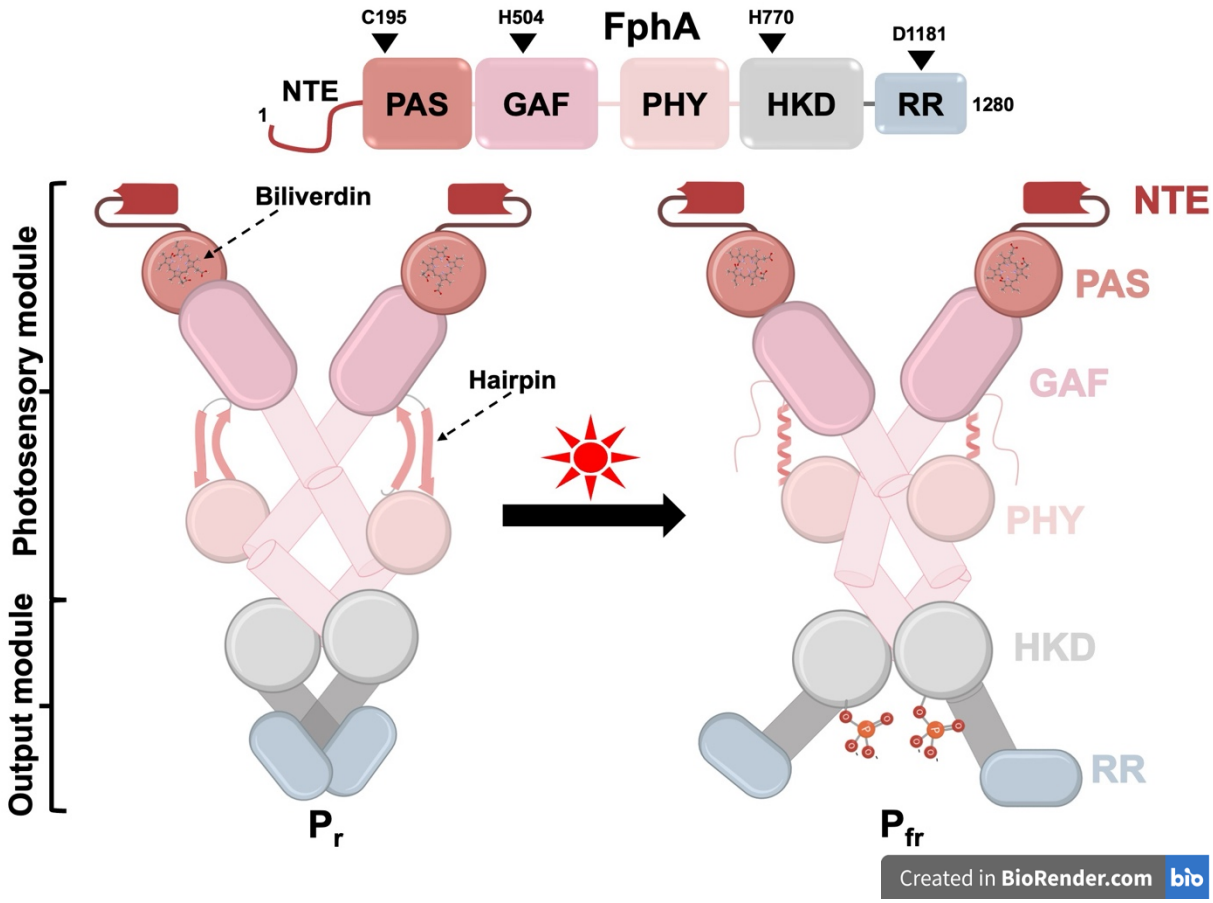

Figure 6: Domain architecture and proposed light induced structural changes of FphA from *A. nidulans*. While the crystal structure of FphA from *A. nidulans* has not yet been solved, its architecture and functional mechanics can be modeled through past identifications of amino acids crucial for its biochemical activity and the structural homology with bacterial and plant phytochromes. The protein is organized into an N-terminal photosensory module comprising a variable extension (NTE) and the PAS, GAF, and PHY domains, followed by a C-terminal output module containing the histidine kinase domain (HKD) and response regulator (RR). Functional FphA exists as a homodimer. Key functional residues include **C195** in the PAS domain, which covalently binds the biliverdin chromophore, and **H504** in the GAF domain, which stabilizes the chromophore pocket. The GAF and PHY domains are linked by a structural interface that exists as β-sheet hairpin in the dark state. Upon red light perception and chromophore isomerization, this hairpin refolds into a shorter α-helix, mechanically pulling the PHY and GAF domains closer together. This conformational change is transmitted to the HKD, triggering autophosphorylation at the histidine residue **H770**. The negative charge of the phosphate groups leads to the exposition of the aspartic acid residue **D1181** on the response regulator which in turn can now accept phosphoryl groups of phosphotransfer proteins. Generated in BioRender and modified after (Brandt *et al.*, 2008; Takala *et al.*, 2020).

1.5 Light response in *A. nidulans*

In the complex soil environment, *A. nidulans* encounters fluctuating light conditions that serve as important signals for survival, governing the transition between vegetative growth and sexual differentiation, the initiation of the pathogenic lifecycle, and the biosynthesis of secondary metabolites (Yu & Fischer, 2019; Bayram & Bayram, 2023). There are several example of different fungal organisms which delay germination under light conditions to improve the viability of sexual spores against harmful UV-radiation or ROS (Fuller *et al.*, 2013; Röhrig *et al.*, 2013; García-Martínez *et al.*, 2015). Another example is the production of compatible solutes as a reaction to desiccation

which is usually on the surface of organic substances and in the presence of light. Here, light serves as a warning signal, preparing the organism for the surrounding conditions and potential threats (Duran *et al.*, 2010; Tisch & Schmoll, 2010). Some species such as *Phycomyces blakesleeanus* even exhibit phototropism (Galland *et al.*, 1985). These physiological responses are highly intricate and demand that the organism precisely discriminates between spectral quality (wavelength) and fluctuating light intensity. The fungal “eye” is very sensitive to low light intensities that a human eye cannot detect (Bayram & Bayram, 2023). To transfer these signals into a stress response and photoadaptation, fungal organisms such as *A. nidulans* employ a photosensory network primarily modulated by the red-light sensing phytochrome FphA and partially by the WCC ortholog LreA/LreB (Light response) together with the sexual master transcription factor VeA (Blumenstein *et al.*, 2005; Purschwitz *et al.*, 2006; Purschwitz *et al.*, 2008; Purschwitz *et al.*, 2009; Yu *et al.*, 2016; Yu & Fischer, 2019).

Recent genome-wide transcriptomic analyses revealed the dominant role of FphA in this system, demonstrating that while LreA and LreB are necessary for blue-light responses, the phytochrome modulates a significantly larger subset of the genome, approximately 1,100 genes, acting as both a transcriptional activator and repressor (Yu *et al.*, 2021). Central to this mechanism is the signal transmission of FphA through the HOG MAPK pathway, specifically interacting with the phosphotransfer protein YpdA to transmit signals from the cytoplasm to the nucleus to activate gene expression via AtfA. Furthermore, FphA shuttles into the nucleus upon light perception and manipulates histone 3 acetylation of light-dependent genes by modulating the activity of the histone acetyltransferases GcnE (general control non-derepressible) and AdaB, although the mechanism behind this process is not known. This regulation identifies FphA with the stimulation of AtfA via the HOG pathway as the primary regulator of light response in *A. nidulans* (Yu *et al.*, 2016).

In contrast to the WCC in *N. crassa,* LreA appears to be more of a repressor of light inducible gene expression by binding together with LreB to the promoter of such genes (Yu & Fischer, 2019; Yu *et al.*, 2021). Together, these proteins promote functionality of the histone deacetylase HdaA and repress GcnE, effectively inhibiting promoter activity in the dark. Therefore, in comparison to the blue light response surrounding the WCC from *N. crassa*, it seems conceivable that LreA and LreB are more utilized to fine-tune the general light response and play a secondary role to the

red-light receptor phytochrome in *A. nidulans* (Yu et al., 2021; Bayram & Bayram, 2023; Corrochano et al., 2025).

As mentioned above, these light receptors do not function in isolation, rather, they coordinate with VeA to control morphology. In the absence of light, VeA predominantly localizes to the nucleus, where it serves as the essential factor for the heterotrimeric velvet complex by bridging VelB with the methyltransferase-like global regulator of secondary metabolism, LaeA (Bayram *et al.*, 2008b). This VelB-VeA-LaeA complex is a prerequisite for sexual morphogenesis (cleistothecia formation) and the activation of secondary metabolite clusters, including those responsible for sterigmatocystin and penicillin biosynthesis (Bayram *et al.*, 2008b). Furthermore, VeA physically associates with LreA and LreB in the dark to suppress the promoter activity of key light-responsive genes, such as *ccgA* (clock-controlled gene A), *abaA* (abacus A) or the conidiation master regulator *brlA* (bristle A) (Yu *et al.*, 2021; Bayram & Bayram, 2023; Bastakis *et al.*, 2025). Under illumination, the regulatory system shifts as the velvet complex dissociates; FphA-mediated signaling triggers the nuclear export of VeA, causing its cytoplasmic accumulation and thereby relieving the repression of the asexual conidiation program (Strohdiek *et al.*, 2025). Interestingly, a subpopulation of VeA remains bound to light-inducible promoters even under these conditions. Recent evidence suggests that FphA can physically interact with VeA to facilitate the activation of these genes, though the precise mechanism regulating this light-dependent recruitment remains elusive (Yu & Fischer, 2019; Yu *et al.*, 2021). This suggests that VeA functions as a dual-role, light-dependent regulator whose cellular function, whether as a repressor of conidiation or an activator of light-inducible genes, is likely determined by dynamic post-translational modifications and changing protein-protein interaction partners (Bayram & Bayram, 2023). Besides phytochrome and LreA/LreB, the genome of *A. nidulans* encodes for a photolyase (CryA) and an opsin (NopA). In *N. crassa,* the orthologs (CRY and NOP-1, respectively) were investigated in their role as negative regulator of the WCC (Olmedo *et al.*, 2010; Olmedo *et al.*, 2013). However, their precise role in the light response of *A. nidulans* is still unclear (Yu & Fischer, 2019).

1.6 The cryptochrome CryA in *A. nidulans*

It is important that differential gene expression, which responds to an outside trigger such as light, is transient, and therefore needs to be negatively regulated. Knowledge

about negative molecular mechanisms in *A. nidulans* is still limited. Although LreA and LreB inhibit gene expression in the dark, they are still positive blue light regulators. In other fungal systems, such as *N. crassa* or *Trichoderma atroviride*, the VVD protein and FRQ are crucial for repressing WCC functionality in a negative feedback loop (Hunt *et al.*, 2010; Schmoll *et al.*, 2010; Gin *et al.*, 2013; Henríquez-Urrutia *et al.*, 2022). This allows the fungi to have a proper day/night cycle and enables photoadaptation for different environmental challenges. *A. nidulans* lacks a VVD or FRQ ortholog and there are no known negative factors of phytochrome. In plants, phytochrome activity is regulated by phytochrome interaction factors (PIFs) and the blue light receptor cryptochrome (Casal, 2000; Más *et al.*, 2000; Wang *et al.*, 2018a; Wang & Lin, 2020a). Additionally, it was suggested that CRY1 acts as a negative regulator of phytochrome by inhibiting the binding to various transcription factors such as COP1 (Constitutively Photomorphogenic 1) or by occupying PIF interaction sites (Li *et al.*, 2011; Pedmale *et al.*, 2016; Wang *et al.*, 2018a). In fungal organisms, only the cryptochrome CRY in *N. crassa* was described in its role as negative regulator, together with NOP-1 and PHY1, of the WCC function. It is therefore conceivable that a cryptochrome protein in *A. nidulans* could act as a negative regulator of the phytochrome action.

Cryptochromes and photolyases constitute a highly conserved superfamily of light-driven photoreceptors (Lopez *et al.*, 2021; Deppisch *et al.*, 2022). They are characterized as flavin-binding proteins that share a conserved Photolyase Homology Region (PHR) domain, which is essential for DNA repair and the binding of the secondary antenna chromophore, usually the folate molecule N_5, N_{10}-methenyl-tetrahydrofolate (MTHF) (Wang *et al.*, 2015). Nested within this PHR domain is the FAD-binding pocket, where the primary chromophore FAD is non-covalently integrated. In contrast to photolyases, cryptochromes possess a unique C-terminal extension (CTE) that is indispensable for protein-protein interactions and downstream regulatory functions (Yang *et al.*, 2000). While photolyases do not directly mediate developmental photoresponses, they utilize light energy to repair DNA damage induced by UV radiation or reactive oxygen species (Sancar, 2003). These enzymes are classified by their substrate specificity: CPD-photolyases repair cyclobutane pyrimidine dimers, whereas 6-4 photolyases target 6-4 photoproducts (Deppisch *et al.*, 2022). Microorganisms, including various fungi and bacteria, typically encode at least one CPD photolyase, while 6-4 photolyases are primarily found in higher eukaryotes such as plants and animals (Bayram *et al.*, 2008a; Li *et al.*, 2025b).

Cryptochromes are further categorized into subfamilies based on their physiological roles: the plant cryptochromes (pCRYs), first identified via CRY1 in *Arabidopsis thaliana*; animal cryptochromes (aCRYs), which include the light-independent mammalian-type (mCRYs) and light-dependent *Drosophila*-type (dCRYs) involved in the circadian clock; and the CRY-DASH group (*Drosophila*, *Arabidopsis*, *Synechocystis*, *Homo*), which represents an evolutionary bridge between photolyases and cryptochromes (Michael *et al.*, 2017; Deppisch *et al.*, 2022). Most fungal species encode a CRY-DASH protein, with roles ranging from the repression of photoinduced conidiation and growth in *Botrytis cinerea* and *Fusarium fujikuroi* to the regulation of circadian rhythms in *N. crassa* and DNA binding in *Mucor circinelloides* (Olmedo *et al.,* 2010; Castrillo *et al.,* 2013; Nsa *et al.,* 2014; Cohrs & Schumacher, 2017; Navarro *et al.,* 2020).

Evidence increasingly indicates "dual-function" proteins where photolyases also serve as light-induced regulators. In diatoms and fish, certain photolyases regulate the circadian clock while maintaining DNA repair activity (Coesel *et al.*, 2009; König *et al.*, 2017; Li *et al.*, 2025b). Similar dual roles exist in fungi: PHL1 in *Cercospora zeae-maydis* regulates repair gene expression under UV light, while in *Trichoderma reesei* and *T. atroviride*, the 6-4 photolyase Cry1 and the CPD photolyase Phr1 perform both photoreactivation and blue/red-light signaling (Berrocal-Tito *et al.*, 2007; Bluhm & Dunkle, 2008; García-Esquivel *et al.*, 2016). In *A. nidulans*, the CPD photolyase CryA functions as a dual-role protein that repairs DNA while simultaneously repressing sexual development through its interaction with the velvet protein VeA. CryA is a nuclear protein whose deletion results in an overabundance of Hülle cells and cleistothecia under light conditions. This phenotype mirrors mutants of sexual transcription factors such as *nsdD* (not in sexual development) and *rosA* (regulator of sexual development) (Bayram *et al.*, 2008a).

Previous biochemical analyses established that CryA utilizes FAD as its primary chromophore and identified MTHF as the predicted secondary cofactor. *In vivo* studies demonstrated that CryA is constitutively localized to the nucleus, remaining unaffected by changes in light, temperature, or carbon sources. Notably, the overexpression of *cryA* leads to the total inhibition of conidiation and pigment synthesis. Furthermore, the confirmed physical interaction between CryA and the phytochrome FphA in the nucleus suggests that CryA may act as a negative regulator by disrupting FphA-driven histone

modifications, thereby modulating the broader light-response network of *A. nidulans* (Landmark, 2022).

1.6 Aim of this work

While the blue-light-sensing White-Collar Complex and the red-light receptor FphA have been extensively characterized, fungal CPF proteins remain poorly understood. They have established roles as negative regulators of light-mediated processes, including circadian rhythms, photosynthesis, and development, across other biological kingdoms (Cohrs & Schumacher, 2017; Kottke *et al.*, 2017; Lopez *et al.*, 2021). The goal of this work is to further characterize CryA in *A. nidulans*, investigating its potential as a negative regulator of FphA-mediated signaling by modulating light-dependent gene expression, histone modifications, or AtfA functionality.

Furthermore, recent evidence revealed that *cryA* expression is regulated by AtfA in response to both light and oxidative stress (Yu *et al.*, 2021; Miskei *et al.*, 2025). To expand on these intriguing findings, this work tries to explore the novel hypothesis that CryA serves as a dual-input sensor for reactive oxygen species (ROS). There are few studies linking cryptochromes and photolyases to ROS sensing (El-Esawi *et al.*, 2017; Zheng *et al.*, 2024; Li *et al.*, 2025a). Therefore, the second part of this study is about integrating the function of CryA into the canonical HOG-pathway and NapA-mediated stress feedback loops. CryA presents an attractive target for genetic manipulations, since it is the only CPF member in the genome of *A. nidulans*. Several *cryA* variants will be investigated by utilizing genetic approaches to characterize CryA as a putative ROS sensor in the general stress response of *A. nidulans*.

2. Results

2.1 CryA is a CPD I photolyase with an N-terminal extension

Cryptochromes and photolyases form the extensive cryptochrome/photolyase family and are present in all kingdoms of life. They are separated in six major subfamilies, depending on the organism and the molecular function they fulfill. While plant cryptochromes and animal cryptochromes are quite specific in their respective kingdom, CRY-DASH and 6-4 and CPD photolyases are more ubiquitous. Fungal organisms predominantly harbor a CRY-DASH protein for cryptochrome functions and either a 6–4 photolyase or a CPD I or II photolyase (Deppisch *et al.*, 2022). On the structural level, CPF members share a high homology in the N-terminal PHR domain, relevant for photoactivation, and the central FAD binding domain which is crucial for forming the chromophore binding pocket (Sancar, 2003; Kiontke *et al.*, 2011). Furthermore, cryptochromes utilize a C-terminal extension for protein-protein interactions and regulatory functions (Yang *et al.*, 2000).

Crucial for the light function is a conserved tryptophan triad which serves as electron donor to reduce FAD^{ox} to $FADH^{-}$ after illumination with light. This leads in the case of a cryptochrome to a conformational shift of the protein and exposes the C-terminal tail which is now able to interact with other proteins. Photolyases utilize the excited FADH*- to transfer the energy to DNA lesions, thereby promoting cleavage and repair of the damaged DNA base (Palayam *et al.*, 2021; Aguida *et al.*, 2024).

Previous work already confirmed that CryA from *A. nidulans* belongs to the CPD I subfamily and contains the necessary conserved tryptophan triad for electron transfer (Bayram *et al.*, 2008a). Additionally, a more recent phylogenetic analysis, including all kingdoms of life, integrated twelve subfamilies instead of the previously known six subfamilies. This comparison categorized CryA as being closer to CPD III and CPD I photolyases (Deppisch *et al.*, 2022; Landmark, 2022). Since most *Aspergillus* species only harbor one CPF protein and are not classified, a new phylogenetic tree was generated using Geneious Prime 2024 **(Fig. 7, Appendix Tab. 16)**. This analysis compared CryA predominantly with other *Aspergillus* members and fungal CPF members known to have dual roles (Berrocal-Tito *et al.*, 2007; Tagua *et al.*, 2015; García-Esquivel *et al.*, 2016; Cohrs & Schumacher, 2017). For simplification, only the major CPF groups were investigated; the CPD photolyases (green), the animal

cryptochromes (ACRYs, violet), the plant cryptochromes (PCRYs, red), and the CRY-DASH proteins (blue).

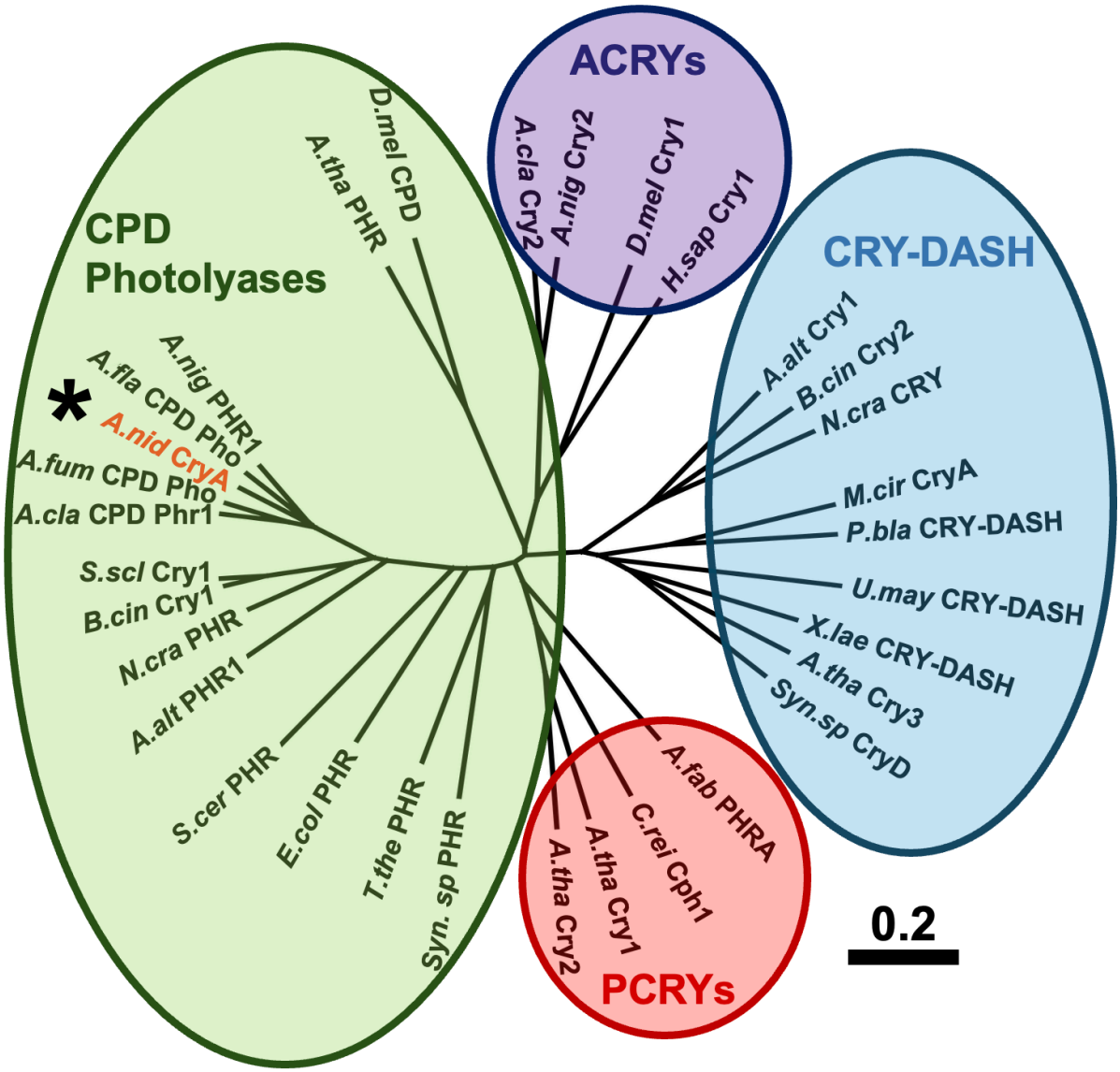

Figure 7: Phylogenetic analysis of CryA from *A. nidulans*. A phylogenetic analysis of CryA together with members of the CPF, and a special focus on fungal representatives, was performed using Geneious Prime 2024. Global alignment was used for sequence alignment with a PAM matrix of 100 and gap costs of 10/1. The phylogenetic tree was generated using the Jukes-Cantor distance model and the Neighbor-Joining algorithm. The subfamilies are CPD photolyases (green), pCRYs (red), aCRYs (violet), and CRY-DASH (blue). CryA is emphasized by an asterisk. The scale bar represents the amino acid substitutions per site.

As described previously, CryA is classified as a CPD I photolyase and clusters with the CPF members of the *Aspergillus* family. In addition, *Aspergillus niger* and *Aspergillus clavatus* harbor an additional animal cryptochrome-like gene distinguishing them from other fungi which usually harbor only a CRY-DASH gene as a cryptochrome (Deppisch *et al.*, 2022). The CPD II photolyases, represented here by *A. thaliana* and *Drosophila melanogaster*, are clearly distinct from the other members of the phylum. CPD III photolyases, predominantly found in yeast and prokaryotes, share a high

degree of evolutionary similarity with both CPD I photolyases and plant cryptochromes. This shows that all photolyases found in the most common *Aspergillus* species are CPD I photolyases. It also reveals that an evolutionary divergence occurred, resulting in the loss of the CRY-DASH protein. This potentially increased the need for CryA to develop regulatory functions besides DNA repair activity (Bayram *et al.*, 2008a).

Next, due to the limited availability of information regarding the structural composition of CryA, the SUPERFAMILY and InterPro domain prediction tools were used to determine the protein architecture. The domain structures of CPF members from *N. crassa*, *A. thaliana*, *Homo sapiens*, and *Escherichia coli*, Phr1 from *T. atroviride*, and Phr1 and CRY2 from *A. niger* were compared to CryA **(Fig 8a).**

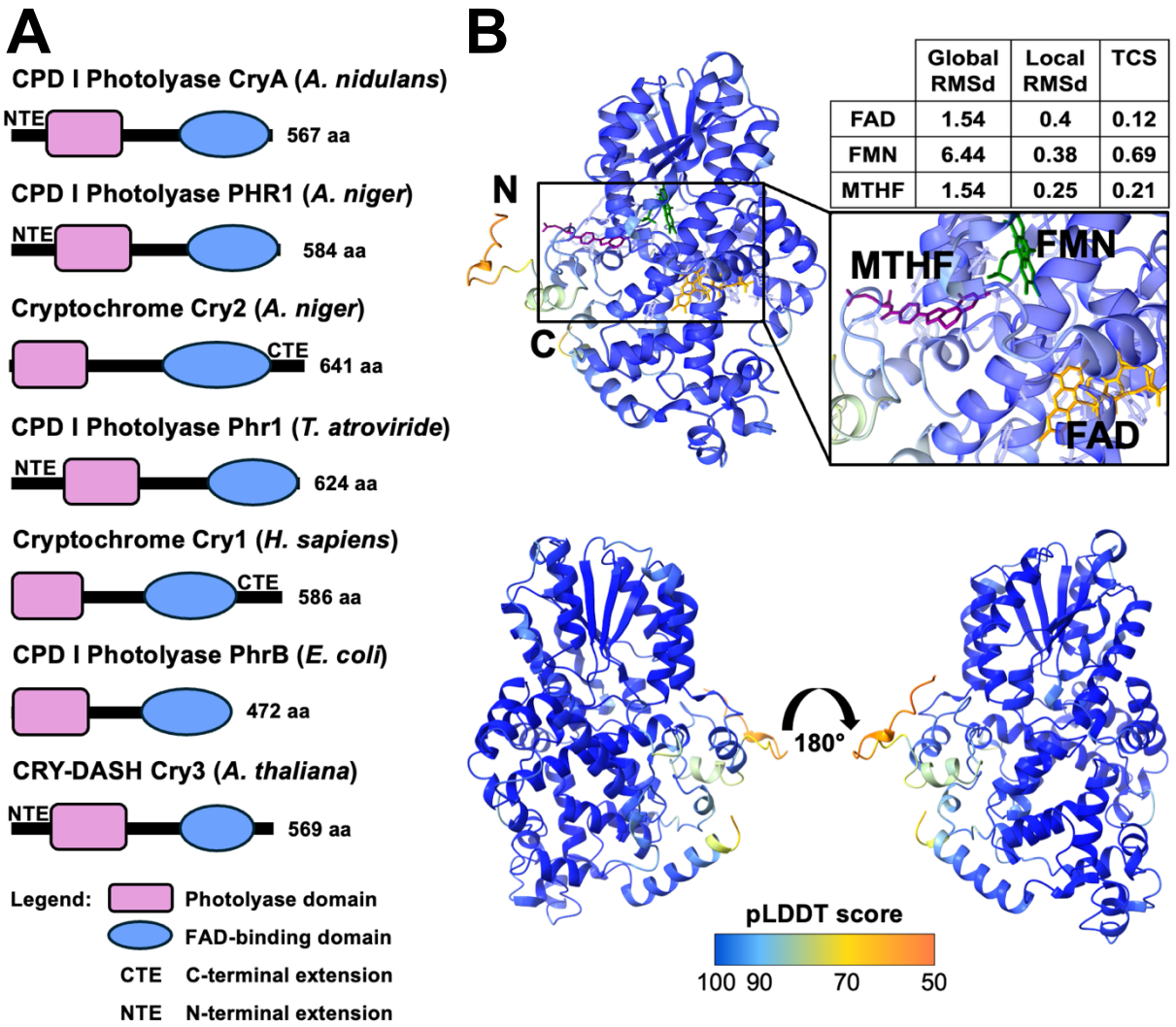

Figure 8: Domain architecture and predicted protein structure of CryA. (A) SUPERFAMILY and InterPro were utilized to predict and compare the conserved domains in CryA with the other CPF members from *A. niger* (PHR1 & Cry2), *T. atroviride* (Phr1), *H. sapiens* (Cry1), *E. coli* (PhrB), and *A. thaliana* (Cry3). The conserved domains are the N-terminal photolyase domain (pink) and the C-terminal FAD-binding domain (light blue). In addition, proteins harbor either a N-terminal extension (NTE) or a C-terminal extension (CTE). The size of each protein domain is arbitrarily proportional to their amino acid sequence length. (B) The protein structure of CryA was predicted with AlphaFold and the structure was used as foundation to predict the chromophores with AlphaFill. The coloration of the protein structure is based on the AlphaFold confidence levels, which are measured through the pLDDT (predicted local distance difference test) score. Blue indicates high confidence and orange indicates low confidence.

The quality of the predicted chromophores is represented by Global and Local RMSD (root mean square deviation) and TCS (transparent clash score) values. Lower scores indicate higher confidence. FAD is colored orange, FMN is colored green, and MTHF is colored purple. The structural AlphaFold prediction of CryA from two viewing angles and the overlaid pLDDT score are detailed below.

CryA contains an N-terminal photolyase domain (pink) and a C-terminal FAD-binding domain (light blue) which are present in all analyzed CPF members. Unlike typical cryptochromes, CryA does not have a variable C-terminal extension that is critical for regulatory function (Palayam *et al.*, 2021). Instead, CryA harbors an untypical and non-specific N-terminal extension which appears to be only present in other eukaryotic CPD photolyases and some CRY-DASHs.

AlphaFold 3 and AlphaFill were utilized to predict the protein structure of CryA and any potential chromophores **(Fig. 8b)**. Most of the core protein structure is highly conserved (>95 pLDDT) except the N- and C-terminus (50-70 pLDDT). The AlphaFill prediction determined with high confidence that CryA utilizes FAD (orange) and MTHF (purple), indicated by the low TCS and RMSd values. In addition, AlphaFill predicts with a lower confidence FMN (green) as a secondary flavin molecule which was described before as an antenna chromophore in some photolyases (Klar *et al.*, 2006). These predictions are concurring with previous results, defining CryA as a folate CPD I photolyase with FAD as main chromophore and possibly FMN and 5,10-MTHF as secondary co-factors (Landmark, 2022).

2.2 CryA uses FAD as main co-factor and 5,10-MTHF and FMN as secondary chromophores

Cryptochromes and photolyases both utilize light to perform regulatory and repair functions. They bind light sensitive molecules, with FAD being described as the main chromophore. In addition, to enhance the light harvesting ability and expand the absorbable spectrum beyond blue light, CPF proteins bind antenna chromophores. These additional co-factors include 5,10-MTHF for the UV-A spectrum, FMN for blue light, and 8-hydroxy-5-deazaflavin (8-HDF), a chromophore that enables some cryptochromes to absorb red and yellow light (Beel *et al.*, 2012; Tagua *et al.*, 2015; Oldemeyer *et al.*, 2020). Although there are no experimental validations present for the chromophores of fungal photolyases, studies about CRY-DASH proteins in *N. crassa*

and *Mucor circinelloides* revealed FAD and 5,10-MTHF as the main chromophores (Froehlich et al., 2010; Navarro et al., 2020).

To experimentally validate relevant co-factors, CryA was introduced in the expression vector pET28a (Novagen) and fused N-terminally to a 6xHis-tag (pAUL13). Next, the vector was integrated in the *E. coli* strain BL21 DE3 and CryA was heterologously expressed and purified. The protein was then analyzed spectroscopically with a photometer to visualize a possible photocycle **(Fig. 9a)**. Afterwards, the protein was denatured and the chromophores separated from the protein pellet. The buffer was replaced with dH_2O, and the released chromophores were analyzed via high performance liquid chromatography (HPLC) **(Fig. 9b)**. FAD, FMN, and 5,10-MTHF (Schircks Laboratory) were used as standards.

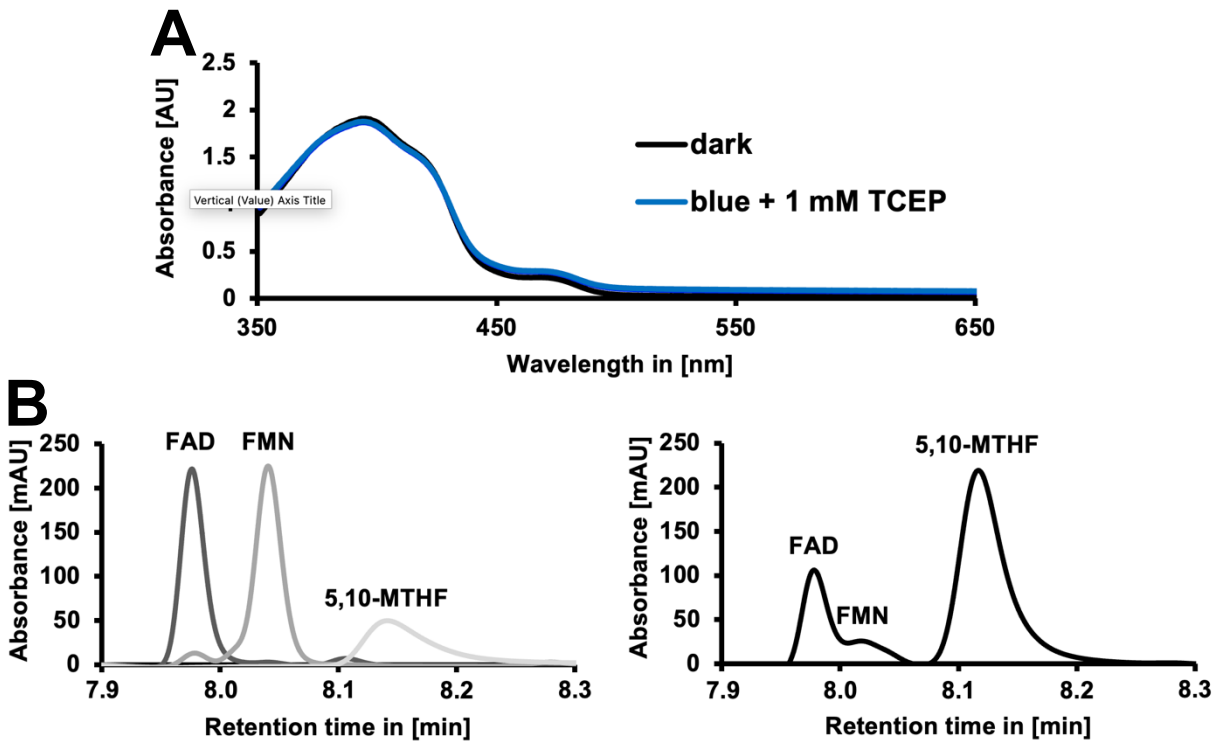

Figure 9: Photometric analysis of CryA and the associated chromophores. (A) Absorption spectrum of CryA in dark conditions or after treatment with blue light and the reducing agent TCEP. Illumination was performed for one minute at a wavelength of 450 nm (200 µmol photons m^{-2} s^{-1}). TCEP was added at the indicated concentration and incubated for 5 minutes at room temperature (RT). The experiment used 77 µM of purified CryA protein. The absorption spectrum was measured under a red safety light. For photometric analysis, the JASCO V-750 (JASCO GmbH) was used. (B) High-performance liquid chromatography of chromophore standards (left) and released chromophores of CryA (right). Monoglutamated 5,10-MTHF was prepared as a standard in 100 % methanol at a concentration of 0.5 mM. Flavine adenine dinucleotide disodium salt (FAD) and riboflavin 5'-monophosphate sodium hydrate (FMN) were used as standards at a concentration of 1 mM in dH_2O. Absorbance was measured at 380 nm. The released CryA cofactors (40 µM concentration) were dissolved in dH_2O, and separation was performed for both the standards and the sample under identical run conditions.

The absorption spectrum of CryA revealed a 470 nm peak, indicative of protein-bound FAD^{ox} as the primary chromophore, and a second, significantly stronger peak

at 380 nm, indicating 5,10-MTHF as the antenna pigment (Navarro *et al.*, 2020). Treatment with blue-light and the reducing agent TCEP (Tris(2-carboxyethyl) phosphine) did not induce an observable photocycle. To verify the bioinformatically predicted chromophores, the protein was denatured, and the chromophores were separated from the protein pellet. Then, the buffer was replaced with dH_2O, and the released chromophores were analyzed via high-performance liquid chromatography (HPLC) **(Fig. 9b)**. The retention times of the CryA cofactors were identical to FAD but showed a small shift to the 5,10-MTHF standard. This observation can be explained by the fact that the 5,10-MTHF found in *E. coli* contains more glutamate residues than the standard form of 5,10-MTHF (Johnson *et al.*, 1988; Navarro *et al.*, 2020). A small third peak with a similar retention time to FMN was detectable, indicating that CryA uses FMN as an additional antenna pigment or relates to an expression artifact in *E. coli* that leads to FMN being loaded in the FAD-binding pocket. In any case, these results verify that FAD and 5,10-MTHF are the main cofactors, and that FMN is possibly a secondary pigment.

2.3 The morphological development of *A. nidulans* is mediated by CryA

Environmental signaling plays a crucial role in the life cycle of *A. nidulans*, determining whether developmental programming switches from vegetative growth to conidia formation or sexual reproduction. Light receptor and how they translate different light signals into molecular responses are especially important for these decisions, since light serves as a warning signal for incoming environmental changes (Yu & Fischer, 2019). Although CryA is predicted to be a photolyase, past studies stated that the blue-light receptor is also involved in regulating the sexual development. Deletion of *cryA* led to overabundance of Hülle cells and higher cleistothecia formation under light conditions, which formed the idea that CryA is a negative regulator of the sexual master regulator Velvet (Bayram *et al.*, 2008a; Bayram *et al.*, 2010).

To further expand on these results, a growth assay experiment was conducted to analyze the influence of light on the phenotype of different *cryA* mutant strains **(Fig. 10a)**. For this experiment, the *A. nidulans* wild-type (WT) was compared to a *cryA* deletion strain, a *cryA* overexpression (*cryA*OE) mutant, and a recomplementation strain of the deletion mutant (+*cryA*). The 2-kb regions upstream and downstream of

the *cryA* open reading frame were combined with the *pyrG* auxotrophy gene and integrated into the pJET1.2 expression vector (pAUL12). The deletion of *cryA* was achieved by homologues recombination via transformation of pAUL12 into the strain sJR2 (sAUL11.2). Recomplementation of the Δ*cryA* strain (sAUL33) was carried out by ectopic integration of *cryA* under the control of the native promoter (pAUL15). CryA overexpression was achieved by placing the *cryA* gene under the control of the inducible *alcA* promoter in the pMCB17apx vector (pAUL5) and ectopically integration in the wild-type strain of *A. nidulans*. The *alcA* promoter is repressed in glucose-containing media, derepressed in glycerol-containing media, and overexpressed in the presence of threonine (Romero *et al.*, 2003). The strains were incubated for seven days on minimal media (MM) with either glucose or threonine under either full darkness or illumination with blue and red light.

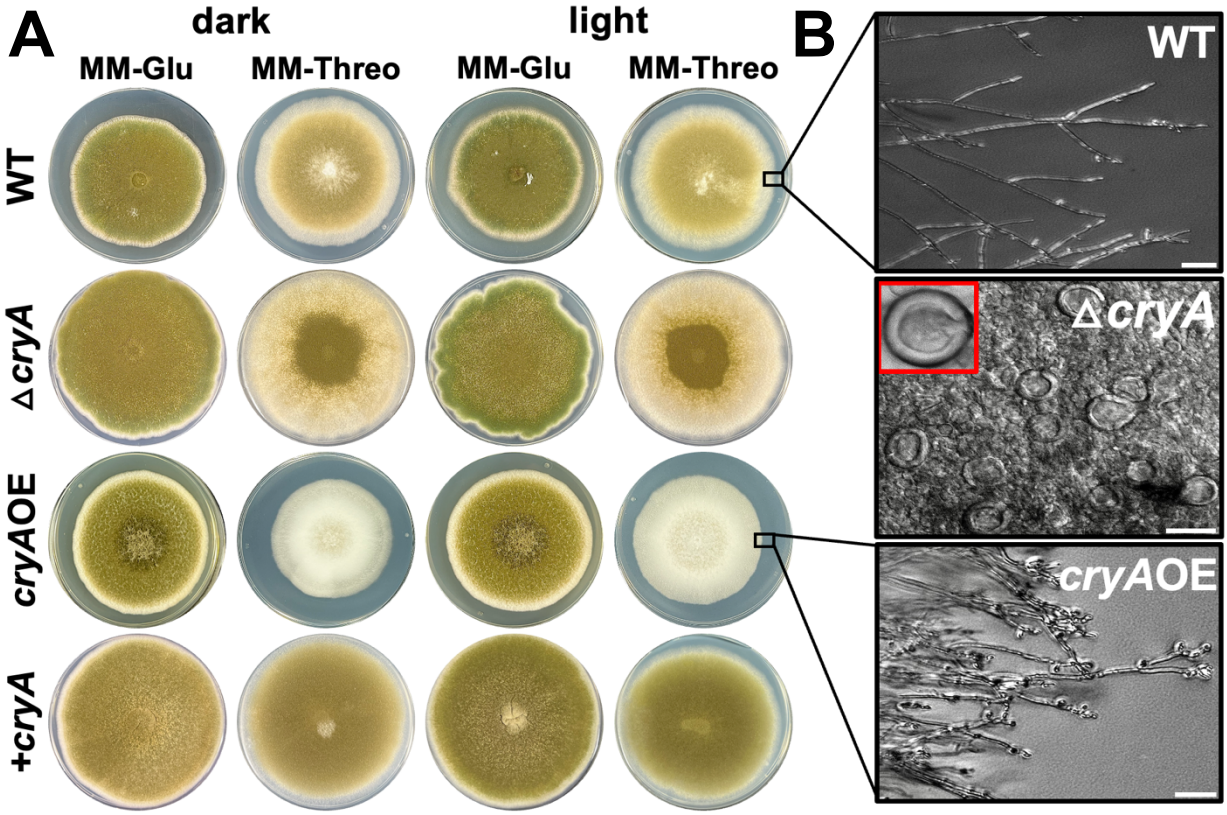

Figure 10: Analysis of the vegetative growth of *cryA* mutants. (A) Comparison of the wild-type strain (WT) with a *cryA* deletion strain (Δ*cryA*), a *cryA* overexpression strain (*cryA*OE), and the Δ*cryA* strain recomplemented with the wild-type gene (+*cryA*). 1,000 spores of the respective strains were inoculated in the center of each plate containing minimal media with either 2 % glucose or 2 % threonine and incubated for 7 days at 37 °C in full darkness (left) or illuminated with blue and red light (200 µmol photons m^{-2} s^{-1}) (right). For each strain eight replicates were analyzed. (B) Microscopic imaging of the wild-type and the *cryA* mutants. The solid plates of the WT strain and the *cryA*OE strain were analyzed. For the Δ*cryA* strain, a liquid culture was inoculated with 10^5 spores and incubated in the dark for three days. Microscopy was performed using a Axio Imager Z1 with the objective W Plan-apochromat 10x/0.5 in the DIC channel. Scale bar represents 100 µm.

The wild-type *A. nidulans* strain and *cryA* mutants exhibited no noticeable phenotypic differences when grown on minimal media containing glucose, where the wild-type strain develops its characteristic green pigmentation. However, cultivating these strains on threonine media revealed significant, light-independent developmental alterations. While the wild-type strain showed a slight loss of pigmentation due to fewer conidia on threonine, overexpressing *cryA* triggered severe growth defects. This overexpression completely abolishes the formation of normal conidiophores and conidia, resulting in stark white colonies. Interestingly, this effect was not light-dependent, suggesting a dark function of CryA. Similarly, deleting *cryA* impaired development, irrespective of the light conditions, causing a reduction in conidia, particularly on threonine media. These defects in the deletion mutant were fully rescued by reintroducing a wild-type copy of the gene. Those phenotypical changes were also visible under the microscope **(Fig. 10b)**. The overexpressing strain displayed hyperbranching hyphae terminating in abnormal, conidia-like structures, indicating the disruption of vegetative growth. While no visible changes were observed in the vegetative hyphae of the Δ*cryA* strain on solid media, high numbers of Hülle cells were observed in liquid culture conditions. These results suggest that CryA is involved in regulating development in *A. nidulans*, and that changes in the protein levels result in severe growth deficiencies.

Because threonine as the carbon source and minimal media as a growth medium are not ideal for studying developmental changes in *A. nidulans*, the experiment was repeated using glycerol to derepress the *alcA* promoter. The strains were incubated in darkness on complete media (CM) under low-oxygen conditions or grown during illumination with either blue or red light, for seven days, in order to study the effects on cleistothecia abundance **(Fig. 11a)**. Similarly to previous observations, the overexpression strain displayed a white phenotype without visible pigmentation on glycerol-containing media under low oxygen conditions. Interestingly, access to atmospheric oxygen and persistent illumination suppressed this effect, indicating that other light receptors, such as phytochrome or white-collar proteins, can counteract the effects of CryA. The Δ*cryA* strain exhibited stark yellow pigmentation under all conditions, indicating the formation of large quantities of cleistothecia. This alteration was partially inhibited under red light, which may be related to phytochrome functions that repress the sexual cycle. The consequences on the phenotype of the Δ*cryA* strain were partially reversed in the complementation strain.

Microscopy revealed that the overexpression strain did not form any cleistothecia, irrespective of the growth conditions, while the Δ*cryA* had a high abundance of cleistothecia **(Fig. 11b)**. This effect was quantified for all strains grown in darkness or under blue- or red-light conditions **(Fig. 11c)**. The quantification revealed that cleistothecia numbers in the Δ*cryA* strain was significantly increased independently of light in comparison to the WT. This effect was partially restored in the +*cryA* recomplementation strain. In contrast, overexpression of *cryA* led to full abolishment of cleistothecia formation. In conclusion, although CryA is classified as a photolyase, these results further prove that it fulfills the role of a cryptochrome by regulating developmental processes in *A. nidulans.*

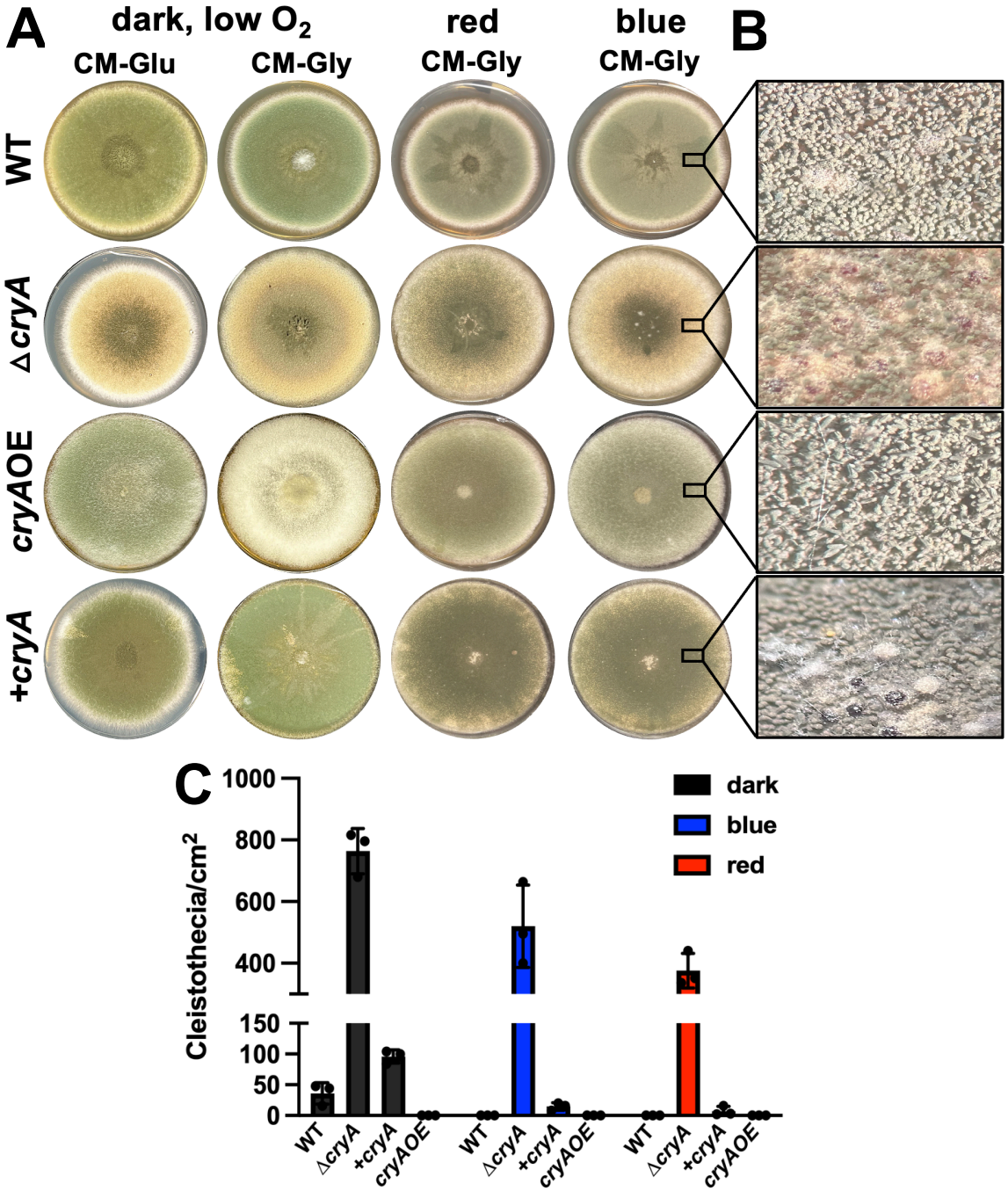

Figure 11: Analysis of the growth and reproduction of *cryA* mutants. (A) Growth assay of wild-type, the Δ*cryA* strain, the *cryA*OE strain, and the re-complementation strain +*cryA* on CM-media with different growth conditions. 10^5 spores were inoculated on complete media with 1 % glucose (CM-Glu) or 1 % glycerol (CM-Gly) and grown for 7 days at 37 °C in full darkness and enclosed with parafilm to ensure low oxygen conditions or illuminated with red or blue light (200 µmol photons m^{-2} s^{-1}) and atmospheric oxygen levels. (B) Microscopy of developed cleistothecia of the wild-type and the *cryA* mutants. Microscopy was performed using the Stemi DV4. (C) Cleistothecia count of the *cryA* mutants under different light conditions. For each strain and condition, biological triplicates and technical quadruplicates were used. Cleistothecia were counted in a 3 cm radius around the center of the plate, and the counting spots were randomized.

2.4 CryA inhibits the production of secondary metabolites

Light does not only impact the developmental decisions of *A. nidulans*, but it is also crucial to produce metabolites. There are several comparative studies about the effect of light on the expression of genes involved in secondary metabolite accumulation (Keller *et al.*, 2005; Bayram *et al.*, 2008b; Röhrig *et al.*, 2013; Gerke & Braus, 2014; Bayram *et al.*, 2016; Frawley *et al.*, 2020; Bastakis *et al.*, 2025). The trimeric velvet complex is crucial for the switch to sexual development and secondary metabolite synthesis. The complex is suppressed by light and subsequently photoreceptor activity which leads to a significant lower secondary metabolites such as sterigmatocystin and other pigments (Bayram *et al.*, 2008b; Bayram *et al.*, 2016). Since CryA is proposed as a negative regulator of VeA, it may play a role in regulating secondary metabolite production. To test this hypothesis, the wild-type strain and the *cryA* deletion strain were grown in the dark or under constant illumination for one week, as were the +*cryA* recomplementation strain, and the *cryA* overexpression *cryA*OE strain. The extracted metabolites were analyzed via thin-layer chromatography (TLC) (**Fig. 12)**. Experimental analysis revealed several additional bands in the Δ*cryA* strain compared to the wild-type, signaling the emergence of new metabolites upon the deletion of *cryA*. These bands were significantly more pronounced in samples grown in the dark. Notably, these metabolic changes were fully reversed in the *cryA* recomplementation strain, which mirrored the WT profile. Conversely, the *cryA* overexpression strain exhibited a visible reduction in total metabolites.

The influence of CryA on the secondary metabolite profile was even more striking when observing the crude extracts directly. The dark-grown extract displayed a distinct brownish hue, while the light-grown sample turned a deep green, indicating the synthesis of additional pigments. This pigment production was entirely abolished in the overexpression strain, which yielded an almost clear liquid. Collectively, these results demonstrate that CryA acts as a repressor of secondary metabolism, with its inhibitory effect being particularly dominant in the dark.

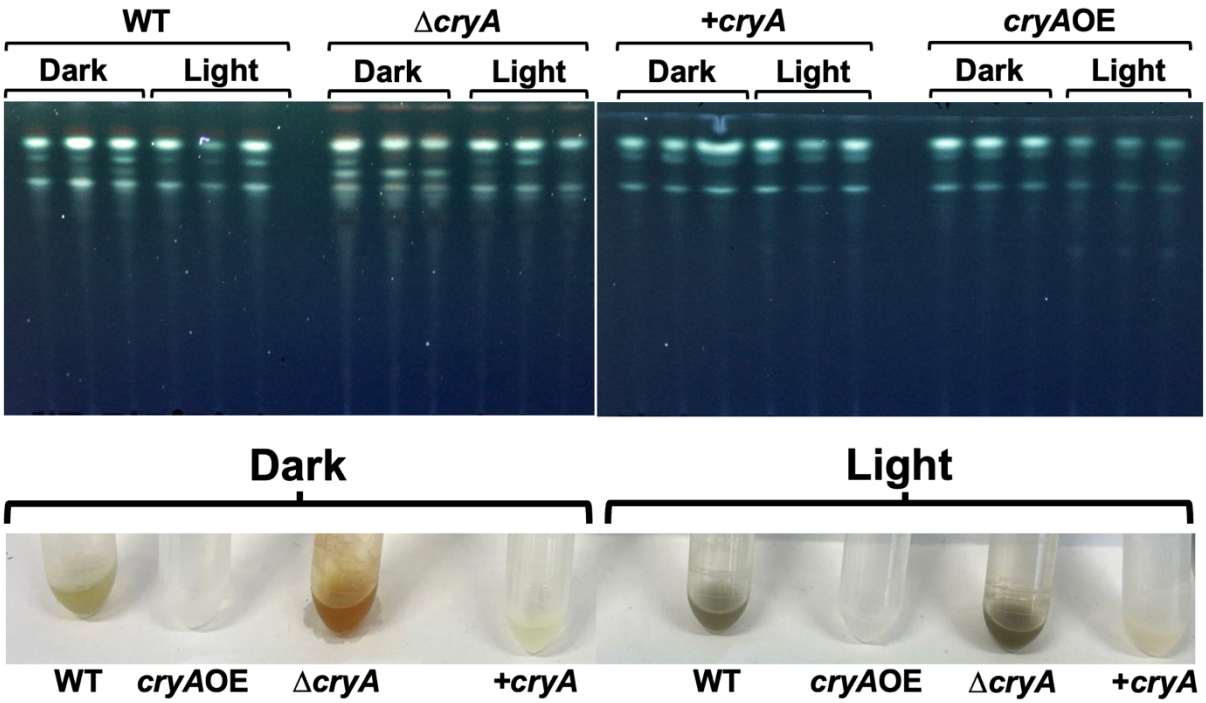

Figure 12: Analysis of the secondary metabolite profile in *cryA* mutants. Thin-layer chromatography of the WT, the Δ*cryA* strain, the *cryA*OE strain, and the recomplementation strain +*cryA*. The strains were grown as triplicates for 7 days either in complete darkness or illuminated with blue and red light (200 µmol m^{-2} s^{-1}) before harvesting. The secondary metabolites were extracted using toluene precipitation. TLC was performed for 25 minutes, and the plate was then illuminated with UV light (365 nm) to visualize the samples' fluorescence. The extracted samples used for TLC are visualized in the bottom part.

2.5 CryA is a nuclear protein

Overexpression or deletion of cryA resulted in severe growth deficiencies and developmental phenotypes. These results suggest that CryA is a regulatory protein that controls developmental processes, such as asexual conidiation and sexual reproduction, through either DNA modifications and/or protein-protein interactions. Most of these developmental systems are closely regulated in the nucleus by several important, interconnected master regulators, such as Velvet A or Stunted A (StuA) (Miller *et al.*, 1992; Vargas-Pérez *et al.*, 2007; Bayram *et al.*, 2008b).

To test, where CryA localizes in *A. nidulans* the protein was tagged N-terminally with GFP under the control of the *alcA* promoter to visualize it *in vivo* (pAUL6) and transformed ectopically in *A. nidulans* wild-type (sAUL3) **(Fig. 13a)**. HOECHST 33342 (ThermoFisher Scientific) was used for nuclear staining. Fluorescence microscopy revealed that CryA localizes exclusively in the nucleus of vegetative hyphae. Changes in the growth conditions, such as different carbon sources, temperature, or light quality, did not influence the localization (Landmark, 2022). Because CryA is involved in light-regulated development, the significance of its localization in conidia under different

light conditions was additionally investigated **(Fig. 13b)**. The nuclear localization sequence (NLS) of StuA, which was tagged with DsRed, was used for nuclear staining (sAUL38) (Toews *et al.*, 2004). CryA only localized in the nucleus of conidia, regardless of light.

In conclusion, the regulatory effect of CryA is connected to nuclear processes and appears to be not dependent on blue-light or the developmental stage.

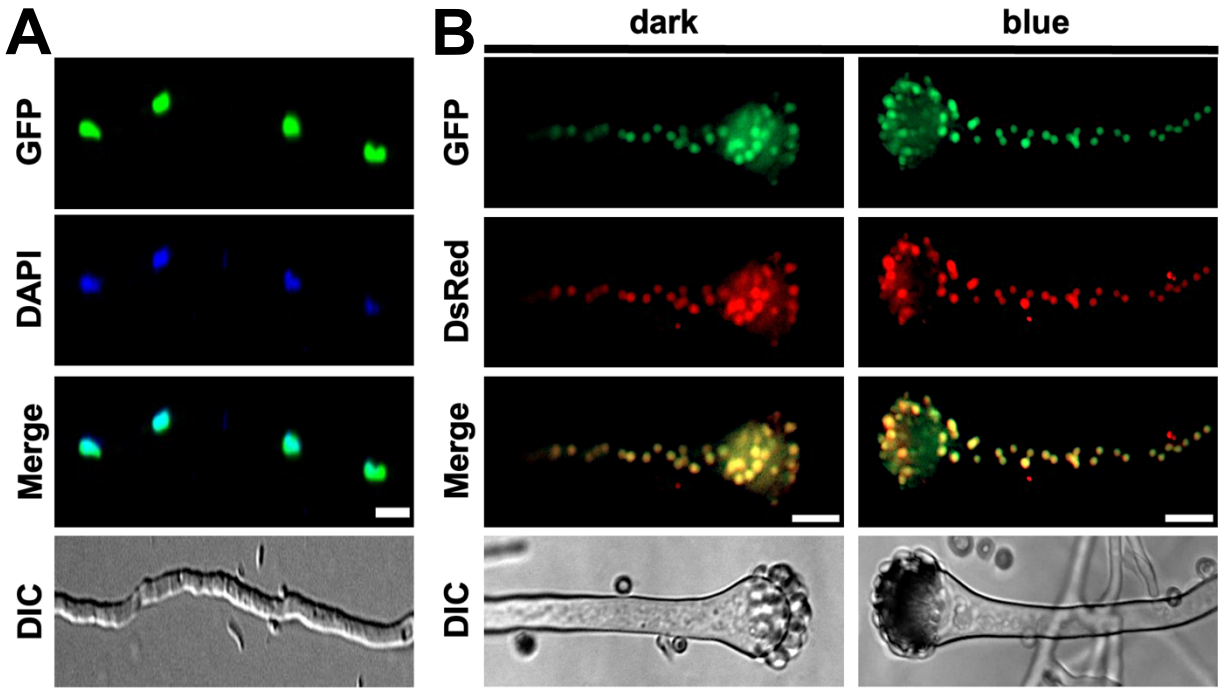

Figure 13: Microscopic analysis of the intracellular localization of CryA. (A) CryA was fused N-terminally to GFP under the control of the *alcA* promoter. Spores were incubated overnight at 25 °C in minimal media with 2 % glycerol instead of glucose to induce the promoter. Nuclei were stained with HOECHST. The scale bar represents 5 µm. Microscopy was performed using the Axio Imager Z1 with the objective W Plan-apochromat 60x/0.5 with the indicated fluorescence channels. (B) Localization of CryA in conidia with different light conditions. CryA was fused N-terminally to GFP under the control of the *alcA* promoter. Spores were incubated overnight at 37 °C in solid minimal media with 2 % threonine instead of glucose to induce the promoter. Nuclei were visualized with the NLS of *stuA* fused to DsRed. Microscopy was performed using the Axio Imager Z1 with the objective W Plan-apochromat 10x/0.5 with the indicated fluorescence channels. The scale bar represents 10 µm.

2.6 The early light response in *A. nidulans* is inhibited by CryA

A. nidulans uses photoreceptors to detect environmental changes and adapt accordingly. This systemic response is defined by an early light response, a burst of gene expression activating subsequent regulators to initiate developmental changes. For instance, transcription factors involved in photoadaptation, such as the asexual master regulator BrlA, the *fluffy* protein family FlbA-FlbE, and the conidiation factor ConJ, regulate the switch from vegetative growth to asexual conidiation when exposed to light for an extended period (Corrochano *et al.*, 1995; Wieser & Adams, 1995; Ruger-

Herreros *et al.*, 2011). Expression analysis of *A. nidulans* revealed that over 1,000 genes are differentially expressed after exposure to light and the activity of the red-light receptor FphA. Interestingly, the expression of *cryA* appeared to be under the control of FphA and SakA, indicating that CryA accumulates in the nucleus after light exposure (Yu *et al.*, 2021).

To confirm, whether CryA expression is light dependent, a quantitative real time PCR (qRT-PCR) was performed **(Fig. 14a)**. For this experiment, mycelia of the wild-type strain of *A. nidulans* were either kept in complete darkness or exposed to 15 minutes of blue and red light prior to harvesting and extracting the RNA. The expression analysis confirmed that the transcript levels of *cryA* are increased after light treatment. This signifies the connection between CryA function and the light response. To observe the impact of CryA on the expression profiles of various light-dependent genes, RNA was extracted from the different *cryA* mutant strains and qRT-PCR was performed (**Fig. 14b)**. The genes *ccgA* and *ccgB* (clock-controlled gene), and *AN11314* were selected since they are strongly upregulated after short-term light treatment (Yu *et al.*, 2021). Meanwhile, *conJ*, *brlA*, and *flbB* were chosen to study alterations in the asexual development (Ruger-Herreros *et al.*, 2011).

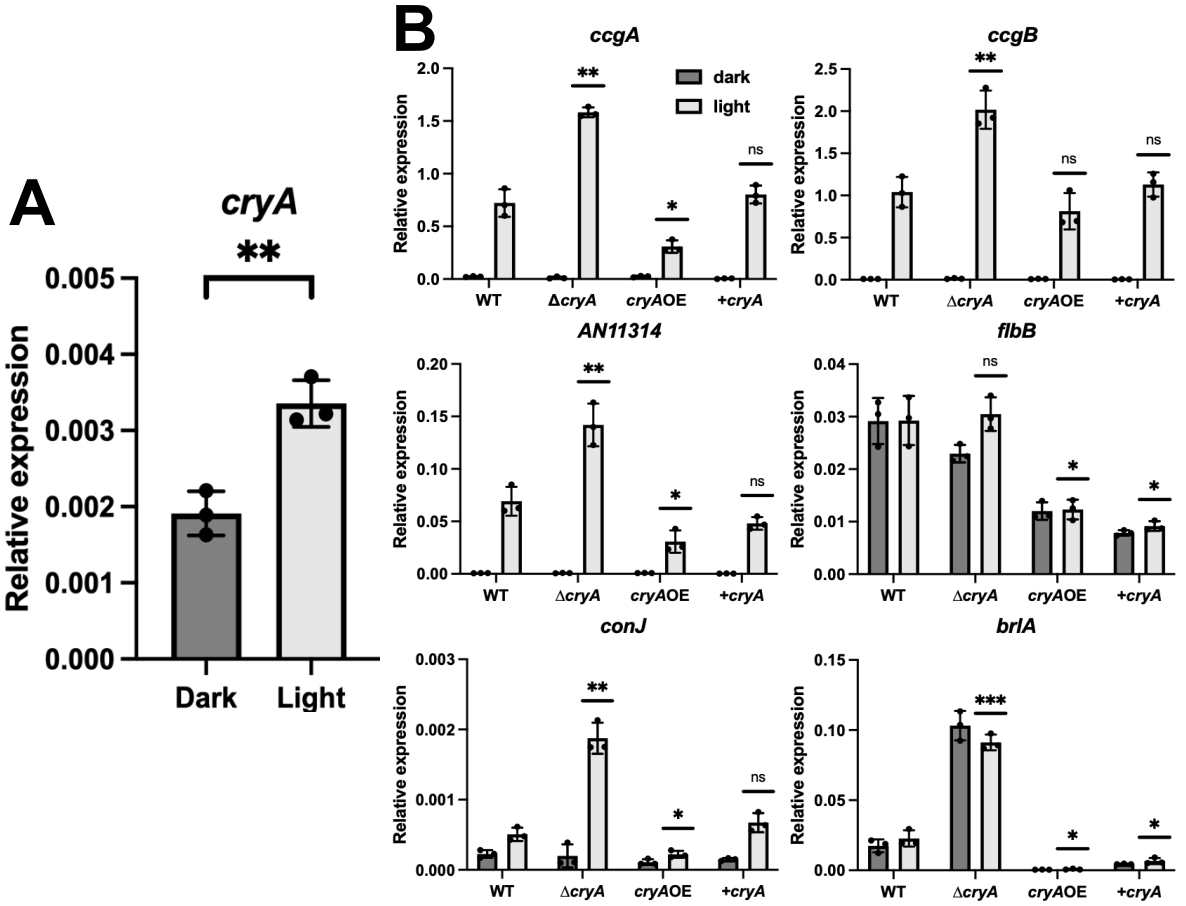

Figure 14: Expression analysis of *cryA* and light dependent genes. (A) Analysis of the *cryA*-expression level in darkness and after light treatment. $1.5*10^8$ spores of WT strain were incubated for 16 h in 10 ml minimal media at 37 °C in the dark. Light samples were illuminated for 15 minutes with blue and red light (200 µmol photons m^{-2} s^{-1}) simultaneously before harvesting the mycelia under green safety light. For the histone 2b (*h2b*) gene was used as housekeeping gene for normalizing the expression. Error bars represent the standard deviation of three biological and two technical replicates. For statistical analysis, an unpaired, parametric two-tailed Student's t-test was performed, using a 95 % confidence interval, **p≤0.01. Dots represent each individual biological replicate. (B) Expression profile analysis of early light responsive genes and transcriptions factors involved in asexual development in in wild type compared to the Δ*cryA* strain, the complementation strain +*cryA*, and a *cryA*-overexpression strain. $1.5*10^8$ spores of the respective strains were incubated for 16 h in 10 ml minimal media with 2 % threonine at 37 °C in the dark. Light-treated samples were illuminated for 15 minutes with blue- and red light (200 µmol photons m^{-2} s^{-1}) simultaneously before harvesting the mycelia under green safety light. For the qRT-PCR *h2b* was used as housekeeping gene for normalization. Error bars represent the standard deviation of three biological and two technical replicates. For statistical analysis, an unpaired, parametric two-tailed Student's t-test was performed between the wild-type and the respective mutant strains using a 95 % confidence interval, ^{ns}p>0.05, *p≤0.05, **p≤0.01, ***p≤0.001. Dots represent individual biological replicates.

Deletion of *cryA* resulted in a significant upregulation of most of the analyzed genes compared to the wild-type after light treatment. Complementation of the *cryA* deletion restored the light activation comparable to the WT. In contrast, the overexpression mutant exhibited significant downregulation of all studied genes. This effect was independent of light for the initiators of asexual development, *brlA* and *flbB*, which explains the previously observed phenotype of complete abolishment of conidia formation. These findings suggest that nuclear CryA levels increase after light treatment, after which CryA inhibits transcription of light-dependent genes and prevents the switch from vegetative growth to asexual conidiation.

To follow up on these results, it appeared of interest to see whether CryA also influences the late light response. After the initial burst of gene expression *A. nidulans* enters a phenomenon called photoadaptation, which is defined by a downregulation of light controlled genes after prolonged exposure. This allows the fungus to fine-tune the light response under varying light conditions (Ruger-Herreros *et al.*, 2011). The previous expression analysis only focused on the effect of CryA on light dependent genes after 15 minutes of treatment. To expand on this, the WT, together with the Δ*cryA* strain and the *cryA*OE strain, were illuminated for 60 or 120 minutes before harvesting the mycelia, extracting the RNA, and performing qRT-PCR for *ccgA* and *brlA* **(Fig. 15)**. The photoadaptation assay uncovered that *ccgA* expression in the WT decreases significantly after prolonged exposure. In contrast, *brlA* gene expression increases with longer illumination times, indicating the switch from vegetative growth to asexual conidiation. However, the expression of both genes decreased significantly after prolonged illumination compared to the WT in the Δ*cryA* strain. This suggests that CryA only affects the early light response phase and is not necessary for late adaptation.

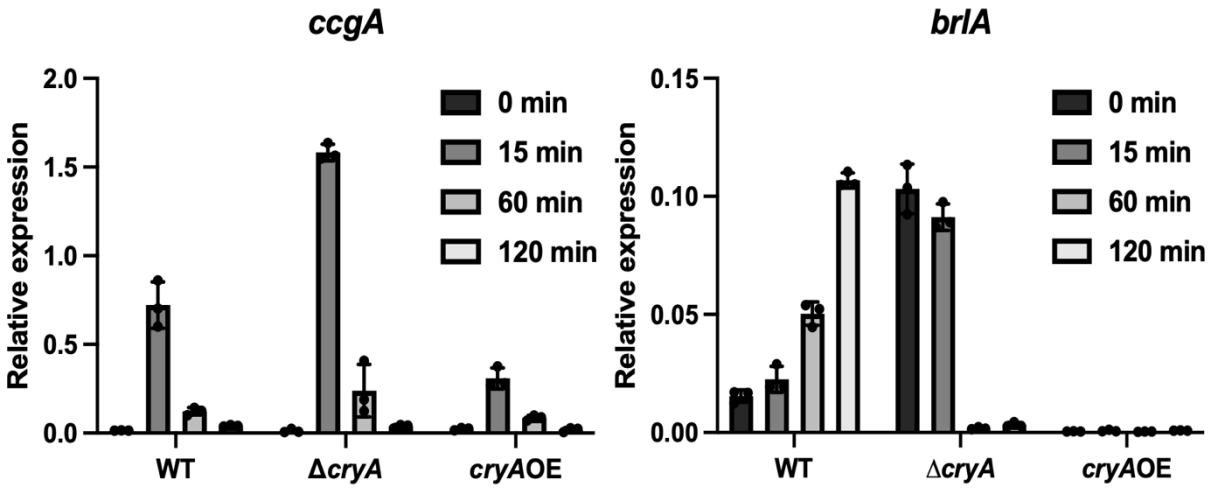

Figure 15: Photoadaptation assay of the Δ*cryA* strain compared to the WT and the *cryA*OE strain. $1.5*10^8$ spores of the respective strains were incubated for 16 h in 10 ml minimal media supplemented with 2 % threonine at 37 °C in the dark or illuminated for the indicated time with blue and red light (200 µmol photons m^{-2} s^{-1}) simultaneously before harvesting the mycelia under green safety light. For the qRT-PCR the *h2b* gene was used as housekeeping gene for normalizing the expression. Error bars represent the standard deviation of three biological and two technical replicates. Dots represent each individual biological replicate.

2.7 CryA interacts with the red-light receptor FphA

There is only one example of a fungal cryptochrome acting as a negative regulator of the light response. In *N. crassa*, the WCC is solely responsible for activating the light response. This activity is somewhat negatively regulated by the CRY-DASH protein CRY-1, together with the phytochrome PHY-2 and the opsin NOP-1 (Olmedo *et al.*, 2010; Olmedo *et al.*, 2013). In *A. nidulans*, the phytochrome FphA acts as the main photoreceptor by activating the HOG-pathway to stimulate AtfA function and promoting histone acetylation of light dependent genes (Hedtke *et al.*, 2015; Yu *et al.*, 2016; Yu *et al.*, 2021). Therefore, it seems likely that the negative effect of CryA on the light response in *A. nidulans* is due to the inhibition of phytochrome function through genetic manipulation or direct protein-protein interactions.

To discriminate between those two possibilities AlphaFold 3 was utilized to test whether CryA and FphA can interact **(Fig. 16a)**. FphA was modelled as a homodimer, and only the PAS, GAF, PHY domains without the N-terminal extension (195-753 aa) were used for the interaction analysis to improve visual quality. AlphaFold predicted with a low predicted template modelling (pTM) score of 0.44 and an interface predicted template modelling (ipTM) score of 0.33 that the interaction between CryA and FphA is localized around the PAS and GAF domain. Repeating the interaction prediction with full length phytochrome did not change the interaction site with CryA (results not shown). The low interaction scores are explained by FphA's generally low pLDDT value

(roughly 60-70), which results in lower confidence scores overall **(Fig. 16b)** (Evans *et al.*, 2021). Because the AlphaFold prediction was inconclusive, a BiFC (bimolecular fluorescence complementation) assay was performed **(Fig. 17a)**. This assay is an imaging technique that visualizes protein-protein interaction in living cells. It involves splitting a fluorescent protein into two non-fluorescent fragments. One fragment is fused to each of the two candidate proteins. If the proteins interact, the fragments come into close proximity and spontaneously reassemble into a functional, glowing fluorophore. This method is valuable for determining the precise cellular location of an interaction, but the interaction itself is irreversible (Lai & Chiang, 2013).

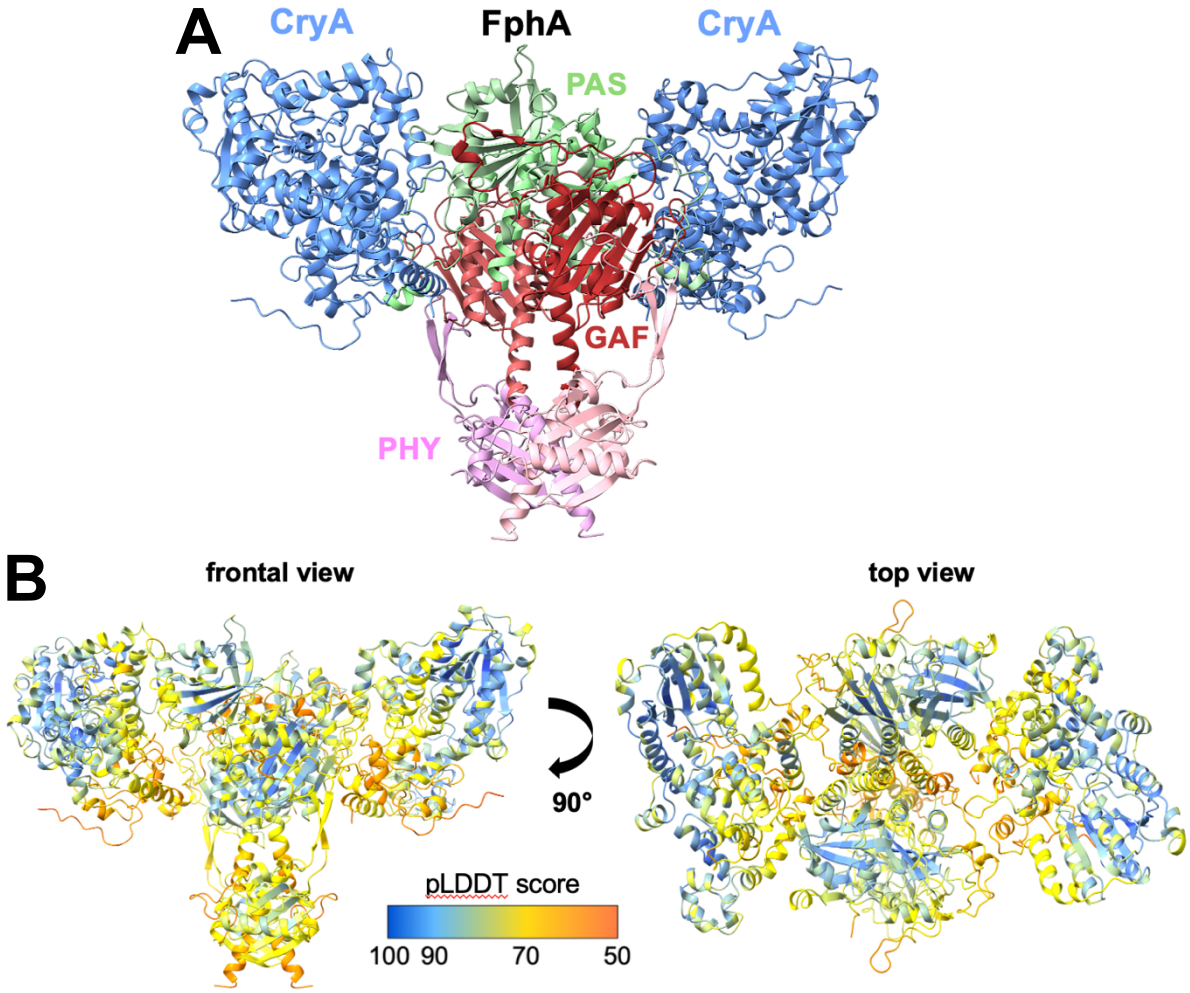

Figure 16: AlphaFold prediction of the interaction between CryA and FphA. (A) AlphaFold3 was used to predict the interaction between the phytochrome dimer and CryA (light blue). To improve visibility, only the conserved PAS (green), GAF (red), and PHY (pink) domains of the photosensory domain of phytochrome, excluding the N-terminal extension, are displayed. (B) Interaction between CryA and FphA with overlaid pLDDT values from two viewing angles.

Both CryA (pAUL3 & pAUL4) and FphA (pJP4 & pJP5) were N-terminally tagged with either half of the yellow fluorescent protein (YFP) under the control of the *alcA*

promoter and introduced together *in vivo* (sAUL34 and sAUL35). Fluorescence microscopy revealed that the proteins interact together in the nucleus. As an additional control, the WC-1 homologue LreA was N-terminally fused to YFPN under the control of the *alcA* promoter (pALBL9) and transformed *in vivo* (sAUL39) to perform the BiFC assay **(Fig. 17b)**. The interaction analysis did not result in any detectable signal.

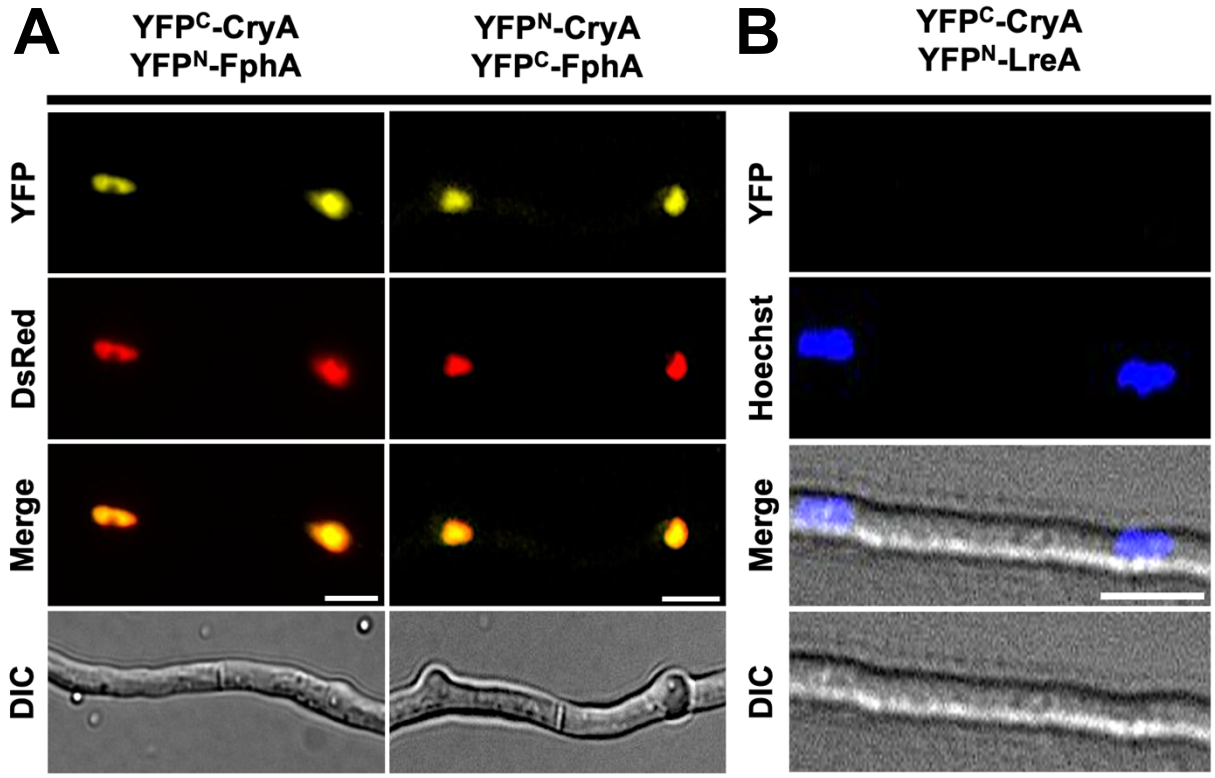

Figure 17: BiFC assay between CryA and the photoreceptors FphA and LreA. (A) CryA and FphA were fused N-terminally to either half of YFP under the control of the *alcA* promoter. Spores were incubated overnight at 25 °C in minimal media with 2 % threonine instead of glucose to induce the promoter. The nucleus was visualized using the NLS of *stuA* fused to DsRed. The scale bar represents 5 µm. (B) CryA and LreA were fused N-terminally to either half of YFP under the control of the *alcA* promoter. Spores were incubated overnight at 25 °C in minimal media with 2 % threonine instead of glucose to induce the promoter. The nuclei were stained using HOECHST 33342. The scale bar represents 5 µm. Microscopy was performed using the Axio Imager Z1 with the objective W Plan-apochromat 60x/0.5 with the indicated fluorescence channels.

For confirming the interaction between CryA and FphA, the biolayer interferometry (BLI) assay was selected as an *in vitro* method**.** This optical based method analyzes the binding kinetics of two proteins by measuring the interference pattern of white light which is reflected by a biolayer of two interacting proteins. For this experiment, one protein serves as bait protein and is immobilized on a biosensor via antibody/antigen interaction. The bound protein is then submerged in varying concentrations of the second interaction partner, the analyte. Depending on the thickness of the biolayer and the measurable kinetics of the association and dissociation of the second protein, an interaction constant between the two interaction

partners can be measured (Sultana & Lee, 2015). To perform the BLI-assay both proteins had to be purified. For CryA, the expression vector pAUL12 was used. FphA was introduced into the pASK-iba3plus vector (IBA Lifescience), fused to a C-terminal strep-tag® and expressed heterologously in *E. coli* BL21 DE3 (Brandt *et al.*, 2008). For the expression of the chromophore biliverdin, which is not naturally produced in *E. coli*, the heme oxygenase BphO from *Pseudomonas aeruginosa* was co-transformed and expressed (Yu *et al.*, 2019). Both proteins were purified and success of the extraction was verified via SDS-PAGE **(Fig. 18a)**. CryA has an apparent protein mass of 65 kilodaltons (kDa), while FphA has an apparent size of 140 kDa. For both proteins, a strong band at the expected size was detectable. Since purification of FphA resulted in a high number of contaminants, a size exclusion chromatography (SEC) was performed to remove contaminations and only purify functional FphA dimer. SEC is a technique used to separate proteins based on their size and conformation. Bigger proteins interact less with the SEC column's matrix, resulting in a lower elution volume. Smaller proteins can enter the matrix's pores, which increases their elution volume. These elution volumes can be compared with a calibration run of the elution volume of known protein standards to determine the apparent protein mass **(Fig. 18b)**.

Size exclusion chromatography of FphA produced three major peaks, the smallest of which had an apparent protein mass of 370 kDa **(Fig. 18c)**. Because both the protein size and conformation are critical for the elution volume, the third maximum was validated via absorption spectroscopy to confirm the purification of functional phytochrome dimer **(Fig. 18d)**. The sample was measured after being kept in the dark or illuminated with red light (680 nm) for 2 minutes to induce a conformational shift to the P_{fr} form. Spectroscopic measurements revealed the functional shift from the P_r to P_{fr} form of FphA.

Next, the BLI assay was performed **(Fig. 19a)**. For this, both proteins were diluted in BLI buffer, and CryA was used as the bait protein. The functional dimer of FphA was diluted in increasing concentrations and used as the analyte. Prior to measurements, FphA was illuminated with white light. The BLI assay revealed an interaction constant (K_d) of 0.0682 µM, indicating high affinity between CryA and FphA and confirming their physical interaction (Frenzel & Willbold, 2014; Kamat & Rafique, 2017; Jug *et al.*, 2024). Since the interaction between FphA and CryA was predicted to occur at the chromophore binding site of FphA, it is reasonable to assume that CryA inhibits chromophore function.

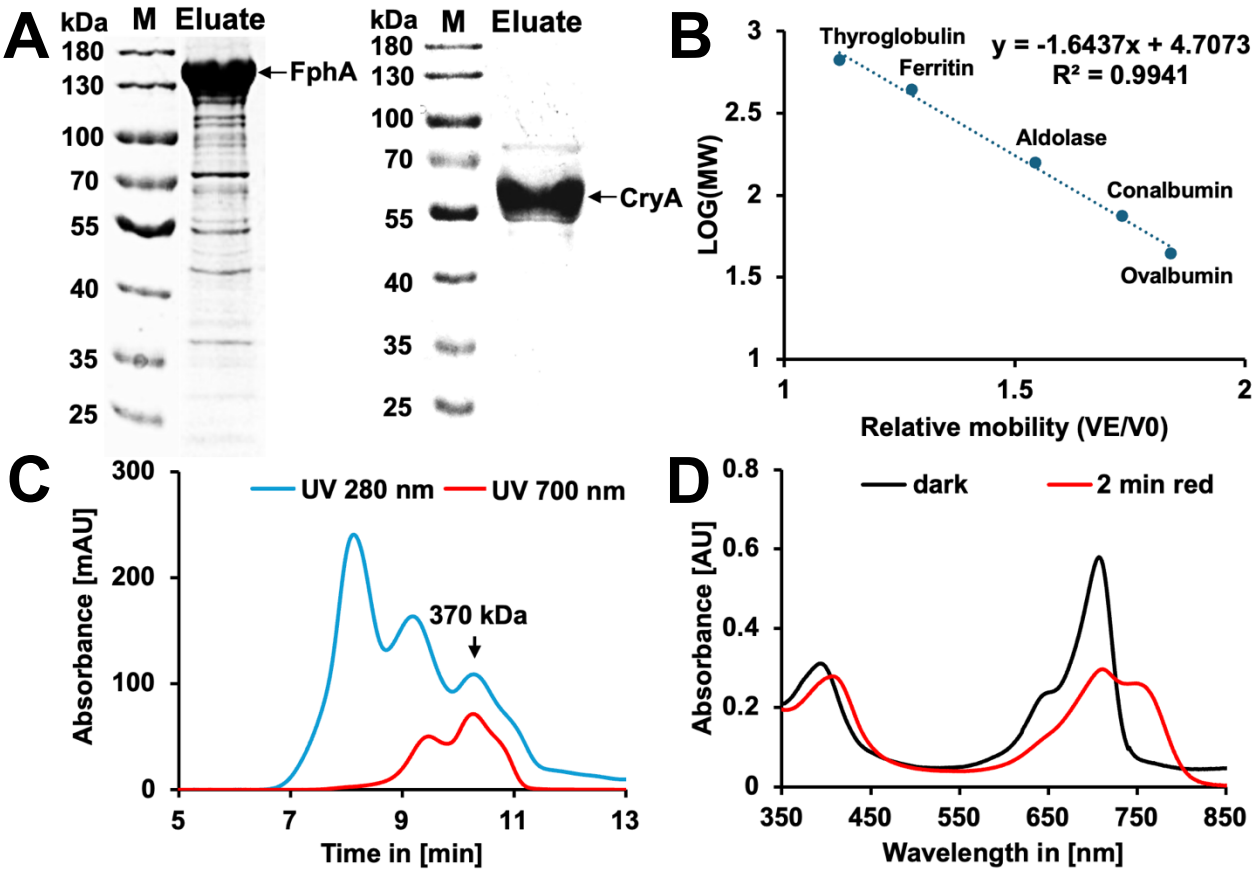

Figure 18: Heterologous expression of CryA and FphA. (A) SDS-PAGE of heterologously expressed and purified FphA (left) and CryA (right) from *E. coli*. PageRuler™ Prestained Protein Ladder 180 kDa was used as protein standard. (B) Calibration of the Superdex 10-300 GL column (Cytiva) with known protein standards (blue) was used to identify the purified phytochrome dimer after SEC. Standards were Thyroglobulin (669 kDa), Ferritin (440 kDa), Aldolase (158 kDa), Conalbumin (75 kDa), and Ovalbumin (44 kDa). (C) Size exclusion chromatography of FphA after purification. UV light of 280 nm (light blue) and 700 nm (red) was used to detect functional FphA as dimer (size with tag: ~284 kDa, calculated size after SEC: ~370 kDa). (D) Spectroscopic analysis of FphA dimer (14 µM) after SEC. The sample was kept in the dark (black line) or illuminated for 2 min with red light (red line) before the measurement.

To test this theory, the FphA^{C195A} cysteine mutant was generated, as Cys195 is critical for biliverdin binding (pAUL103) (Brandt *et al.*, 2008). The FphA^{C195A} protein was purified from *E. coli*, as was done previously for the wild-type FphA protein. Then, the BLI assay was repeated with CryA as the bait and FphA^{C195A} as the analyte **(Fig. 19b)**. Without bound biliverdin, the interaction constant K_d dropped significantly to 0.345 mM, suggesting that the chromophore of FphA is relevant for protein interaction with CryA.

In conclusion, protein-protein interaction experiments confirmed that CryA and FphA interact physically in the nucleus, and functional FphA dimer with the bound chromophore is crucial for the interaction.

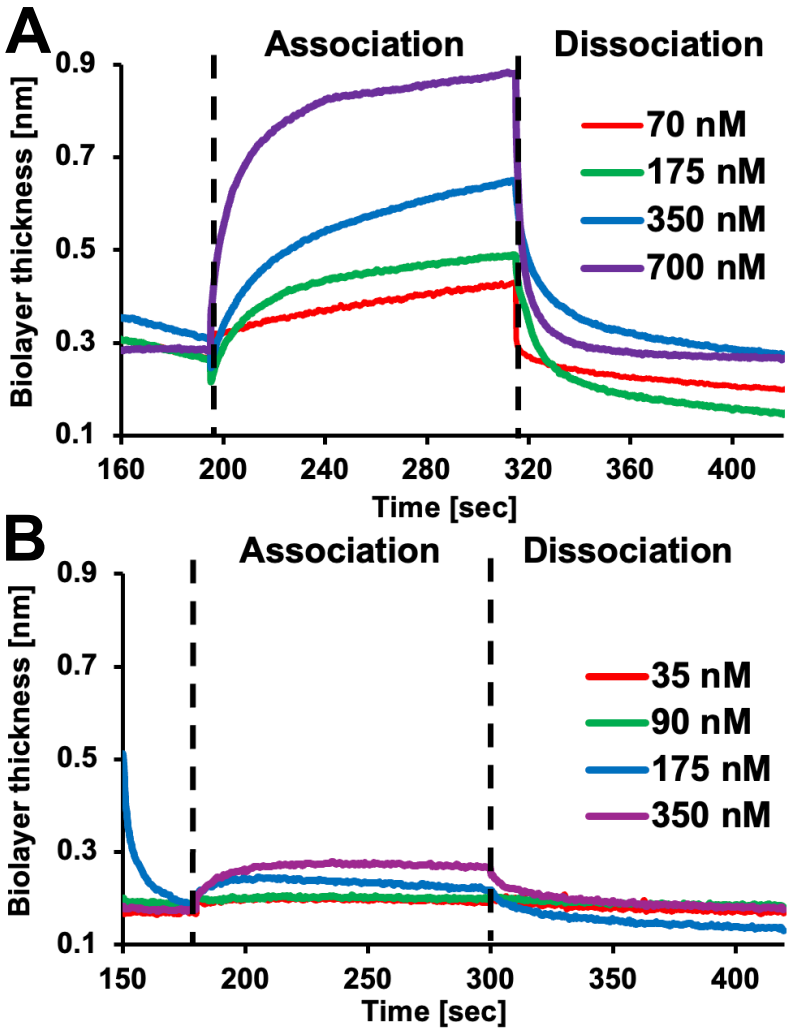

Figure 19: BLI assay of CryA with FphA and FphA^{C195A}. (A) Biolayer interferometry analysis with purified CryA with 6xHis-tag and FphA with Strep-tag. CryA was immobilized as bait with a concentration of 30 nM on a Nickel-nitrilotriacetic acid (NTA) biosensor. Phytochrome was prepared at the indicated concentrations, and association/dissociation kinetics were recorded to calculate the Kd value with the BLI software of the system. All protein solutions were made up in BLI buffer. The individual steps were all carried out in 0.5 ml tubes with the following settings: 30 s baseline step in BLI buffer, 120 s loading step of CryA, 45 s second baseline step in BLI buffer, 120 s association step with the indicated FphA concentration, 120 s dissociation step in BLI buffer. For the analysis, a global fit with a step correction for the start of the association and dissociation were selected. As reference BLI buffer without phytochrome was used. (B) Biolayer interferometry analysis with purified CryA with 6xHis-tag and FphA^{C195A} with Strep-tag. CryA was immobilized as bait with a concentration of 30 nM on a Nickel-nitrilotriacetic acid (NTA) biosensor. Phytochrome was prepared at the indicated concentrations, and association/dissociation kinetics were recorded to calculate the K_d value with the BLI software of the system. All protein solutions were made up in BLI buffer. The individual steps were all carried out in 0.5 ml tubes with the following settings: 30 s baseline step in BLI buffer, 120 s loading step of CryA, 30 s second baseline step in BLI buffer, 120 s association step with the indicated FphA^{C195A} concentration, 120 s dissociation step in BLI buffer. For the analysis, a global fit with a step correction for the start of the association and dissociation were selected. As reference BLI buffer without phytochrome was used.

2.8 Histone modification of FphA dependent genes is inhibited by CryA

FphA is the primary component of light-dependent gene activation in *A. nidulans* (Yu et al., 2021). Besides triggering the HOG-pathway to modulate AtfA activity, FphA can also enter the nucleus to modify histone 3 acetylation via recruiting the histone

acetyltransferases AdaB and GcnE (Hedtke *et al.*, 2015; Yu *et al.*, 2020). Because CryA and FphA appear to interact exclusively in the nucleus, one might ask whether CryA prevents histone modifications of light- and, therefore, FphA-dependent genes. To test this hypothesis, a chromatin immunoprecipitation (ChIP) experiment with *A. nidulans* wild-type as control and the Δ*cryA* strain was carried out **(Fig. 20)**. As a control, the abundance of histone 3 (H3) was compared to the abundance of acetylated H3K9, using *actA* as the control gene and *ccgA* as the target gene of FphA. For this experiment, antibodies against H3 (Abcam) and acetylated H3K9 (Merck Millipore) were used for immunoprecipitation, and the abundance of precipitated chromatin was compared to the input control. In the *cryA* deletion strain the abundance of acetylated H3K9 of *ccgA* was enriched significantly in comparison to the WT, signifying that CryA prevents histone modification of FphA through direct nuclear interaction.

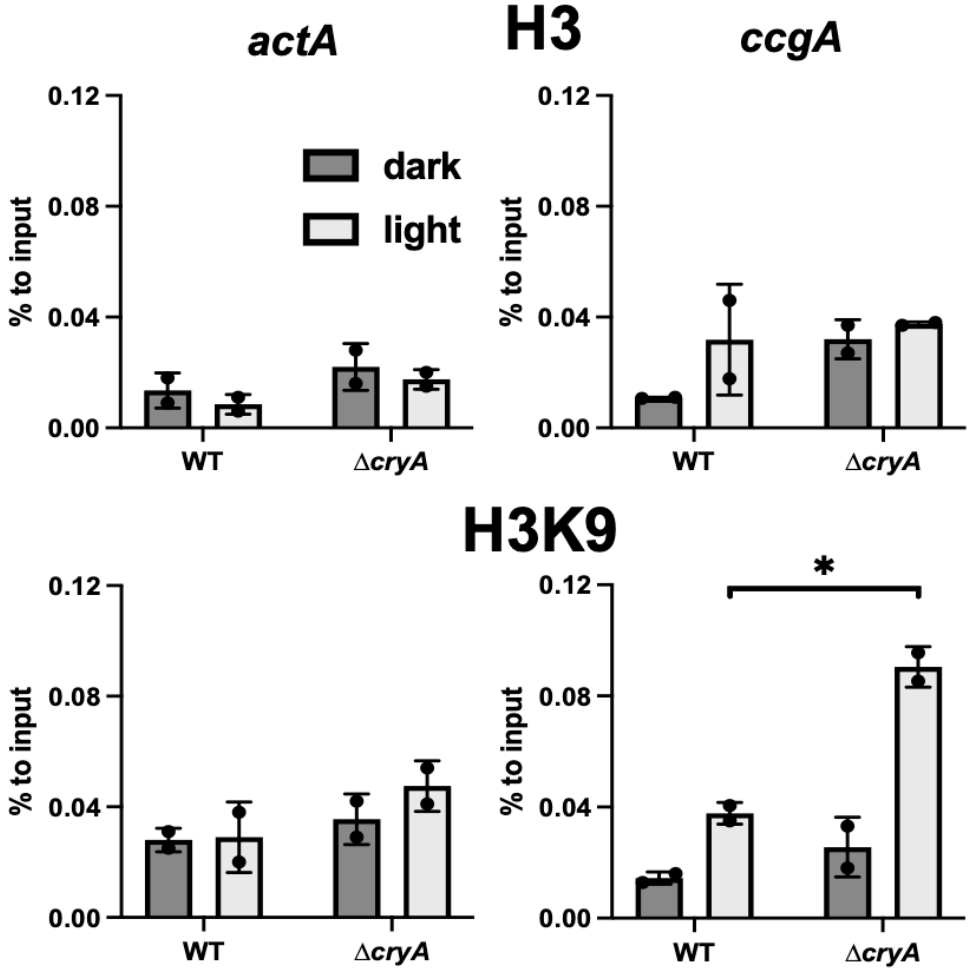

Figure 20: Chromatin immunoprecipitation of light-induced histone acetylation. For the ChIP analysis, four biological replicates of each strain were incubated overnight in 50 mL of minimal media at 37 °C. Before fixation with formaldehyde, two replicates were illuminated (200 µmol photons m^{-2} s^{-1}) and two were kept in darkness. Then, the replicates were combined into two. ChIP was performed using antibodies against histone 3 (top) and acetylated lysine 9 of histone 3 (bottom), and qRT-PCR was used for *ccgA* as target gene and the control gene *actA*. The abundance of the immunoprecipitated product was compared to the total chromatin input. Error bars represent the standard deviation of two biological and two technical replicates. An unpaired, parametric, two-tailed Student's t-test with a 95 % confidence interval was performed for statistical analysis, *p≤0.05. Dots represent individual biological replicates.

FphA does not only activate gene expression after absorption of red light but can also use blue light to induce the light response (Yu *et al.*, 2021). To test, if the inhibitory effect of CryA on FphA is independently of the light quality, qRT-PCR was carried out comparing the WT strain with the Δ*cryA* and a Δ*fphA* strain (sJP2) as control **(Fig. 21)**. In this experiment, the strains were either kept in the dark or illuminated separately with blue (465 nm) or red (680 nm) light. In addition to the target genes *ccgA*, *ccgB*, and *AN11314* of FphA, the light dependent gene *AN8930* was selected because it did only respond to treatment with red light (Yu *et al.*, 2021). The expression of all analyzed genes was significantly reduced in the Δ*fphA* strain and notably stronger in the Δ*cryA* strain. As expected, *AN8930* exhibited significant upregulation only after red light illumination in the *cryA* deletion strain. The absence of interaction between CryA and LreA in the nucleus suggests that CryA inhibits FphA in response to both red and blue light.

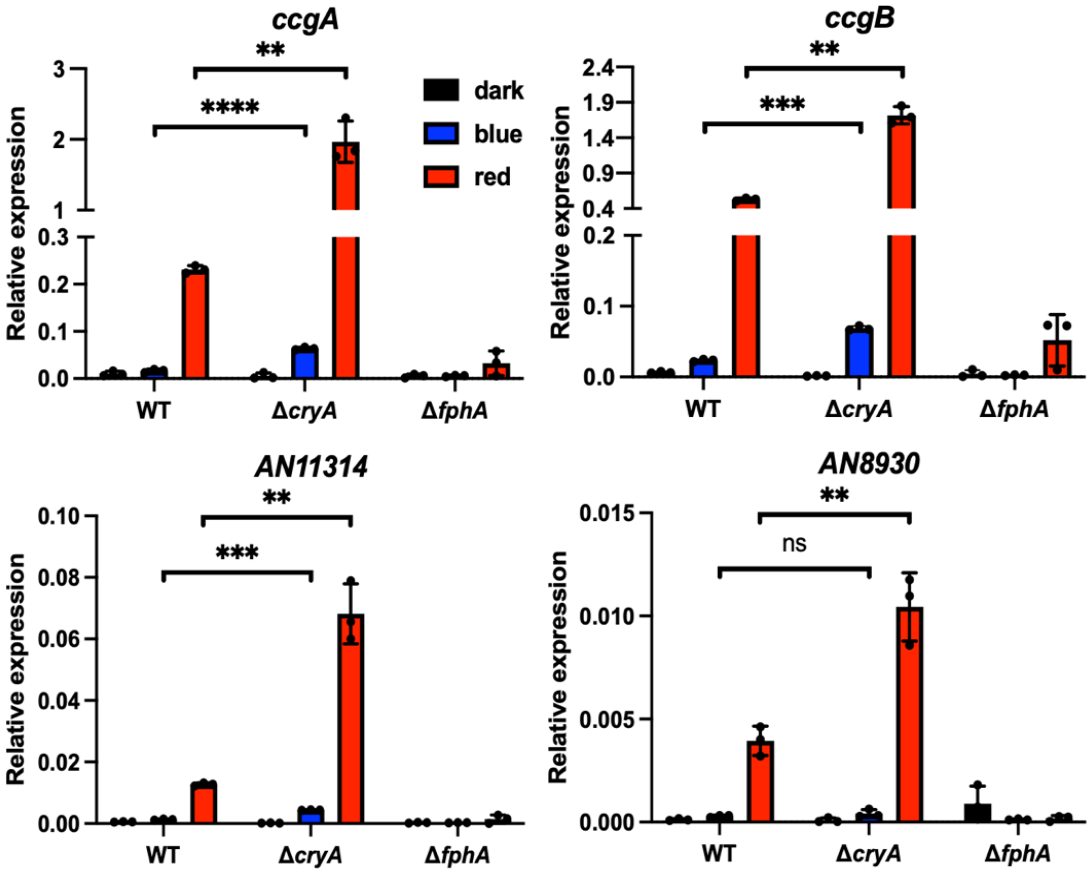

Figure 21: Analysis of the expression of red-light-dependent genes. qRT-PCR of different red-light regulated genes in wild-type compared to a Δ*cryA* and Δ*fphA* strains. 1.5*10^8 spores of the respective strains were incubated for 16 h in 10 ml minimal media with 2 % glucose at 37 °C completely in the dark or were illuminated for 15 minutes with blue- or red light (200 µmol photons m^{-2} s^{-1}) before harvesting the mycelia under green safety light. For the qRT-PCR *h2b* was used as housekeeping gene for normalizing the expression level. Error bars represent the standard deviation of three biological replicates and two technical replicates. For statistical analysis, an unpaired, parametric two-tailed Student's t-test was performed, using a 95 % confidence interval, ^{ns}p>0.05; **p≤0.01; ***p≤0.001; ****p≤0.0001. Dots represent individual biological replicates.

To confirm that the upregulation of gene expression in the Δ*cryA* strain is a result from the absence of the CryA inhibitory effect on FphA functionality, a qRT-PCR was performed using a Δ*cryA*/Δ*fphA* double deletion strain (sAUL23) compared to the WT **(Fig. 22)**. The double deletion mutant was generated by crossing the deletion strains Δ*cryA* and Δ*fphA* (sJP2) together. The target genes *ccgA, ccgB*, *AN11314,* and *brlA* were selected for expression analysis due to their dependence on FphA activity. The double mutant showed no significant increase in gene expression when exposed to light and exhibited a notable decrease for the transcription factor *brlA*. This suggests that transcriptional activation is primarily initiated by FphA and then modified in a negative manner by CryA.

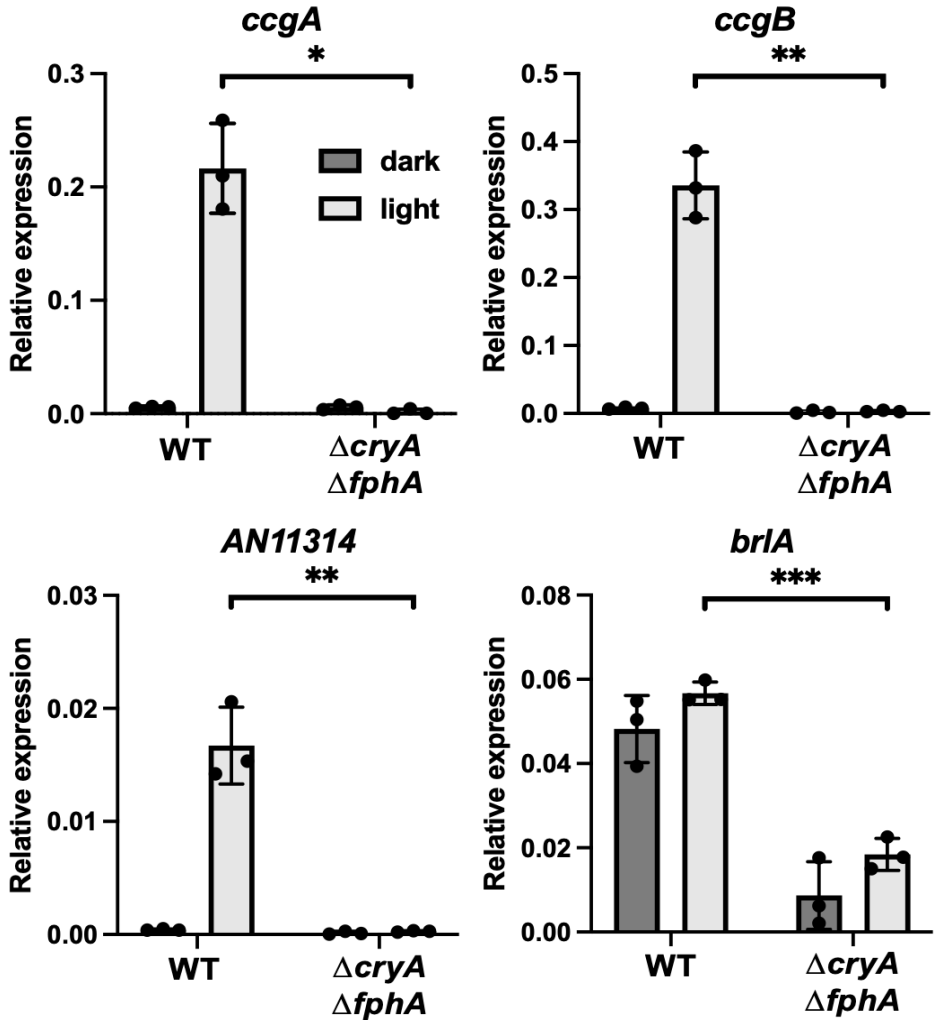

Figure 22: Expression analysis of FphA dependent genes. Expression analysis of FphA dependent genes in wild-type compared to the double deletion strain Δ*cryA*/Δ*fphA*. $1.5*10^8$ spores of the respective strains were incubated for 16 h in 10 ml minimal media with 2 % glucose at 37 °C completely in the dark or were illuminated for 15 minutes with blue- or red light (200 µmol photons m^{-2} s^{-1}) before harvesting the mycelia under green safety light. For the qRT-PCR *h2b* was used as housekeeping gene for normalizing the expression level. Error bars represent the standard deviation of three biological replicates and two technical replicates. For statistical analysis, an unpaired, parametric two-tailed Student's t-test was performed, using a 95 % confidence interval, *p≤0.05; **p≤0.01; ***p≤0.001. Dots represent individual biological replicates.

2.9 The expression of *cryA* is activated through oxidative stress

Light serves as an important early warning system for incoming stresses, such as temperature shifts, UV-radiation, or higher concentrations of ROS (Rodriguez-Romero *et al.*, 2010). AtfA plays a critical role in the adaptation of *A. nidulans* because it serves as a convergence point for various stress stimuli and activates the general stress response (Balázs *et al.*, 2010; Hagiwara *et al.*, 2016; Miskei *et al.*, 2025). Recent studies examined the role of AtfA in *A. nidulans* in response to the oxidative stress factor menadione. Interestingly, *cryA* expression was significantly increased by AtfA following menadione treatment (Kocsis *et al.*, 2023).

To replicate these results, qRT-PCR was performed of wild-type *A. nidulans* to compare the effects of menadione and, in addition, hydrogen peroxide on *cryA* expression **(Fig. 23)**. Menadione is a xenobiotic agent that generates superoxides through redox cycling, primarily in the mitochondria. This leads to toxic intracellular concentrations of ROS (Loor *et al.*, 2010; Goffart *et al.*, 2021). In addition to menadione, H_2O_2 was selected as a source of direct ROS damage. Hydrogen peroxide damages fungal cells primarily through oxidative stress, it generates highly reactive hydroxyl radicals via the Fenton reaction that damage lipids, proteins, and DNA, disrupting cellular function (Goffart *et al.*, 2021; Yaakoub *et al.*, 2022).

Expression analysis revealed that the expression of *cryA* is significantly increased after treatment with H_2O_2. This effect was even stronger after treatment with menadione. These results suggest that intracellular damage through ROS is followed by an increase of *cryA* expression as part of the oxidative stress response.

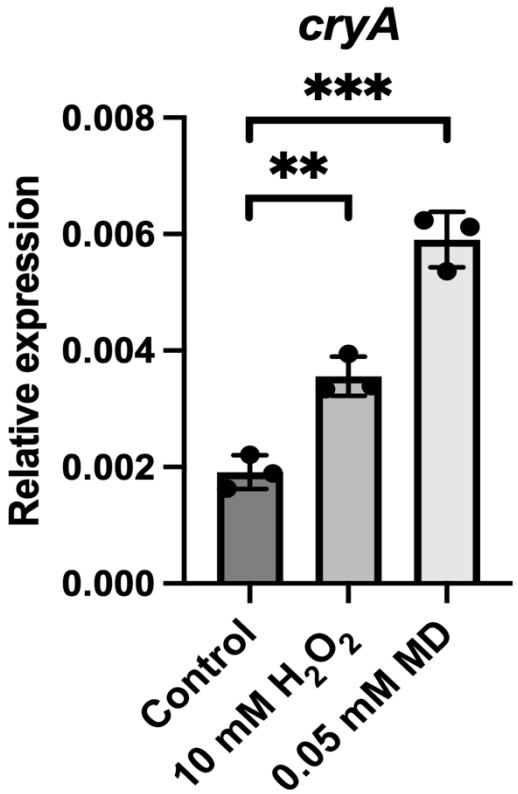

Figure 23: Analysis of *cryA* expression after treatment with different ROS. 1.5*10^8 spores of *A. nidulans* wild-type were incubated for 16 h in 10 ml minimal media with 2 % glucose at 37 °C completely in the dark. For the stress assay, the samples were either kept in the dark (control, dark grey) or transferred in new media supplemented with either 10 mM H_2O_2 (grey) or 0.05 mM menadione (MD, light grey) for 25 min before harvesting the mycelia under green safety light. The concentrations were estimated empirically. For the qRT-PCR *h2b* was used as housekeeping gene for normalizing the expression level. Error bars represent the standard deviation of three biological replicates and two technical replicates. For statistical analysis, an unpaired, parametric two-tailed Student's t-test was performed, using a 95 % confidence interval, **p≤0.01; ***p≤0.001. Dots represent individual biological replicates.

2.10 The oxidative stress response is modulated by CryA

There are not many studies about the role of CPF members in the oxidative stress response. The functions of these proteins depend on the organism and subsequent subfamily of cryptochrome/photolyase. Interestingly, the oxidation of light activated $FADH^-$ back to FAD^{ox} produces H_2O_2 as a byproduct (Ahmad, 2016; Aguida *et al.*, 2024). This led to studies about plant cryptochromes, such as CRY1 and CRY2 in *A. thaliana,* which were described in their role as ROS producing proteins, thereby serving in intracellular signaling (El-Esawi *et al.*, 2017). Another example describes the photolyase CPDphr of the blind cavefish *Phreatichthys andruzzii* with a novel function in ROS sensing. CPDphr can perceive and repair DNA damage triggered through endogenous ROS in a light independent manner (Li *et al.*, 2025a).

No information is available regarding the role of fungal cryptochromes or photolyases in stress perception and regulation in connection to the HOG-pathway. Therefore, a stress assay was conducted using different stress stimuli that are

described to activate the HOG-pathway (Hagiwara *et al.*, 2009a; Duran *et al.*, 2010; Winkelströter *et al.*, 2015; Yu *et al.*, 2016; Yaakoub *et al.*, 2022) **(Fig. 24a)**. For this stress assay, the growth of WT *A. nidulans* was compared to the Δ*cryA* strain, the *cryA*OE strain, and the Δ*fphA* strain as a control. In addition to menadione and H_2O_2 for induction of oxidative stress, high concentrations of sodium chloride were selected to observe the response to high osmotic pressure (Han & Prade, 2002). The stress assay revealed that both NaCl and menadione inhibited the growth of all strains. However, the Δ*cryA* strain exhibited increased growth and conidiation on menadione. Additionally, only the Δ*cryA* strain displayed visible growth on 10 mM H_2O_2, suggesting that CryA controls resistance to oxidative stress agents.

To expand on these results regarding CryA's role in defending against ROS, a gene expression analysis of antioxidants involved in defending against H_2O_2 was carried out **(Fig. 24b)**. In particular, the primary catalases *catA* and *catB* were selected for their importance in the resistance against H_2O_2 in vegetative hyphae and spores (Kawasaki *et al.*, 1997; Kawasaki & Aguirre, 2001). Additionally, the thioredoxin and glutathione systems were examined because they play a critical role in managing intracellular ROS levels by controlling the thiol-disulfide equilibrium (Sato *et al.*, 2009; Liu *et al.*, 2025). All analyzed genes were significantly upregulated in the WT after treatment with 10 mM H_2O_2. In contrast, the *cryA* deletion strain exhibited a significant upregulation of catalase B, most likely contributing to the survival on H_2O_2. This stark increase occurred even under non-stress conditions. Notably, the other antioxidant genes besides *catB* displayed significant downregulation compared to the wild-type. This suggests that CryA regulates the stress response rather than completely inhibiting it.

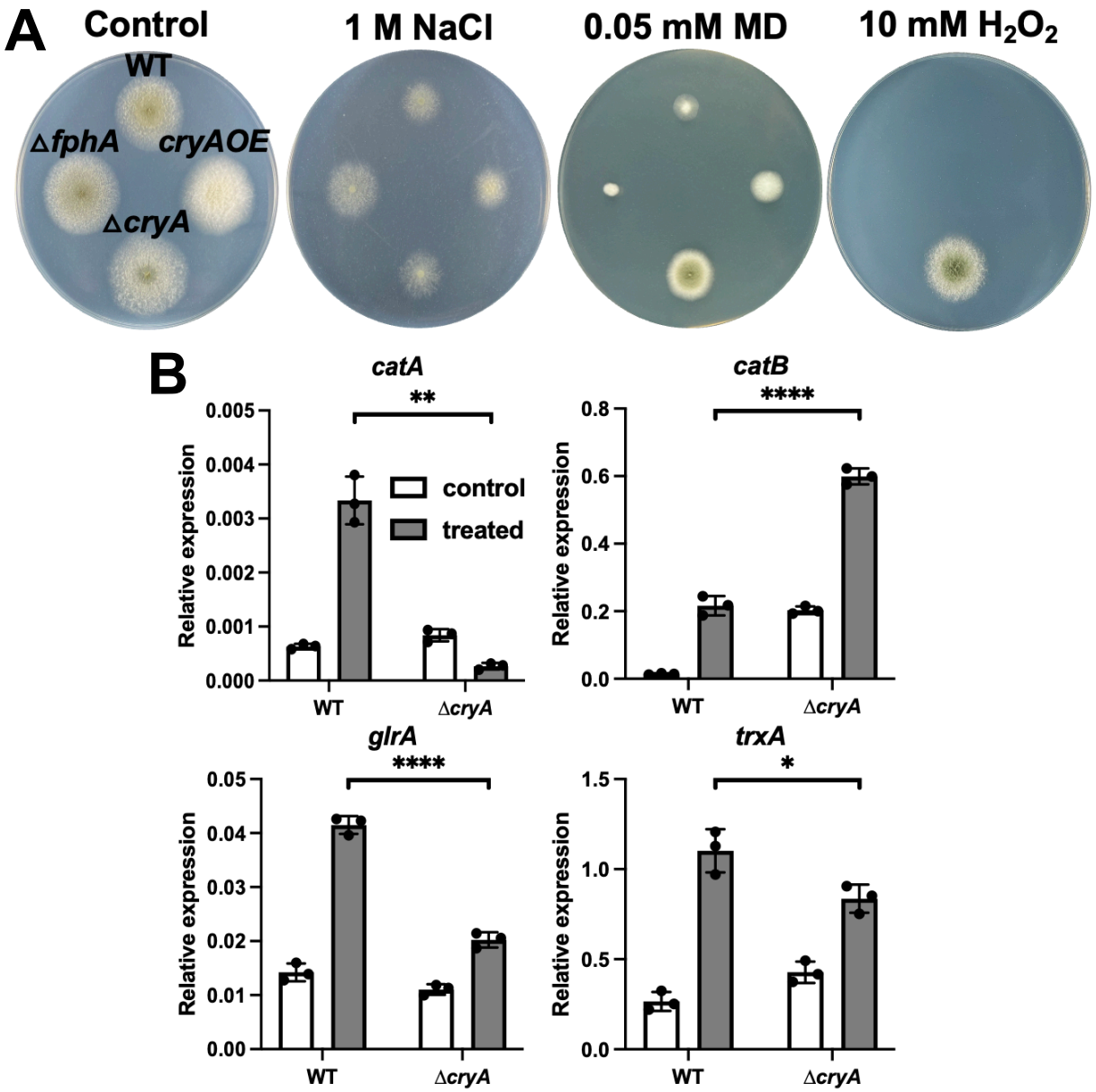

Figure 24: Stress assay and expression analysis of the wild-type compared to the Δ*cryA* strain, the Δ*fphA* strain, and the *cryA*OE strain. (A) Stress assay of the WT compared to the *cryA*-deletion strain (Δ*cryA*), the *cryA*-overexpression strain (*cryA*OE), and the *fphA*-deletion strain (Δ*fphA*) exposed to either 1 M NaCl, 0.05 mM menadione (MD), or 10 mM H_2O_2. 1,000 spores of the respective strains were inoculated as colonies and incubated for 5 days at 30 °C in white light (200 µmol photons m^{-2} s^{-1}) on minimal media supplemented with 2 % threonine and the respective stress factors. At least 8 replicates per condition were analyzed. (B) Expression analysis of antioxidant genes in WT compared to the *cryA*-deletion strain. $1.5*10^8$ spores of the respective strain were incubated for 16 h at 37 °C in minimal media in darkness. Prior to harvesting in green safety light, the mycelia were either kept in the dark (control, white) or transferred in new minimal media supplemented with 10 mM H_2O_2 for 25 min (treated, grey). For the qRT-PCR *h2b* was used as housekeeping gene for normalizing the expression level. Error bars represent the standard deviation of three biological replicates and two technical replicates. For statistical analysis, an unpaired, parametric two-tailed Student's t-test was performed, using a 95 % confidence interval, ^{ns}>0.05; *p≤0.05; **p≤0.01; ****p≤0.0001. Dots represent individual biological replicates.

2.11 CryA interacts with the bZIP transcription factor AtfA

The expression of *cryA* is described to be regulated by light and FphA (Yu *et al.*, 2021). CryA interacts with FphA, which inhibits its function in the nucleus and prevents histone

acetylation. Previous results indicated that CryA is expressed in response to oxidative stress under the control of AtfA (Kocsis *et al.*, 2023; Miskei *et al.*, 2025). Therefore, it is meaningful to consider whether CryA can interact with AtfA and modify its functions similarly to how it responds to light and FphA. To test this hypothesis, a BiFC assay was performed with CryA (pAUL3 & pAUL4) and AtfA (pALBL33 & pALBL34) *in vivo* **(Fig. 25)**. The strains sAUL20 (YFPC-CryA & YFPN-AtfA) and sAUL21 (YFPN-CryA & YFPC-AtfA) were generated and Hoechst 33342 was used for nuclei staining. Interaction between the two proteins could be observed in the nuclei of *A. nidulans*. The nuclear interaction was also detected under different light conditions (results not shown).

In summary, *cryA* expression is controlled by AtfA and oxidative stress, together with FphA and the light response. Similar to its negative impact on the light response, CryA most likely accumulates in the nuclei and interacts with AtfA, thereby modifying the oxidative stress response.

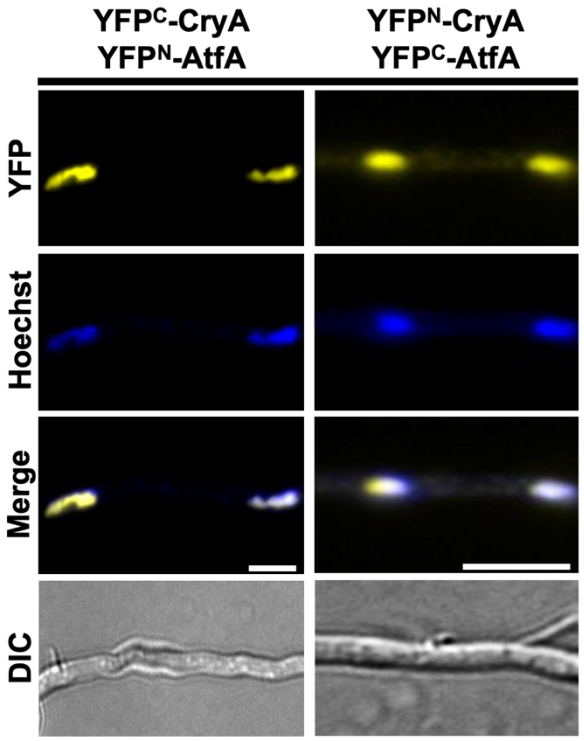

Figure 25: BiFC assay between CryA and the bZIP transcription factor AtfA. CryA and AtfA were fused N-terminally to either half of YFP under the control of the *alcA* promoter. Spores were incubated overnight at 25 °C in minimal media with 2 % threonine instead of glucose to induce the promoter. The nuclei were stained using HOECHST 33342 The scale bar represents 5 µm.

2.12 Perception of H_2O_2 induces shuttle of CryA to the mitochondria

Several proteins are involved in the signaling mechanism against oxidative stress and shuttle between different intracellular compartments (Vargas-Pérez *et al.*, 2007). One example is the bZIP transcription factor NapA, which resides in the cytosol under low-stress conditions but is imported into the nucleus after oxidation through ROS (Mendoza-Martínez *et al.*, 2017). Since CryA appears to be involved in the oxidative stress signaling mechanism, we investigated whether exposure to high concentrations of H_2O_2 would affect CryA localization similarly *in vivo* **(Fig. 26)**. sAUL3 was selected for fluorescence microscopy and MitoTracker was used for staining of the mitochondria to improve visualization. Treatment of CryA with 10 mM H_2O_2 led to an immediate shuttle (approximately 1 min) out of the nuclei to the mitochondria.

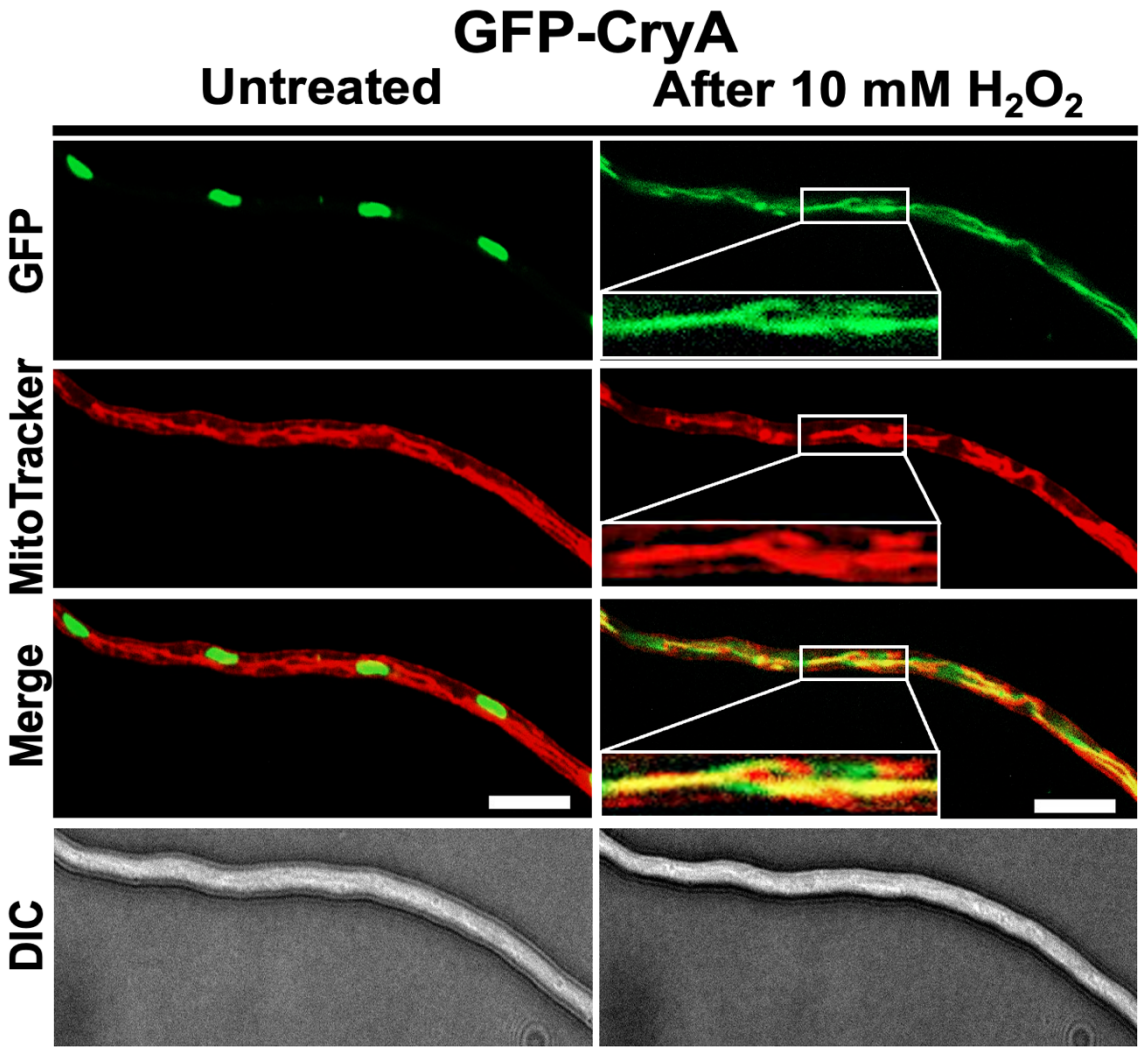

Figure 26: Localization of CryA before and after treatment with 10 mM H_2O_2. 1,000 spores were incubated overnight at 25 °C in minimal media with 2 % threonine to induce the promoter activity. MitoTracker staining was used to visualize mitochondria. The scale bar represents 10 µm.

This result was surprising as previous domain predictions did not reveal any conserved mitochondria transit sequence (MTS). In addition, treatment with menadione did not induce an intracellular shuttle (results not shown). These findings provide a possible molecular connection between CryA and its role in ROS signaling.

2.13 N-terminal extension of CryA determines intracellular localization

The H_2O_2 induced shuttle of CryA from the nucleus to the mitochondria was an unexpected result and is a mechanism which was not described for any CPF member before. Typically, cryptochromes harbor a C-terminal NLS, whereas some CRY-DASH members, such as Cry3 from *A. thaliana*, contain a N-terminal motif for plastidial or mitochondrial import (Kleiner *et al.*, 1999; Kleine *et al.*, 2003; Kiontke *et al.*, 2020). The predicted N-terminal extension of CryA is highly disordered and only present in other eukaryotic CPD photolyases and CRY-DASH proteins. To further analyze the NTE, a sequence alignment was performed using Geneious Prime 2024 between the NTE of CryA (1-70 amino acids) and Cry2 from *A. thaliana*. **(Fig. 27a)**. Only the first 92 amino acids of CryA are shown in the sequence comparison. The alignment revealed that the first 70 amino acids of the NTE are unique to CryA; the consensus region of both proteins begins at Met71 of CryA.

To test the importance of the NTE for intracellular localization, truncated variants of the NTE were generated. For the truncation, either the first 20 (pAUL32) or 60 amino acids (pAUL34) were removed, and the truncated variants were N-terminally tagged with GFP under the control of the *alcA* promoter (sAUL24 & sAUL26). These variants were then analyzed via fluorescence microscopy **(Fig. 27b)**. The truncation mutants localized without additional exogenous factors such as H_2O_2 exclusively at the mitochondria. These results suggest that the first 20 amino acids and the NTE in general is important for nuclear import and retention.

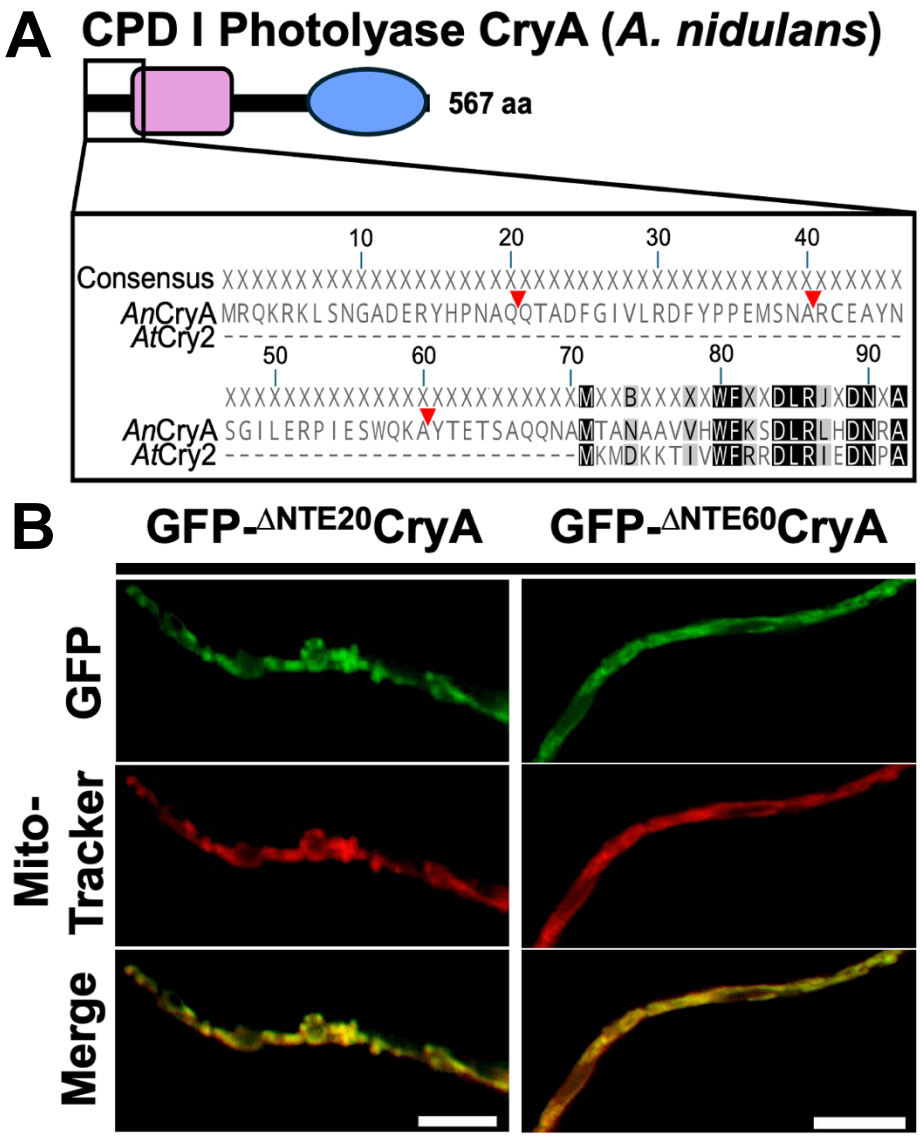

Figure 27: Functional analysis of the NTE of CryA. (A) Comparison between the N-termini of CryA from *A. nidulans* and Cry2 from *A. thaliana*. Geneious Prime 2024 was used for pairwise alignment with a global alignment with free end gaps, a Pam-matrix of 100 and gap costs of 10/1. Red triangles mark the chosen lengths for the truncation mutants. (B) Fluorescence microscopy of a strain expressing truncation mutants of the N-terminal extension of CryA. Strains were incubated overnight at 25 °C in minimal media with 2 % threonine to induce promoter activity. MitoTracker staining was used to visualize mitochondria. The scale bar represents 10 µm.

Although a few other CPF proteins can localize to the mitochondria, the mechanism behind this process remains unclear (Yasui *et al.*, 1992; Kleine *et al.*, 2003; Takahashi *et al.*, 2011; Takahashi *et al.*, 2014; Zheng *et al.*, 2024). The rice CPD II photolyase was able to repair UV-induced damage in plastids and mitochondria (Takahashi *et al.*, 2011). A lysine-arginine-lysine (KKR) motif in the N-terminus of the rice CPD photolyase was important for nuclear retention (Takahashi *et al.*, 2014). Additionally, studies on the CPD photolyase of *S. cerevisiae* revealed the role of yeast photolyases in mitochondrial DNA repair. Here, the methionine-histidine-tryptophan-phenylalanine-arginine motif (MHWFR) is predicted as a mitochondrial transit

sequence and appears crucial for the photoreactivation of mitochondrial DNA (Yasui *et al.*, 1992). Interestingly, a sequence comparison between CryA and both the CPD I and CPD II photolyases revealed similar sequence motifs in the N-terminus of CryA. More precisely, the Lys4-Arg5-Lys6 motif (KRK) resembles the nuclear localization signal (NLS) found in rice photolyase, while the Val78-His79-Trp80-Phe81-Lys82 motif (VHWFK) shares high identity with the MTS of yeast photolyase.

To test whether these amino acids are crucial for organelle targeting, the motifs were substituted with alanine, either as a single mutation or both motifs together. The $^{\Delta NLS}$CryA mutant (pAUL81), the $^{\Delta MTS}$CryA mutant (pAUL82), and the $^{\Delta MTS\Delta NLS}$CryA (pAUL83) mutant were then fused N-terminally to GFP under the control of the *alcA* promoter and then integrated *in vivo* (sAUL40 & sAUL41 & sAUL42). Intracellular localization of the motif mutants was analyzed via fluorescence microscopy **(Fig. 28)**. Similar to the NTE truncation mutant, substitution of the functional NLS resulted in the loss of nuclear retention and import. Unexpectedly, deleting the MTS motif did not abolish mitochondrial localization, but it did prevent CryA from being imported into the nucleus. Deletion of both motifs led to exclusive cytoplasmic localization of CryA. These results suggest that the KRK motif is essential for nuclear retention. Additionally, the expected loss of nuclear and mitochondrial import occurred with the deletion of both motifs, though this could also be a byproduct of nonfunctional CryA synthesized artificially.

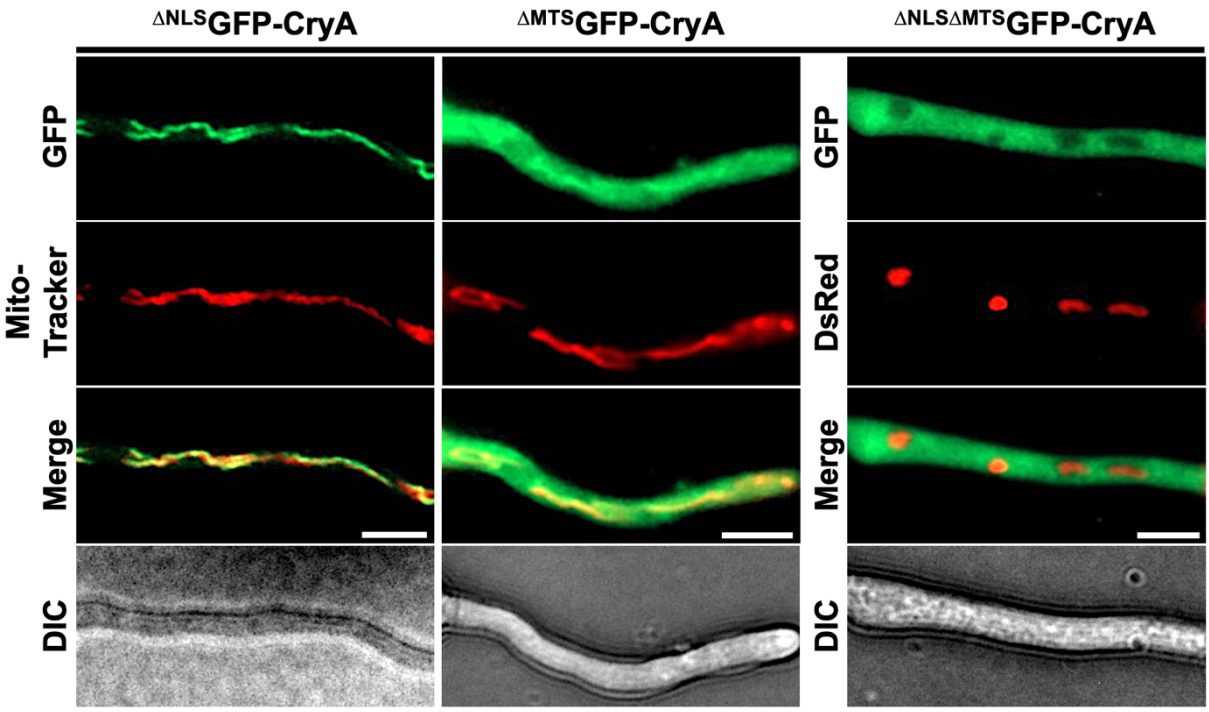

Figure 28: Analysis of the intracellular localization of the $^{\Delta NLS}$CryA mutant, the $^{\Delta MTS}$CryA mutant, or the $^{\Delta MTS\Delta NLS}$CryA mutant. Fluorescence microscopy was utilized to visualize the GFP signal of the $^{\Delta NLS}$CryA mutant, the $^{\Delta MTS}$CryA mutant, and the $^{\Delta MTS\Delta NLS}$CryA. Strains were incubated overnight at 25 °C in minimal media with 2 %threonine to induce promoter activity. MitoTracker staining was used to visualize mitochondria. For sAUL42, the NLS of *stuA* tagged with DsRed was used to visualize the nucleus. The scale bar represents 5 µm.

2.14 The cysteine Cys42 in CryA is crucial for the response to H_2O_2

The rapid shuttling of CryA from the nucleus to the mitochondria suggests a conformational shift as the molecular mechanism. Interestingly, a similar mechanism has been described for the bZIP transcription factor NapA in response to the perception of oxidative stress. This transcription factor resides in the cytosol, where an exposed nuclear export signal (NES) prevents its import into the nucleus. Upon the oxidation of two conserved cysteines by H_2O_2, a conformational shift is triggered that masks the NES and promotes transport to the nucleus (Mulford & Fassler, 2011; Mendoza-Martínez *et al.*, 2017). A similar mechanism might be present in CryA. The NTE contains one cysteine, Cys42, which is predicted to be in close proximity to two other cysteines, Cys387 and Cys391, to form disulfide bridges **(Fig. 29a)**. To determine the importance of Cys42 in ROS perception, a point mutation (CryA^{C42A}) was created by replacing the cysteine with an alanine. The CryA^{C42A} mutant was tagged N-terminally with GFP (pAUL92) and introduced into *A. nidulans* (sAUL32) to study its response to exogenous H_2O_2 **(Fig. 29b)**. Unlike the wild-type CryA, the cysteine mutant was not exported out of the nucleus after contact with hydrogen peroxide. This result confirms that Cys42 is a conserved amino acid crucial for the CryA shuttle from the nucleus to the mitochondria.

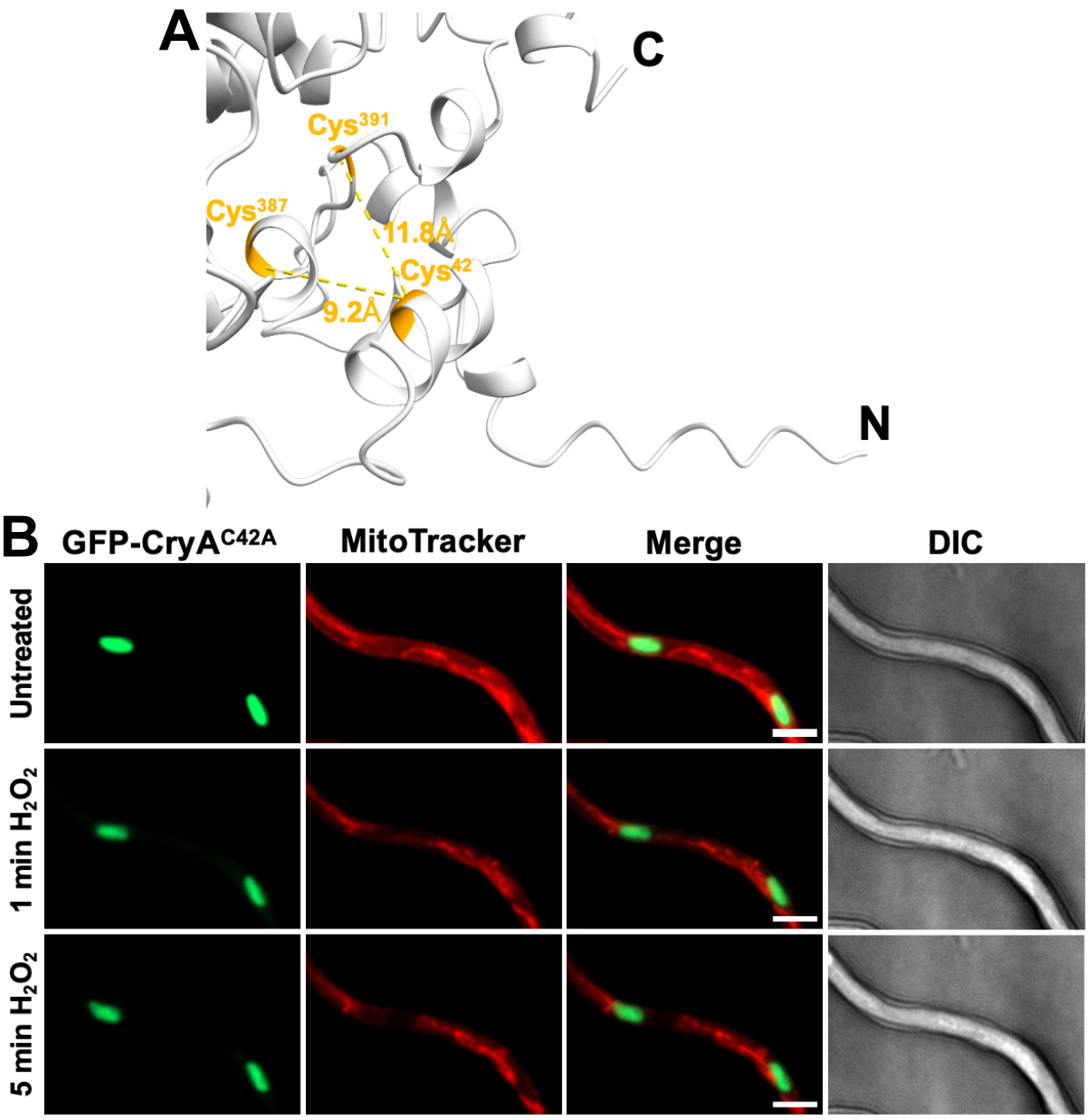

Figure 29: Analysis of the role of Cys42 in the mitochondrial shuttle of CryA. (A) AlphaFold 3 and ChimeraX were used to visualize the cysteines (orange) in the NTE. The distance between the cysteines is given in angstroms. (B) Fluorescence microscopy was used to localize CryA^{C42A} before and after exposure to 10 mM H_2O_2. Spores were incubated overnight at 25 °C in minimal media with 2 % threonine to induce promoter activity. MitoTracker staining was used to visualize mitochondria. The scale bar represents 5 µm.

Next, to study the effect of H_2O_2 on the different localization mutants a stress assay with various concentrations of H_2O_2 was performed **(Fig. 30a)**. For this assay both the $^{\Delta NTE}$CryA (pAUL44) variant and the CryA^{C42A} (pAUL93) variant were integrated into the pMCB17apx vector under the control of the *alcA* promoter and transformed in the Δ*cryA* strain. The growth assay was conducted comparing the WT strain to the Δ*cryA* strain and strains either overexpressing $^{\Delta NTE}$CryA (sAUL30) or the CryA^{C42A} point

mutant (sAUL37). While all strains were resistant to lower concentrations of H_2O_2, only the Δ*cryA* strain and the overexpression strain of CryA^{C42A} were able to survive on 7.5 mM H_2O_2 or higher concentrations. In contrast, overexpression of $^{\Delta NTE}$CryA reinstated the susceptibility to H_2O_2. To expand on the growth assay, a quantitative analysis for the expression of antioxidant genes in the CryA mutant strain was carried out **(Fig. 30b)**. For this analysis, the catalases A & B together with the glutathione and thioredoxin system were examined. Treatment with H_2O_2 led to a significant downregulation of all analyzed genes in the $^{\Delta NTE}$CryA strain. However, for the CryA^{C42A} overexpression strain *catB* and *glrA* revealed a strong upregulation.

In summary, these results, together with the growth assay, indicate for a localization dependent role of CryA in the oxidative response.

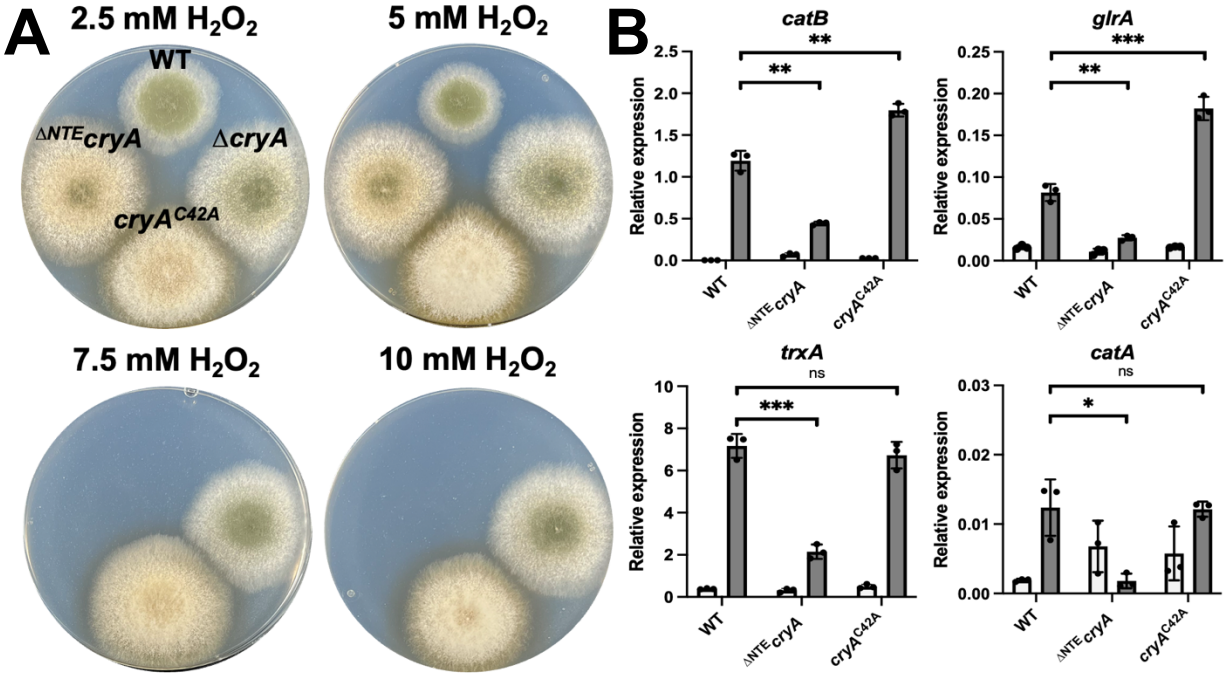

Figure 30: Analysis of the stress response to hydrogen peroxide in the WT, the truncation mutant $^{\Delta NTE}$*cryA*, and the cysteine mutant *cryA*^{C42A}. (A) Comparison of wild-type colonies with the *cryA* deletion, the Δ*cryA* strain re-complemented with an overexpression mutant of the N-terminal truncation mutant of CryA ($^{\Delta NTE}$*cryA*), and re-complementation of the Δ*cryA* strain with the cysteine mutant (*cryA*^{C42A}). 1,000 spores were point inoculated and grown for five days at 30 °C on minimal media with 2 % threonine in white light (200 µmol photons m^{-2} s^{-1}) with the indicated concentrations of H_2O_2. For each concentration at least eight replicates were analyzed. (B) Expression analysis of genes responding to oxidative stress in the wild type, $^{\Delta NTE}$*cryA*, and *cryA*^{C42A} strains. 1.5*10^8 spores of the respective strains were incubated for 16 hours in 10 ml of minimal medium at 37 °C in complete darkness. Before harvesting, the mycelia were transferred to pre-warmed liquid minimal media, either without supplements (control, white) or with 10 mM H_2O_2 (treated, gray), under green safety light. They were then incubated for 25 minutes. For qRT-PCR, *h2b* was used as the housekeeping gene to normalize expression levels. Error bars represent the standard deviation of three biological and two technical replicates. An unpaired, parametric, two-tailed Student's t-test was performed for statistical analysis using a 95 % confidence interval, ^{ns}p>0.05; *p≤0.05; **p≤0.01; ***p≤0.0001. Dots represent individual biological replicates.

2.15 CryA mediates the menadione-induced oxidative stress response

The N-terminal extension and cysteine 42 play an important role in CryA's mechanism of perceiving and responding to H_2O_2 treatment. While hydrogen peroxide damages the entire cell through the undesirable oxidation of DNA, proteins, and lipids, other oxidative stress factors, such as paraquat and menadione, directly target the mitochondrial respiratory system and induce the generation of harmful superoxides (Castello *et al.*, 2007; Loor *et al.*, 2010). Because CryA plays a role in the mitochondrial response to oxidative stress, analyzing how CryA mutants respond to menadione treatment was appealing. To test this, a growth assay was conducted, comparing the WT with the Δ*cryA* strain, the $^{\Delta NTE}$CryA overexpression strain, and the CryA^{C42A} overexpression strain **(Fig. 31a)**. All CryA mutant strains exhibited increased resistance on media containing 0.05 mM menadione (MD). In contrast, Wild-type *A. nidulans* was not able to grow on menadione-containing media after five days. The $^{\Delta NTE}$CryA strain appeared to be the most adapted to menadione-induced stress, while the CryA^{C42A} overexpression strain displayed only weak growth. This indicates that the deletion or interruption of the normal molecular function of CryA removes the inhibitory effect on the oxidative stress response. To confirm this hypothesis, a quantitative analysis of the primary antioxidant genes was performed **(Fig. 31b)**. In addition to the catalases (*catA* and *catB*), the thioredoxin system (*trxA*), and glutathione reductase (*glrA*), the two antioxidants (*prxA* and *cetJ*) were included because they have been shown to be up-regulated by menadione treatment (Kocsis *et al.*, 2023). qRT-PCR revealed that *catB,* along with *trxA* and the peroxiredoxin gene *prxA* was significantly upregulated in all CryA mutant strains compared to the WT. The expression of *catA* and *glrA* was mostly identical to that of the wild-type. Interestingly, complete deletion of *cryA* resulted in the most significant increase in expression levels as opposed to the cysteine mutation which only promoted a slight increase in relative expression levels.

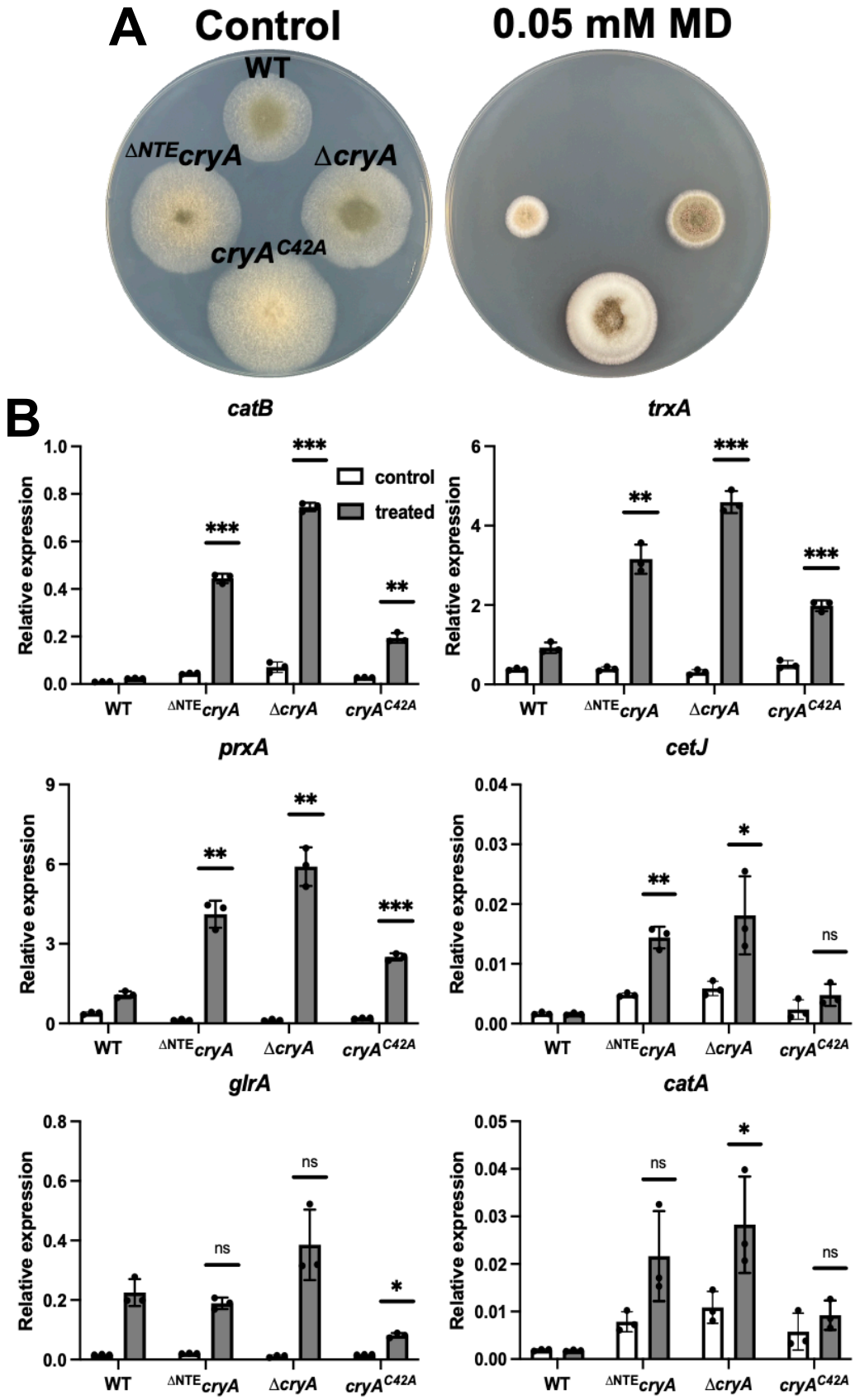

Figure 31: Analysis of the stress response to menadione in the WT, the *cryA* deletion strain, the truncation mutant $^{\Delta NTE}$*cryA*, and the cysteine mutant *cryA*^{C42A}. (A) Comparison of wild-type colonies with the *cryA* deletion, the Δ*cryA* strain re-complemented with an overexpression mutant of the N-terminal truncation mutant of CryA ($^{\Delta NTE}$*cryA*), and re-complementation of the Δ*cryA* strain with the cysteine mutant (*cryA*^{C42A}). 1,000 spores were grown for 5 days at 30 °C on minimal media with 2 % threonine in light (white light with 200 µmol photons m^{-2} s^{-1}) with no supplements (control) or 0.05 mM menadione (MD). (B) Expression analysis of genes responding to oxidative stress in wild type, the $^{\Delta NTE}$*cryA* strain, and the *cryA*^{C42A} strain. 1.5*10^8 spores of the respective strains

were incubated for 16 h in 10 ml minimal media at 37 °C completely in the dark. Before harvesting, the mycelia were transferred to pre-warmed liquid minimal media without supplements (control, white) or 0.05 mM menadione (treated, grey) under green safety light and incubated for 25 minutes. For the qRT-PCR *h2b* was used as housekeeping gene for normalizing the expression level. Error bars represent the standard deviation of three biological and two technical replicates. For statistical analysis, a two-tailed Student's t-test was performed and compared to the wild-type and the respective mutants, $^{ns}p>0.05$; *p≤0.05, **p≤0.01, ***p≤0.0001. Dots represent the individual biological replicates.

2.16 ROS and blue light induce homodimerization of CryA

The molecular function of cryptochromes depends on the activation through light and subsequent homodimerization. This phenomenon is mostly described for plant cryptochromes which form homo- or even tetramers upon light perception. Interestingly, the N-terminal photolyase domain, together with the C-terminal extension, appears to be crucial for oligomer formation (Sang *et al.*, 2005; Wang & Lin, 2020b; Palayam *et al.*, 2021).

Several SEC experiments were performed using heterologously expressed CryA (pET28a) to investigate whether CryA can oligomerize upon light perception or after contact with H_2O_2 **(Fig. 32)** For these experiments, 31 nM of CryA was either kept in the dark or illuminated continuously with blue light (450nm). Alternatively, it was treated with 10 µM H_2O_2, to induce dimer formation. SEC confirmed that CryA primarily elutes as a monomer (with an apparent size of ~75 kDa), indicating that CryA is a monomeric protein without an external signal. Additionally, a secondary maximum with an apparent size of 105 kDa was visible in the dark, indicating a small fraction of dimerized CryA. In contrast, treatment with blue light or H_2O_2 led to a significantly higher maximum for homodimerized CryA. These results suggest that blue light and ROS can induce homodimerization of CryA. As an additional control, the cysteine deletion mutant should have been purified to ascertain whether blue light or ROS could still induce CryA dimer formation. Unfortunately, this experiment could not be conducted due to time constraints.

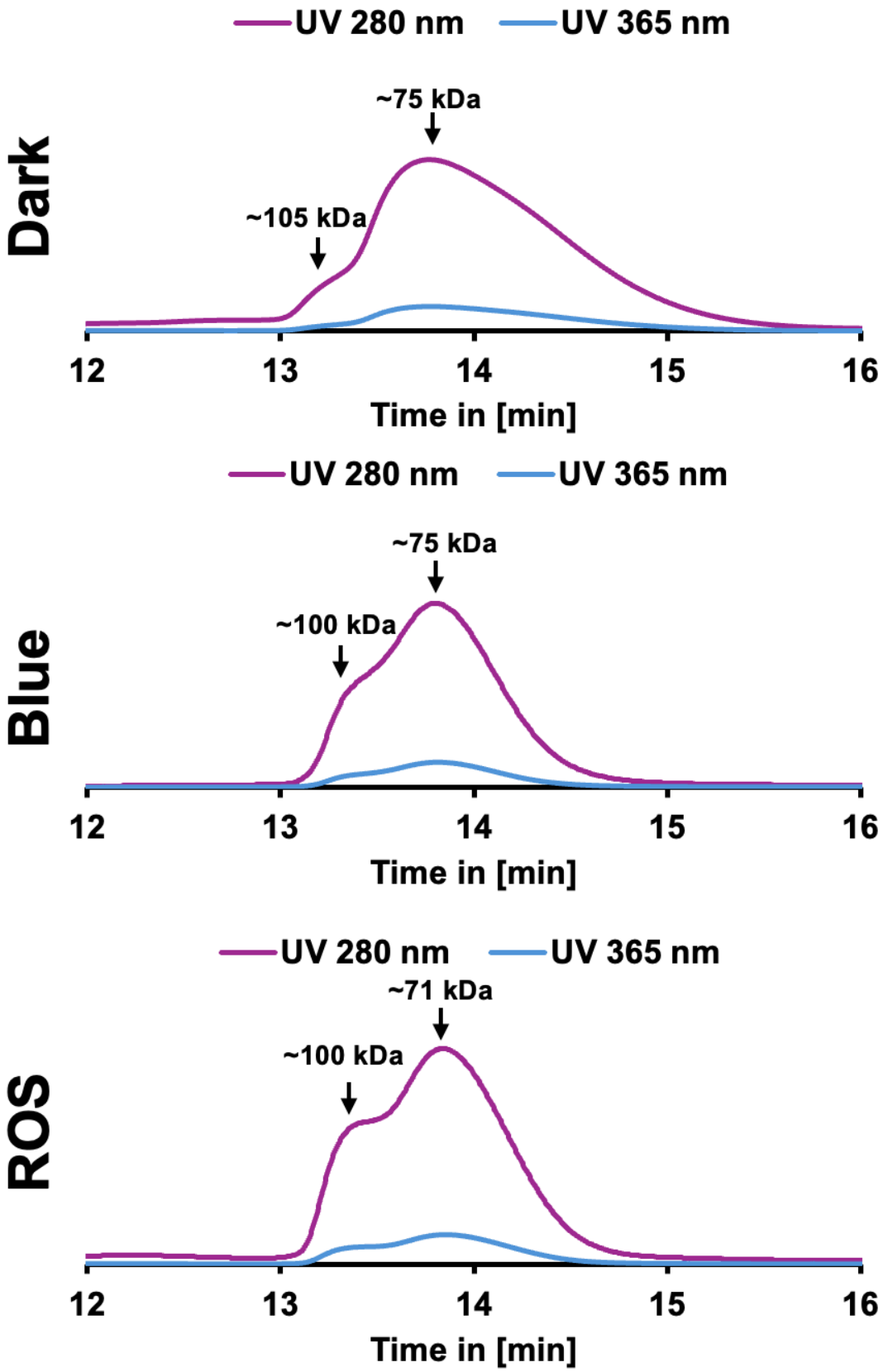

Figure 32: Size exclusion chromatography of purified CryA under different run conditions. CryA was N-terminally tagged with a 6x-His tag and purified from *E. coli*. UV absorption was measured at 280 nm (pink) or 365 nm (blue). The predicted protein mass of tagged CryA as a monomer is 67 kDa (134 kDa as a dimer). The indicated apparent protein sizes are calculated using the calibration with known protein standards (see 2.7, Fig. 18).

2.17 The photolyase CPDphr from *P. andruzzii* is a canonical photolyase

In light of the now well-established role of fungal CryA as an intracellular sensor of oxidative stress, we were keen to further study other members of the cryptochrome/photolyase family to determine whether they exhibit redox sensitivity. We therefore had the opportunity to collaborate with Prof. Nick Foulkes' group, who are interested in studying photolyases in several fish species. One promising candidate emerged in the cavefish *P. andruzzii*. In this species, the CPD photolyase CPDphr responds to oxidative stress in the dark by repairing ROS-induced DNA damage (Li *et al.*, 2025a). As these results revealed interesting parallels with those obtained regarding oxidative stress and CryA in *A. nidulans*, we investigated whether CPDphr could fulfil similar functions.

The blind cavefish *P. andruzzii* is an interesting species for studying light responses **(Fig. 33a)**. It is thought that this species evolved in lightless caves for over 2 million years, which makes it interesting in terms of its photophobic behaviour towards blue light, despite the fact that it is completely blind (Ercolini & Berti, 1975; Ercolini *et al.*, 1982). Several studies have been conducted on the circadian rhythm of *P. andruzzii*, which has been described as the first animal clock that does not rely on light (Mejia, 2011; Lloyd *et al.*, 2018). Despite these evolutionary conditions, the genome of *P. andruzzii* contains several photoreceptors, including the CPD photolyase CPDphr. Since life in hypoxic conditions leads to the generation of intracellular ROS, might provide an evolutionary pressure on these photoreceptors to develop additional functions such as light-independent photoreactivation (Li *et al.*, 2025a)

To investigate the evolutionary relationship between CPDphr and fungal photolyases, a phylogenetic tree was created by primarily comparing animal and fungal photolyases **(Fig. 33b, Appendix Tab. 17)**. Additionally, some prominent prokaryotic and plant photolyases were included to facilitate a more accurate comparison of evolutionary distance.

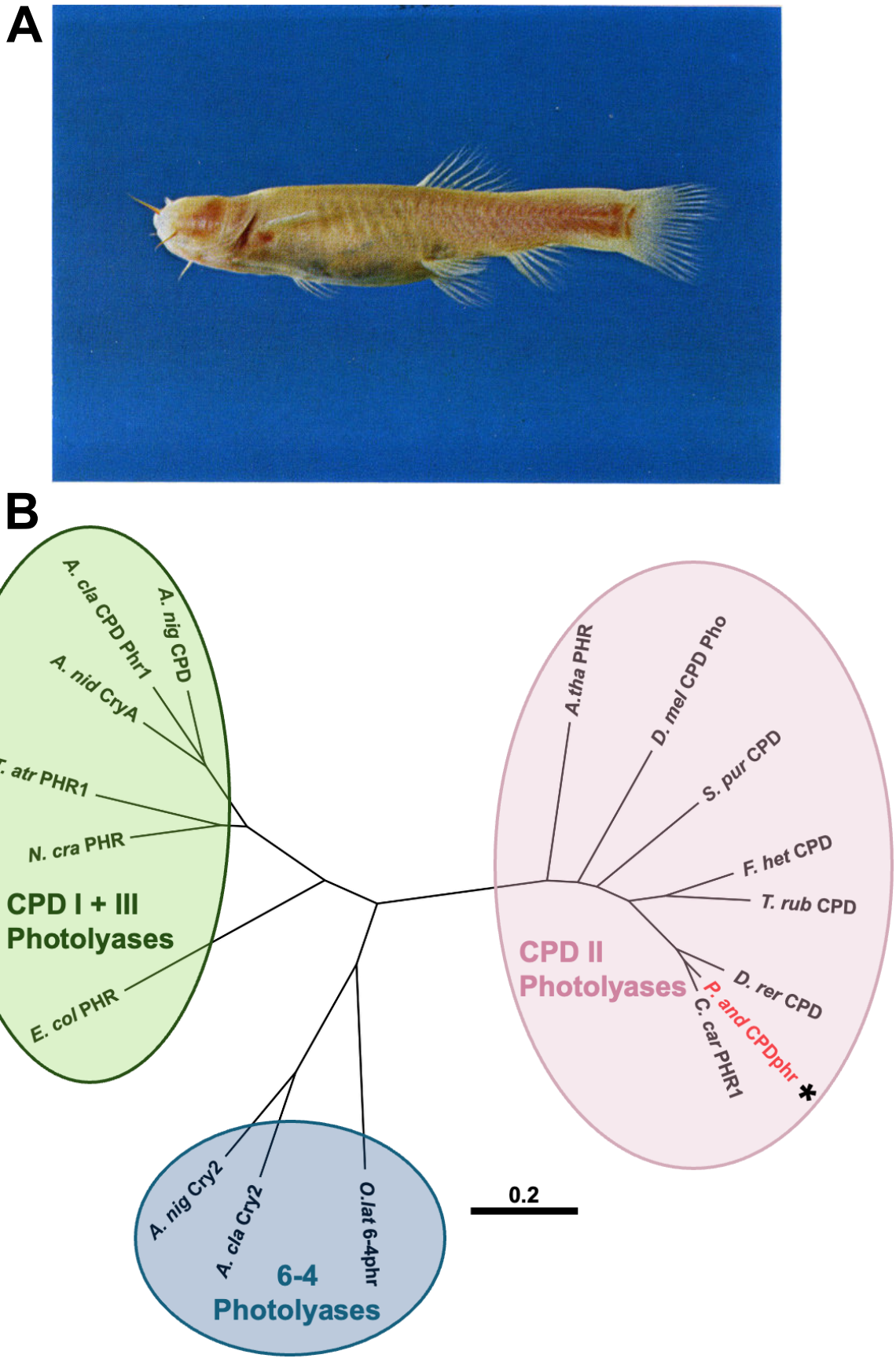

Figure 33: Phylogenetic analysis of the CPD photolyase CPDphr of *P. andruzzii*. (A) Photography of the Somalian cavefish *P. andruzzii* (Ercolini et al., 1982). (B) A phylogenetic analysis of CPDphr together with other photolyases, with special focus on fungal and animal photolyases, was performed using Geneious Prime 2024. Global alignment was used for sequence alignment with a PAM matrix of 100 and gap costs of 10/1. The phylogenetic tree was generated using the Jukes-Cantor distance model and the Neighbor-Joining algorithm. The

subfamilies are CPD I + III photolyases (green), 6-4 photolyases (blue), and CPD II photolyases (pink). The scale bar represents the amino acid substitutions per site.

The phylogenetic analysis reveals that the photolyase of *P. andruzzii* clusters separately from fungal photolyases, alongside other CPD II photolyases. CPD I and CPD III photolyases form a distinct group, but the 6-4 photolyase from the medaka fish clusters with the cryptochromes found in animals, such as *A. clavatus* and *A. nidulans*. The fact that 6-4phr from *Oryzias latipes* was described as a photolyase that can modulate the vertebrate clock suggests that these additional CPF proteins in the *Aspergillus* family may be connected to fungal circadian rhythms (Li *et al.*, 2025b).

Next, to evaluate whether CPDphr can be expressed as a functional protein, its coding sequence, kindly submitted by Nick Foulkes's group, was integrated into the pASK-iba3plus vector (pAUL107) and expressed in *E. coli* BL21 DE3. The protein was then purified using a StrepTrap XT column (Cytiva) on an Äkta FPLC system, and the success of the purification was verified via absorption spectroscopy **(Fig. 34)**. CPDphr was either kept in the dark and measured directly after purification or treated with 1 mM TCEP as an electron donor and then illuminated for one minute with blue light (450 nm) to induce the reduction of FAD^{ox}. The absorption spectrum of CPDphr exhibits two maxima at 380 nm and 450 nm, resembling a canonical FAD^{ox} spectrum (Evans *et al.*, 2013). Unlike CryA, which has a significantly stronger peak at 365 nm, it appears that CPDphr does not contain a secondary antenna chromophore such as 5,10-MTHF. Illumination with blue light and the addition of the reducing agent TCEP initiated the reduction of FAD^{ox}, recognizable by the decrease in absorption at 450 nm and the increase in green absorption. Furthermore, after resting in the dark for one day at 4 °C, the photocycle of CPDphr resets to the oxidized FAD state. These results indicate that CPDphr has a functional photocycle and confirms functionality of the protein.

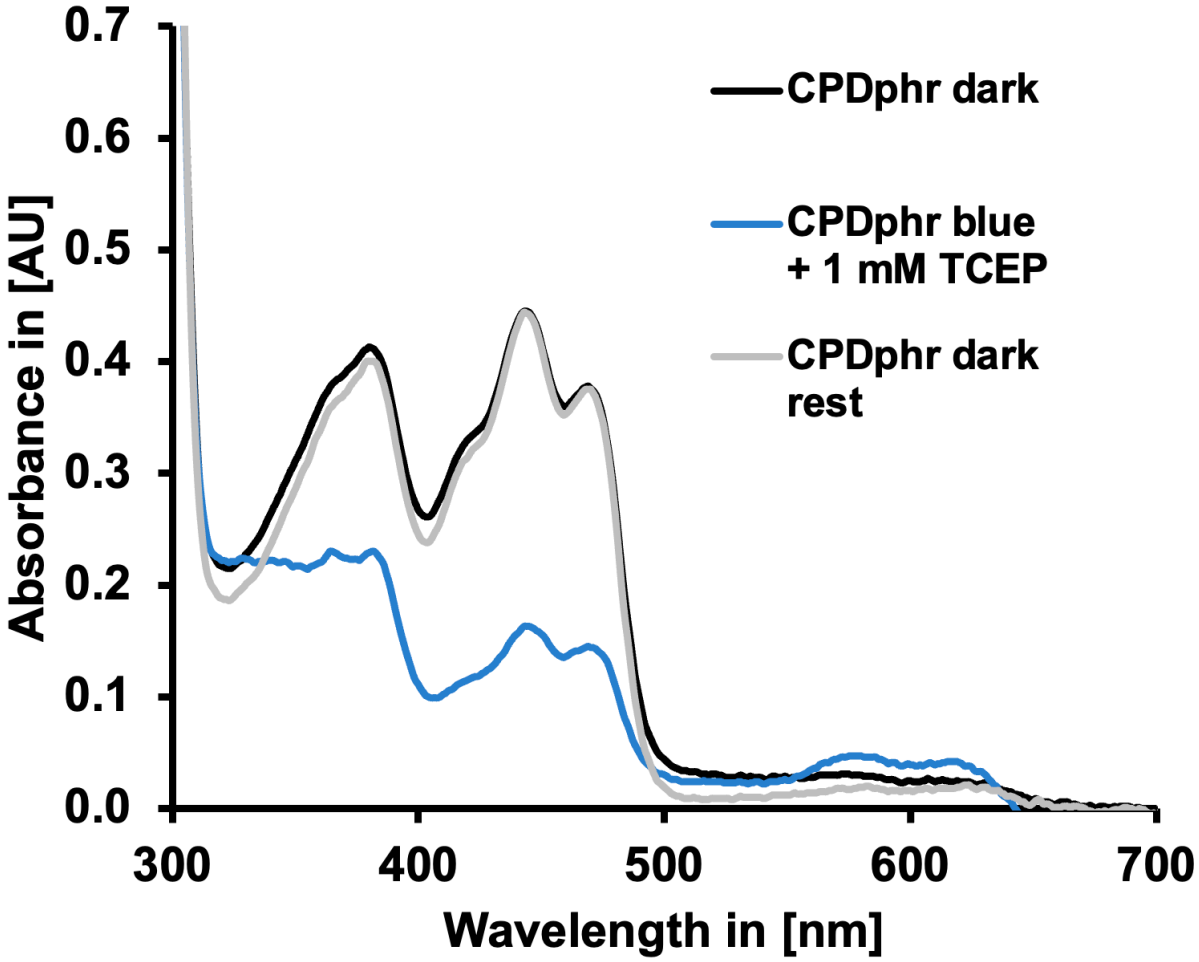

Figure 34: Absorption spectrum of the photolyase CPDphr from *P. andruzzii*. CPDphr was spectroscopically analyzed directly after purification (black), after treatment with blue light and the reducing agent TCEP (blue), or after a resting time of one day at 4 °C in the dark (grey). Illumination was performed for one minute at a wavelength of 450 nm (200 µmol photons m^{-2} s^{-1}). TCEP was added at the indicated concentration and incubated for 5 minutes at room temperature. Spectroscopic measurement was performed using the Implen NP-80.

2.18 The Cys50 in CPDphr modulates the intracellular localization in *A. nidulans*

In order to evaluate CPDphr as an intracellular redox sensor and to compare its intracellular functions with those of CryA, it was deemed valuable to analyze whether CPDphr responds in a similar manner to exogenous ROS as CryA does. To test this hypothesis, the protein's coding sequence was cloned into the pMCB17apx vector and fused to N-terminal GFP under the control of the *alcA* promoter (pAUL106). The vector was then transformed into *A. nidulans* (sAUL43), and the fluorescence signal was analyzed under a fluorescence microscope **(Fig. 35a)**. Unlike CryA, which is exclusively nuclear, the overexpression of GFP-CPDphr resulted in nuclear and cytosolic localization. To see if CPDphr can shuttle in *A. nidulans*, cells expressing

GFP-CPDphr were treated with 10 mM H_2O_2 **(Fig. 35a)**. Similar to CryA, contact with exogenous hydrogen peroxide triggered the mitochondrial association of CPDphr. However, only the cytosolic protein appeared to shuttle to the mitochondria, whereas the nuclear protein remained in the nucleus.

The N-terminal extension (NTE) of CPDphr contains a cysteine residue (Cys50), which may be involved in sensing reactive oxygen species. To test if the H_2O_2-induced conformational shift and subsequent shuttle are a result of Cys50 oxidation, the deletion mutant CPDphr^{C50A} (pAUL108) was generated and transformed into *A. nidulans* (sAUL44). Fluorescence microscopy was performed identically to that of the native CPDphr **(Fig. 35b)**. The Cys50 deletion mutant was now exclusively localized in the nucleus, and treatment with hydrogen peroxide did not result in any mitochondrial signal. These results suggest that CPDphr responds to exogenous ROS similarly to CryA. Additionally, the Δ*cryA* strain should have been recomplemented with the *CPDphr* gene under the control of the native *cryA* promoter to determine whether CPDphr can rescue the phenotype under oxidative stress. This experiment was not conducted due to time constraints.

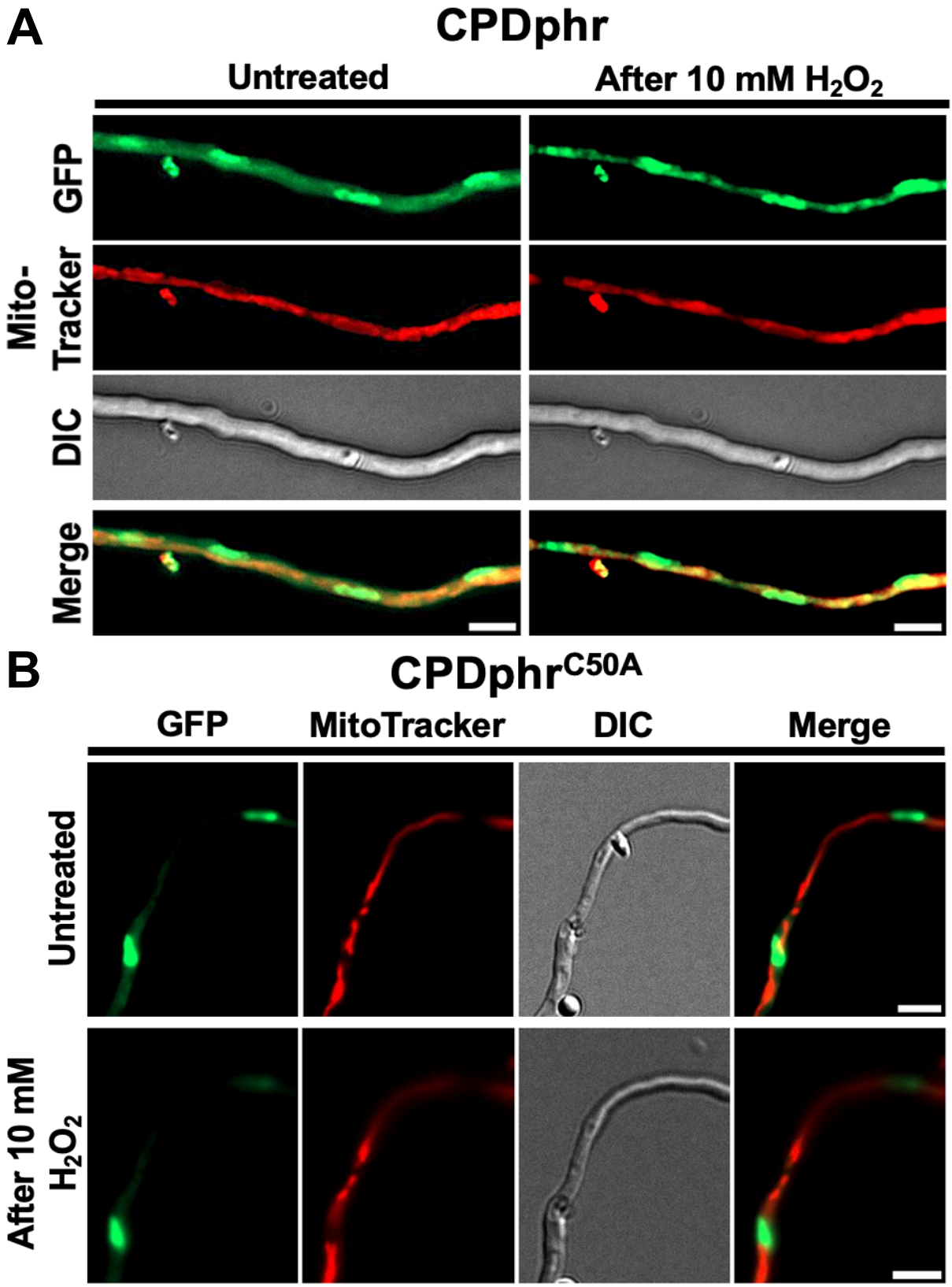

Figure 35: Localization of CPDphr and CPDphr^{C50A} before and after treatment with 10 mM H_2O_2. (A) Analysis of the fluorescence signal of the CPDphr photolyase fused to GFP before and after treatment with hydrogen peroxide. 1,000 spores were incubated overnight at 25 °C in minimal media with 2 % threonine to induce the promoter activity. MitoTracker staining was used to visualize mitochondria. The scale bar represents 5 µm. (B) Analysis of the fluorescence signal of the cysteine deletion mutant CPDphr^{C50A} fused to GFP before and after treatment with hydrogen peroxide. 1,000 spores were incubated overnight at 25 °C in minimal media with 2 % threonine to induce the promoter activity. MitoTracker staining was used to visualize mitochondria. The scale bar represents 5 µm.

3. Discussion

Light plays a critical role for fungal organisms as it serves as an early morning precursor signal, followed by various stress factors throughout the day. Since fungi are sessile organisms, they must employ a highly adaptive system to cope with and survive in changing environmental conditions. Photoreceptors, a conserved group of proteins with a light-sensitive chromophore that allows absorption of a specific wavelength of visible light, are a central part of this regulatory system (Yu & Fischer, 2019). The blue-light-sensitive WCC and the red-light-dependent phytochromes are the most well-described in fungal organisms. While the WCC is primarily known for its role in the circadian rhythm of *N. crassa*, phytochromes are major initiators of the light response in *A. nidulans* (Olmedo et al., 2013; Hedtke et al., 2015; Yu et al., 2016). Although many results show that phytochrome promotes the light response in *A. nidulans*, little is known about how the fungus regulates this response.

The results presented here show that photolyase CryA from *A. nidulans* is a CPD I photolyase that contains FAD and 5,10-MTHF as chromophores. CryA expression is stimulated by light and CryA is a nuclear protein. Deletion or overexpression of *cryA* interferes with the development and secondary metabolism of *A. nidulans*. CryA interacts directly with FphA and AtfA in the nucleus, where it negatively regulates the light response by preventing histone modification via FphA. Notably, CryA also responds to reactive oxygen species, negatively affecting resistance to oxidative stress through interaction with AtfA. When H_2O_2 is applied, CryA leaves the nucleus and rapidly travels to the mitochondria. This behavior depends on a cysteine residue in an N-terminal extension of the protein. A similar molecular mechanism has been identified in the CPD photolyase CPDphr from *P. andruzzii*, suggesting evolutionary conservation of photolyases with regard to oxidative stress. These findings establish CryA as a key regulator of general stress and light responses in *A. nidulans* and reveal a nuclear-mitochondrial shuttle as a novel regulatory mechanism, identifying CryA as a potential ROS sensor. CryA will be discussed in three parts: (i) its light-independent functions in development; (ii) its role in the light response; and (iii) its involvement in adapting to oxidative stress.

3.1 The light-independent functions of CryA

A. nidulans employs a tightly regulated network of developmental systems that act synergistically or antagonistically to precisely regulate reproduction, growth, and differentiation, depending on the environment (Blumenstein *et al.*, 2005; Rodriguez-Romero *et al.*, 2010). In soil, *A. nidulans* favors sexual reproduction over asexual conidiation to increase genetic diversity and prepare for environmental changes (Bayram *et al.*, 2008b; Rodriguez-Romero *et al.*, 2010; Ruger-Herreros *et al.*, 2011). In this dark environment with stable thermal fluctuations and low oxygen levels, the trimeric Velvet complex (composed of VeA, VelB and LaeA) is localized in the nucleus and acts as a positive master regulator of sexual morphogenesis and secondary metabolism (Bayram *et al.*, 2008b; Bayram *et al.*, 2016). Upon perceiving light, phytochrome binds to VeA and LaeA, promoting the nuclear export of VeA and subsequent disassembly of the Velvet complex. This is followed by genetic reprogramming of the reproductive cycle, initiating asexual development (Purschwitz *et al.*, 2009; Röhrig *et al.*, 2013). Interestingly, CryA has been suggested as a light-dependent inhibitor of *veA* expression. In a *cryA* deletion strain, the formation of Hülle cells and the number of cleistothecia increased (Bayram *et al.*, 2008a).

To expand on these results, several growth assays were conducted comparing a *cryA* deletion strain with a *cryA* overexpression strain regarding their vegetative growth and number of cleistothecia. Intriguingly, the overexpression strain exhibited a strong reduction in pigment synthesis, cleistothecia numbers, and conidia production, resulting in white (fluffy) colonies. This effect was light-independent, indicating an additional role for CryA in the repression of development in *A. nidulans*. Furthermore, this effect was also visible in expression profiles of the overexpression strain. The expression of several asexual transcription factors was severely downregulated.

This raises the question of how CryA can perform regulatory functions in the dark. Early studies of the mammalian circadian clock revealed a class of light-independent cryptochromes that interact with the CLOCK-BMAL1 complex, thereby inhibiting the circadian rhythm (Griffin *et al.*, 1999; Chaves *et al.*, 2006). Furthermore, recent studies have shown that CRY1 and CRY2 from *A. thaliana* also harbor regulatory functions independently of light and can interact with the plant phytochrome PhyB, despite lacking the essential CTE domain for protein interactions (Hughes *et al.*, 2012; Zeng *et al.*, 2025). The oligomer state is crucial for determining whether functions occur in the dark or are activated by light. Non-photoexcited CRY2 does not form a

homodimer and can therefore inhibit the transcription of cell-division genes. Upon perceiving blue light, CRY2 homodimerizes and triggers long root formation (Zeng *et al.*, 2025).

A similar mechanism may be present for CryA. SEC experiments revealed that CryA homodimerizes upon treatment with either H_2O_2 or blue light, whereas dark conditions mostly result in a monomer. This structural differentiation, dependent on external factors, may explain how CryA modulates developmental decisions in the dark and the early light response to red and blue light, as well as the oxidative stress response. Cys42, which is important for ROS sensing, may be essential for dimer formation. Blue light absorption can induce ROS production through the oxidation of photoactivated FADH-, which could contribute to the formation of disulfide bridges between two CryA proteins (Arthaut *et al.*, 2017; El-Esawi *et al.*, 2017). It would be valuable to study, via *in vitro* assays, whether $CryA^{C42A}$ can dimerize and whether it retains its physiological functions in the dark.

The photolyase CPDphr in *P. andruzzii* is capable of independently repairing DNA damage induced by oxidative stress. This novel function can be explained by the notable fact that it survived in complete darkness for over a million years, resulting in photoreceptors becoming redundant or additional functions evolving, as described in CPDphr (Li *et al.*, 2025a). A similar case may also apply to CryA in *A. nidulans*. Typically, most fungal organisms harbor at least two different CPF members in their genome: one CPD photolyase for DNA repair and one CRY-DASH for blue-light-induced regulatory functions (Tagua *et al.*, 2015; Deppisch *et al.*, 2022). However, the majority of the *Aspergillus* species only harbor one CPD I photolyase, which might have led to the acquisition of new regulatory functions (Bayram *et al.*, 2008a). Interestingly, such dual-mode photolyases with dark functions have primarily been described in fungal organisms until now. The photolyase PHR1 from *T. atroviride* represses the activity of the WCC homologues BLR1 and BLR2 (blue light receptors) in darkness yet remains crucial for photoreactivation (Berrocal-Tito *et al.*, 2007; García-Esquivel *et al.*, 2016). The 6-4 photolyase PHL1 from *C. zeae-maydis* plays a key role in the expression of other photoreceptors independently of light (Bluhm & Dunkle, 2008). These results suggest that additional functions are evolutionary conserved for CPF proteins in fungal organisms in order to fine-tune responses in different light conditions.

Deletion of *cryA* resulted in a significant increase in secondary metabolism, particularly in the dark. This was indicated by the appearance of several additional bands in the TLC analysis, as well as a deep brownish hue, which contrasts starkly with the greenish color of the WT. This overproduction of additional metabolites was completely abolished in the overexpression mutant, as evidenced by the complete loss of color and significantly fewer bands on the TLC. The increased numbers of cleistothecia and Hülle cells in the *cryA* deletion strain suggest that CryA represses sexual reproduction and metabolite synthesis, which are generally under the control of the velvet complex (Bayram *et al.*, 2008b; Gerke & Braus, 2014; Bayram *et al.*, 2016; Strohdiek *et al.*, 2025). However, functional protein-protein interaction between CryA and VeA was not observed (results not shown). Therefore, these results allow only to speculate about a possible function of CryA in development. Recent studies have revealed the zinc cluster transcription factor SclB (sclerotia-like B) to be a major transcription factor for asexual development and secondary metabolism. Deletion of *sclB* results in yellowish/white colonies and fewer conidia, which is attributed to significantly weaker expression of the conidiation factors *brlA* and the fluffy genes (*flbB–flbE*). Furthermore, SclB promotes the production of several polyketides, notably emericellamide and sterigmatocystin (Thieme *et al.*, 2018; Bastakis *et al.*, 2026). Surprisingly, recent results revealed that SclB also modulates the switch from vegetative growth to asexual development in *A. nidulans* and promotes expression of *veA* and *velB* light-independently (Bastakis *et al.*, 2026).

The *cryA*OE strain exhibits a comparable phenotype to the deletion strain of *sclB*, accompanied by similar changes in gene expression of asexual transcription factors and reduction of secondary metabolism. These results indicate that CryA can possibly suppress the activity of SclB, either genetically or through direct interaction, explaining the stark differences in asexual and sexual development in the *cryA* mutant strains. Further experiments, such as interaction studies between CryA and SclB, are needed, but it appears likely that CryA modulates the activity of different developmental master regulators and plays a key role in balancing asexual conidiation and sexual reproduction. In addition, while light generally suppresses secondary metabolism, CryA may act as a light-independent inhibitor of velvet functions, helping to maintain homeostasis in non-stress conditions.

3.2 The role of CryA in the light response

The activation of light-dependent genes should be a transient process; otherwise, the organism would waste too much energy in prolonged illumination conditions throughout the day. Therefore, the effect of promoting the light response needs to be negatively regulated in order to enable precise control at varying light levels (Bayram & Bayram, 2023). In *N. crassa*, positive regulation through the WCC is fine-tuned at two different stages in blue light conditions. The expression of the circadian rhythm-associated protein FRQ is activated by the WCC. FRQ then heterodimerizes with the frequence-interacting helicase FRH, which leads to the recruitment of several protein kinases and subsequent hyperphosphorylation and inactivation of the WCC. This process resembles a classic negative feedback loop and resets the clock in *N. crassa* (Cheng et al., 2001; Froehlich et al., 2003; Schafmeier et al., 2005; Hunt et al., 2010*)*. The fungus also employs an additional regulatory system in the form of the blue light-dependent protein VVD, which dampens the activity of the WCC. VVD disrupts the homodimerization of WC-1 and WC-2 by competitively interacting with WC-1, thereby inhibiting late photoadaptation in *N. crassa* (Hunt et al., 2010; Gin et al., 2013; Olmedo et al., 2013; Dasgupta et al., 2015).

A similar process has now been observed with CryA in *A. nidulans*. Here, *cryA* expression depends on FphA and AtfA following light exposure. CryA accumulates and interacts with both proteins, thereby disrupting the activation of its own expression and the light response in general. Therefore, the negative action of CryA could be considered a photoadaptation process, given that *cryA* is light-induced and acts comparable to a negative feedback loop. However, CryA does not interrupt late photoadaptation steps for light-dependent genes. Therefore, it appears likely that CryA fine-tunes the early light response in a manner similar to the VVD homologue from *T. reesei*: the PAS/LOV domain-containing inhibitor of the light response, Envoy 1 (ENV1). This protein, together with the CPF members Phr1 and Cry1, negatively regulates the photoresponse, which is controlled by the WC-1 homologue BLR1, in several *Trichoderma* species (Berrocal-Tito *et al.*, 2007; Tisch *et al.*, 2014; Lokhandwala *et al.*, 2015; García-Esquivel *et al.*, 2016; Schmoll, 2018). As there are no VVD or FRQ orthologues present in the genome of the *Aspergillus* family, CryA and its orthologues could potentially serve as replacements for these proteins. Interestingly, the two important pathogens *A. fumigatus* and *A. flavus* exhibit late photoadaptation of light-dependent genes which has a stark influence on the stress response and the

secondary metabolism (Fuller *et al.*, 2013; Idnurm, 2013; Fuller *et al.*, 2016; Jia *et al.*, 2024). However, it is unclear what exactly mediates this process. Now that CryA has been described as a negative regulator of phytochrome activity in *A. nidulans*, it would be valuable to analyze the role of other *Aspergillus* photolyase orthologues in light/stress sensing, regarding their high degree of homology with CryA. Given the importance of the stress response in determining *A. fumigatus'* ability to infect human cells, further research in this area is warranted (Keller *et al.*, 2005).

The concurrent interactions of CryA with both FphA and AtfA in order to modulate the photoresponse raise the intriguing question of why this pathway requires two-sided regulation. The phytochrome FphA localizes to the cytoplasm, where it initiates the HOG pathway through its interaction with the phosphotransfer protein YpdA. This binding event triggers a MAP kinase signaling cascade, which transfers the signal into the nucleus to ultimately activate the transcription factor AtfA (Idnurm & Bahn, 2016; Yu *et al.*, 2016). In addition to this cytoplasmic function, a fraction of FphA also has a nuclear function in chromatin remodeling, which is inhibited by CryA (Hedtke *et al.*, 2015). Because AtfA functions downstream of FphA, the physical interaction between CryA and AtfA effectively regulates the transcriptional effect of FphA. Crucially, this CryA-AtfA complex modulates not only the light response but also the oxidative stress pathway. Consequently, CryA inhibits both functional roles of FphA and integrates this signaling together with the light-independent modulation of the oxidative stress response.

While this regulation clearly relies on direct protein-protein interactions, the precise biochemical mechanism remains to be elucidated. It is currently unknown whether CryA binding induces conformational shifts in its target proteins, creates steric hindrance that blocks other binding partners, or directly alters the kinase or phosphatase activity of FphA. Similar mechanistic paradigms are well-documented in plants; for instance, in *A. thaliana*, the cryptochromes CRY1 and CRY2 physically interact with the transcription factors PIF4 and PIF5, thereby competing with phytochrome and preventing downstream signaling (Pedmale *et al.*, 2016). It has also been demonstrated that CRY1 and CRY2 can functionally interact with the phytochrome PhyA. In this scenario, however, PhyA mediates the phosphorylation of both cryptochromes (Casal, 2000; Más et al., 2000; Wang et al., 2018a). Consistent with these regulatory mechanisms, light-dependent physical interactions have been documented between several phytochrome and cryptochrome pairs, specifically PhyA-

CRY1, PhyB-CRY2, and PhyB-CRY1. Within this interactive network, it is proposed that CRY1 functions as a negative regulator of the red-light signaling pathway in plants (Casal, 2000; Hughes *et al.*, 2012). Therefore, it seems likely that a similar mechanism evolved independently in fungal species, which further signifies the link between red-light- and blue-light-dependent systems.

In addition to controlling light-regulated genes, some of which play a role in development, it is unclear whether the developmental effects in *A. nidulans* can be explained by interaction with FphA and/or AtfA. It is conceivable that CryA interacts with other cellular targets in an unknown way. Another possible explanation for the observed phenotypes is the role of CryA in controlling the redox homeostasis of the cell. Treatment with either ROS or blue light induces the formation of a CryA homodimer. Studies have revealed that continuous illumination with blue light induces cryptochrome-dependent H_2O_2 formation, which is hypothesized to serve as an intracellular signal in *A. thaliana* and *Alternaria alternata* (Ahmad, 2016; Arthaut et al., 2017; El-Esawi et al., 2017; Schuhmacher et al., 2024). This process may be similar for CryA. During the initial photoresponse, CryA accumulates and interacts with AtfA and FphA, thereby preventing overstimulation. Following continuous illumination, CryA produces hydrogen peroxide, inducing a conformational shift in the protein and subsequent export out of the nucleus. This negates the effects of CryA, resulting in the upregulation of photopigments and other light-induced genes that protect against prolonged exposure to light. This would explain why the overexpression of *cryA* leads only to the inhibition of the early light response but drops to comparable WT levels after longer illumination intervals. To test this theory, localization studies using CryA tagged with GFP and continuous blue light illumination should be conducted to see whether the protein successfully shuttles to the mitochondria or is retained in the nucleus.

3.3 The role of CryA in the oxidative stress response

In *A. nidulans*, oxidative stress triggers the upregulation of both *cryA* and various anti-stress genes, with the CryA protein interacting with AtfA to fine-tune this genetic response. A notable finding from this study presented here is the rapid translocation of CryA from the nucleus to the mitochondria. Because this shuttling depends on the N-terminal extension, suggests a novel mechanism in which conformational changes in cryptochromes directly dictate its subcellular location. This dynamic raise critical questions regarding how the NTE orchestrates this movement and the ultimate

biological purpose of the translocation. The prevailing hypothesis is that extensive blue and UV light exposure generates high levels of reactive oxygen species, which damage DNA and trigger this shuttling event. By exiting the nucleus, CryA removes its inhibitory effect on the stress response, allowing a stronger expression of protective antioxidant genes and photopigments. This regulatory mechanism closely parallels how light influences the velvet complex, where negative regulatory elements are similarly exported from the nucleus to alter developmental pathways. (Strohdiek *et al.*, 2025). Alternatively, CryA may be translocated to the mitochondria to serve as a rapid-response factor, where it catalyzes DNA repair and prevents the fragmentation of mitochondrial DNA (Takahashi *et al.*, 2011; Takahashi *et al.*, 2014). Previous studies have shown that CryA exhibits DNA repair activity, but this does not appear to be necessary for functional photoreactivation and protection against UV-damage (Bayram *et al.*, 2008a). Consequently, CryA may not be essential for mitochondrial DNA repair after strong UV irradiation but instead exerts a vital regulatory function inside the mitochondria. This aligns with mechanisms identified in *Drosophila*, where CRY activity is closely connected to the respiratory chain; when complexes III and V are inhibited, the resulting spike in intracellular ROS production effectively blocks CRY from regulating the circadian clock (Zheng *et al.*, 2024). Taken together, these findings imply a mechanistic link between CRY and the mitochondrial respiratory chain. Consequently, much like other CPD class I and II photolyases, CryA likely senses and responds to fluctuations in the mitochondrial redox state to promote organelle survival under stress.

The observed response to external ROS by CryA provides a mechanistic basis for the distinct developmental phenotypes of the *A. nidulans cryA* deletion strain and overexpression mutants. This points to the active participation of CryA in the oxidative stress response, a tightly regulated system utilizing multiple pathways to regulate antioxidant enzymes. This regulation is highly dynamic across the *A. nidulans* life cycle, relying on complementary enzymes such as CatA in spores and CatB in vegetative hyphae (Navarro *et al.*, 1996; Kawasaki *et al.*, 1997; Kawasaki & Aguirre, 2001; Yaakoub *et al.*, 2022). In addition, GlrA and TrxA are involved in balancing intracellular redox homeostasis (Sato *et al.*, 2009; Liu *et al.*, 2025). The differential expression of these antioxidant genes in the Δ*cryA* mutant is likely mediated by AtfA. Alongside AtfA, the bZIP transcription factor NapA plays a critical role in orchestrating the oxidative stress response. Upon oxidation by ROS, NapA translocates to the nucleus, where it

actively upregulates key antioxidant defenses, including catalase B, the thioredoxin system, and glutathione reductase (Mendoza-Martínez *et al.*, 2017; Yaakoub *et al.*, 2022; Liu *et al.*, 2025). This provides a parallel signaling pathway, independent of the HOG-pathway, to confer resistance to ROS. In conclusion, the ROS-triggered translocation of CryA serves a dual molecular purpose: it safeguards the mitochondria from oxidative damage while simultaneously relieving CryA-mediated repression in the nucleus, thereby activating stress resistance networks via AtfA, FphA, and potentially NapA.

Equally intriguing is the role of the NTE in the subcellular localization of CryA. While full-length CryA resides in the nucleus and translocates to the mitochondria upon H_2O_2 exposure, mutant CryA lacking the NTE localizes exclusively to the mitochondria. There are two theories: first, the NTE undergoes proteolytic cleavage which exposes a possible MTS; however, in experiments using N-terminally GFP-tagged CryA, the GFP-signal was still visible at the mitochondria, rendering this hypothesis unlikely. Second, nuclear CryA could be degraded and replaced by newly synthesized, mitochondria-targeted CryA. This is also improbable given the near-instantaneous nature of the translocation following H_2O_2 exposure. Therefore, it appears likely that the NTE masks a mitochondrial targeting sequence or inhibits interactions with nuclear export machinery. While mitochondrial localization has been observed in other CPF proteins, the precise mechanism behind it remains to be fully elucidated (Yasui *et al.*, 1992; Brudler *et al.*, 2003; Takahashi *et al.*, 2011; Zheng *et al.*, 2024). The rice CPD II photolyase can repair UV-B light-induced mitochondrial and plastidial DNA damage, which is accompanied by localizing in either mitochondria, plastids, or the nucleus (Takahashi *et al.*, 2011; Takahashi *et al.*, 2014). Interestingly, the KRK motif, which was critical for the nuclear localization of the rice photolyase, is also present in the NTE of CryA. Experimental deletion of the first 20 amino acids, or targeted substitution within this motif, effectively abolished the nuclear import of the protein. Furthermore, the MHWFR amino acid sequence, which was described to mediate mitochondrial DNA photoreactivation in *S. cerevisiae*, is predicted to function as a mitochondrial targeting sequence for CPD I photolyases (Yasui *et al.*, 1992). A similar motif (VHWFK) is present in CryA immediately after the NTE at positions 78-82. However, deleting this motif alone did not prevent mitochondrial localization, though it did prevent nuclear retention. Only the deletion of both motifs resulted in CryA being localized solely to the cytoplasm. This suggests that the KRK motif is essential for nuclear localization,

whereas changes to the amino acid sequence of the PHR domain result in an artificial signal. Overall, it seems that contact with ROS triggers a conformational change in the NTE, exposing an MTS and resulting in nuclear export and translocation to the mitochondria. This structural remodeling is likely triggered by the oxidation of specific redox-sensitive residues, namely cysteine and methionine. The generation of cysteine disulfide bonds and methionine sulfoxides determine the conformation and activity of proteins, functioning as precise on/off switches that modulate cellular reactions to oxidative stress (Miki & Funato, 2012; Kim *et al.*, 2014; Lim *et al.*, 2019). Substitution of Cys42 to alanine in CryA fully abolished the shuttle after H_2O_2 treatment, supporting the hypothesis that this amino acid is crucial for nuclear retention and mitochondrial transport.

To corroborate these findings, the photolyase CPDphr from *P. andruzzii* was examined. As CPDphr has been shown to perceive ROS light independently, it was deemed important to determine whether this protein exhibits a similar response to exogenous ROS in *A. nidulans*. Sequence analysis revealed that CPDphr contains an N-terminal extension comprising a single cysteine residue. Localization studies revealed that the protein localizes in the nucleus and cytoplasm. Treatment with exogenous H_2O_2 resulted in a shift from the cytoplasm to the mitochondria, though the nuclear signal remained unaffected. Removal of Cys50 abolished cytoplasmic localization and any visible shuttling after treatment with ROS. While there are parallels with the molecular mechanism of CryA, further research is needed to determine whether N-terminal cysteines are conserved and what role they play in sensing oxidative stress. Nevertheless, it seems probable that there is a significant and understudied relationship between light perception and ROS in the cryptochrome/photolyase family.

Investigating dual-localized proteins is inherently challenging, as whole-gene deletion abolishes functions in both compartments simultaneously. However, CryA presents a unique opportunity to investigate its role at both subcellular localizations. While the truncated CryA variant localizes solely at the mitochondria, the cysteine mutation restricts the protein entirely to the nucleus. Initially, formthe 'nucleus-only' variant, it was hypothesized that itw would phenocopy the wild-type, whereas the truncation mutant would mirror full *cryA* deletion. Strikingly, the results demonstrated the opposite. Compared to the full deletion, the 'mitochondria-only' strain was highly susceptible to H_2O_2, showing significantly dampened induction of all tested antioxidant

genes. Conversely, it exhibited resistance to menadione, characterized by substantial antioxidant gene upregulation. Most unexpectedly, the full Δ*cryA* strain displayed even stronger gene activation than the truncation mutant. This implies that mitochondrially localized CryA can still actively suppress the nuclear stress response, strongly indicating the presence of mitochondrial-nuclear communication. This mechanism is similar to the mitochondrial-nuclear retrograde signaling pathway observed in *Schizosaccharomyces pombe*, where the NapA homologue Pap1 is activated to increase efflux activity and restore redox homeostasis (Liu *et al.*, 2025; Fellas *et al.*, 2026).

Consequently, CryA likely modulates AtfA and NapA activity in a localization-dependent manner, regulating intracellular redox levels to prevent mitochondrial dysfunction and fine-tune the overarching stress response. While the truncated CryA variant is exclusively mitochondrial, H_2O_2 induced translocation of full-length CryA results in only a partial shift to the mitochondria. This implies that exposure to hydrogen peroxide triggers the relocation of only a specific fraction of the available CryA pool. Under basal conditions, maintaining a precise equilibrium between nuclear and mitochondrial CryA is likely essential for tightly regulating retrograde communication. Conversely, the cysteine-mutated strain demonstrated high tolerance to H_2O_2 stress, displaying an expression profile closely mirroring the full deletion strain. Although this strain also remained resistant to menadione, gene expression analysis showed only weak upregulation compared to the wild type. This divergence suggests that CryA employs distinct molecular mechanisms in response to menadione versus hydrogen peroxide. Something similar can be observed in the ROS sensor Yap1 in *S. cerevisiae*, where specific cysteine residues are essential for activation by H_2O_2 but remain unresponsive to other forms of ROS such as menadione and diamide (Wemmie *et al.*, 1997; Delaunay *et al.*, 2000). Therefore, Cys42 seems relevant not only for CryA localization, but also for its functionality upon perception of H_2O_2. This explains the phenotypical difference between the full *cryA* deletion phenotype compared to the Cys42 deletion strain.

3.4 Conclusion and model

In summary, this dissertation further demonstrated regulatory functions for the CPD photolyase CryA from *A. nidulans*. CryA plays an extensive role in the adaptation to different stress stimuli and is important for the intracellular activity of several regulators.

The results demonstrate that CryA is a negative regulator of the general stress- and light response in *A. nidulans*, revealing a nuclear-mitochondrial shuttle as a novel regulatory principle. CryA is also identified as a potential ROS sensor. While the general underlying mechanism appears to be like a negative feedback loop, it is not fully elucidated, how CryA can be involved in so many physiological responses **(Fig. 36)**. Furthermore, genome wide analysis of gene expressions in the *cryA* mutant strains under different stress conditions needs to be conducted to further identify molecular targets of CryA. Additionally, integrative studies of more photolyases and cryptochromes and their connection to oxidative stress should be conducted as it appears likely that this is a more conserved mechanism than expected. This would be particularly valuable for studying the CPF proteins of the human pathogen *A. fumigatus* and the plant pathogen *A. flavus*, and their role in the stress response against the target host defense system.

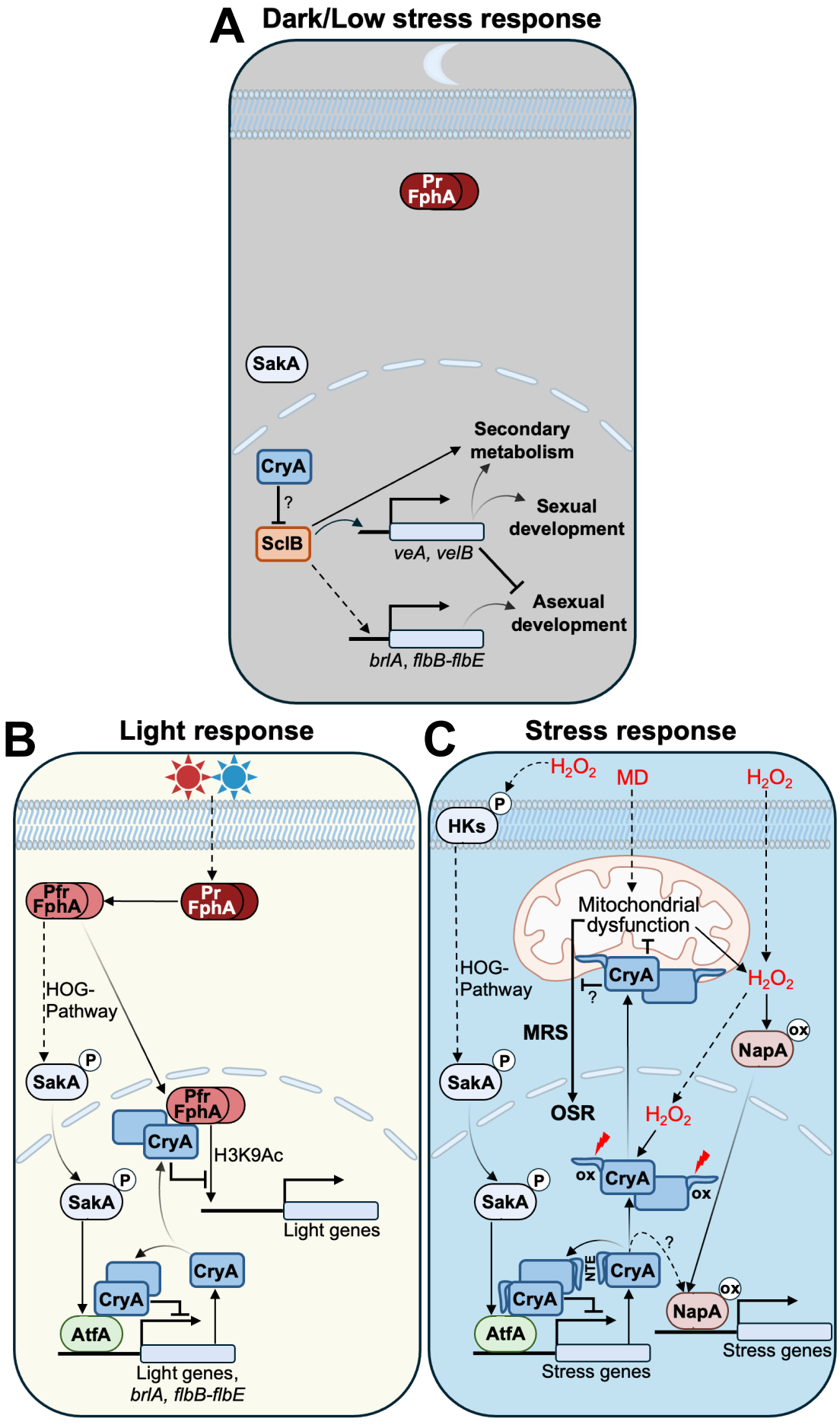
A
Dark/Low stress response
Pr FphA
SakA
CryA
?
SclB
Secondary metabolism
Sexual development
veA, velB
Asexual development
brlA, flbB-flbE
B
Light response
Pfr FphA
Pr FphA
HOG-Pathway
SakA
P
Pfr FphA
CryA
H3K9Ac
Light genes
SakA
P
CryA
CryA
AtfA
Light genes, brlA, flbB-flbE
C
Stress response
H2O2
MD
H2O2
HKs
P
Mitochondrial dysfunction
HOG-Pathway
CryA
?
H2O2
MRS
NapA
ox
SakA
P
OSR
H2O2
ox
CryA
ox
SakA
P
NTE
CryA
CryA
?
ox
NapA
AtfA
Stress genes
Stress genes

Figure 36: Current model of the CryA regulated dark, light, and stress response in *A. nidulans*. (A) In dark and low-stress conditions, CryA is only expressed at a basal level and FphA is inactive and localized in the cytosol. CryA may modulate the developmental machinery of *A. nidulans* by balancing the activity of the master regulator SclB. SclB controls the expression of the sexual transcription factors *veA* and *velB*, as well as the conidiation factors *brlA* and the *fluffy* genes *flbB–flbE*. Furthermore, SclB promotes secondary metabolism in the dark together with the velvet complex. (B) Exposure to red or blue light induces a conformational shift in the homodimerized phytochrome FphA from its inactive (Pr) to its active (Pfr) state. Photoactivated FphA triggers the HOG pathway, transmitting a signal via SakA (HogA) to the nuclear transcription factor AtfA to drive the transcription of light-responsive genes. Additionally, FphA can translocate to the nucleus to mediate targeted chromatin remodeling. Conversely, the blue-light receptor CryA accumulates in the nucleus; upon blue light exposure, it homodimerizes and physically interacts with FphA and AtfA, creating a negative-feedback loop that represses the light response and FphA mediated histone modification. (C) Reactive oxygen species, such as H_2O_2, activate the HOG pathway together with AtfA signaling and induce the nuclear import of NapA to trigger the expression of stress genes. Upon encountering ROS, nuclear CryA homodimerizes and fine-tunes this response by modulating the activation of both NapA and AtfA. Crucially, H_2O_2 exposure oxidizes cysteine 42 within NTE of CryA. This drives a conformational change that forces CryA to translocate from the nucleus to the mitochondria. Once there, CryA mitigates menadione (MD)-induced mitochondrial dysfunction and limits the generation of additional H_2O_2 molecules, thereby suppressing mitochondrial retrograde signaling (MRS) and the subsequent broader oxidative stress response (OSR).

4. Material and Methods

4.1 Chemicals

All chemicals used in this work were obtained from Roth (Karlsruhe), Sigma (Taufkirchen), Invitrogen (Karlsruhe), Roche (Mannheim), Applichem (Darmstadt), IBA (Göttingen), and Serva Feinbiochemica (Heidelberg), unless otherwise stated. Enzymes and DNA and protein markers were provided by New England Biolabs (Frankfurt), Thermo Scientific (Waltham, Massachusetts, USA), and Fermentas (St-Leon-Rot).

4.2 Kits and consumables

All kits and consumables which were used in this work are listed in Table 1.

Table 1: List of the used kits and the manufacturer.

Kit	Manufacturer
NucleoSpin® Plasmid EasyPure	Macherey-Nagel
FastGene Gel/PCR Extraction Kit	NIPPON Genetics EUROPE GmbH
NEBuilder® HiFi DNA Assembly	New England Biolabs
Vivaspin 6 and 20; 10.000, 30.000, 50.000 MWCO	Sartorius AG, Göttingen
TURBO DNA-free™ Kit	ThermoFisher Scientific, Invitrogen
SuperScript Double-Stranded cDNA Synthesis	ThermoFisher Scientific
Luna® Universal One-Step RT-qPCR Kit	New England Biolabs
PD-10 desalting columns packed with Sephadex™ G-25 resin	Cytiva
ChIP DNA Clean & Concentrator	Zymo Research US
Protein G PLUS-Agarose:	Santa Cruz Biotechnology
Anti-Histone H3 antibody	Abcam
Anti-acetyl-Histone H3 (Lys9) antibody	Merck Millipore
Qubit™ Protein Broad Range Assay Kit	Thermo Fisher Scientific
Gel Filtration Markers Kit	Merck Millipore
Thin layer chromatography glass plates	Macherey-Nagel

4.3 Devices

All devices which were used for this work are listed in Table 2.

Table 2: List of the used devices, their names and the manufacturer.

Device	Name	Manufacturer
Centrifuge	Universal 320R Micro Star 21R cooled Sorvall Lynx4000	Andreas Hettich GmbH VWR ThermoScientific
FPLC	ÄktaPure	Cytiva
HPLC	Vanquish Core HPLC systems	Thermo Fisher Scientific
Sonicator	Q800R3	QSonica
Rotary mixer	Multi-Purpose Tube Rotator	Thermo Fisher Scientific
Chromatography columns	StrepTrap XT, 5 ml HisTrap HP, 5 ml Superdex 200 Increase 10/300 GL	Cytiva
Gele documentation system	FastGene® FAS-V Imaging System	Peqlab
Immunoblot imager	Amersham ImageQuant 800	Cytiva
Fluorometer	Qubit™ 4.0	Invitrogen
High pressure homogenizer	EmulsiFlex-C3	Avestin, Inc.
Thermocycler	Labcycler	SensoQuest GmbH
qRT-PCR cycler	CFX Connect Real-Time PCR Detection System	Bio-Rad
Incubator	HT Infors Ecotron B40 MaxQ™ 6000	Edmund Bühler GmbH Memmert GmbH ThermoScientific
Compressor	6-15 Compressor	JunAir

SDS PAGE blotting device + power unit	Power Pac 3000 Mini-PROTEAN Tetra Vertical Electrophoresis Cell Mini Trans-Blot® Cell	Bio-Rad
Photometer	NP-80	Implen
	V-750	JASCO GmbH
Gel electrophorese system	Powersupply EV222 PerfectBlue™ Gelsystem Mini L	Peqlab
Microscope	AxioImager Z1 Stemi DV4	Zeiss
Light boxes	Self-made	Christian Streng
BLItz system	Octet N1	Satorius

4.4 Strains

All strains created and used in this work are listed in Table 3.

Table 3: List of the generated strains and the correspondent genotype.

Strain	Genotype	Reference
sKV103	*pyrG89; pyroA4; veA+*	(Blumenstein *et al.*, 2005)
sJR2	*pyrG89; pyroA4; veA+; ∆nku*::*argB*	(Hedtke *et al.*, 2015)
sJP2	*pyroA4*; ∆*fphA*::*argB, veA+*	(Purschwitz *et al.*, 2008)
sKL15	*pyroA4; alcA(p)::stuA-NLS::DsRed*	(Leister *et al.*, 2025)
sAUL1	*alcA(p)::YFPC::cryA* *alcA(p)::YFPN::fphA* in sKV103	This work
sAUL2	*alcA(p)::cryA::trpC(t)* in sKV103	This work
sAUL3	*alcA(p)::GFP::cryA* in sKV103	This work
sAUL6	*alcA(p)::YFPN::cryA* *alcA(p)::YFPC::fphA* in sKV103	This work
sAUL11.2	∆*cryA* in sJR2	This work
sAUL20	*alcA(p)::YFPC::cryA*	This work

	alcA(p)::YFPN::atfA in sKV103	
sAUL21	*alcA(p)::YFPN::cryA* *alcA(p)::YFPC::atfA* in sKV103	This work
sAUL23	Δ*cryA,* Δ*fphA* Crossing between sAUL11.2 and sJP2	This work
sAUL24	*alcA(p)::GFP::*Δ*NTE20cryA* in sKV103	This work
sAUL26	*alcA(p)::GFP::*Δ*NTE60cryA* in sKV103	This work
sAUL30	*alcA(p)::*Δ*NTE70cryA::trpC(t)* in sAUL11.2	This work
sAUL32	*alcA(p)::GFP::cryA*^{C42A} in sKV103	This work
sAUL33	*cryA(p)::cryA* in sAUL11.2	This work
sAUL34	*alcA(p)::YFPC::cryA* *alcA(p)::YFPN::fphA* in sKL15	This work
sAUL35	*alcA(p)::YFPN::cryA* *alcA(p)::YFPC::fphA* in sKL15	This work
sAUL37	*alcA(p)::cryA*^{C42A}*::trpC(t)* in sAUL11.2	This work
sAUL38	*alcA(p)::GFP::cryA* in sKL15	This work
sAUL39	*alcA(p)::YFPN::lreA* *alcA(p)::YFPC::cryA* in sKV103	This work
sAUL40	*alcA(p)::GFP::*$^{\Delta KRK}$*cryA* in sKV103	This work
sAUL41	*alcA(p)::GFP::*$^{\Delta VHWFK}$*cryA* in sKV103	This work
sAUL42	*alcA(p)::GFP::*$^{\Delta KRK\Delta VHWFK}$*cryA* in sKV103	This work
sAUL43	*alcA(p)::GFP::CPDphr* in sKV103	This work
sAUL44	*alcA(p)::GFP::CPDphr*^{C50A} in sKV103	This work

4.5 Plasmids

All plasmids generated and used in this work are listed in Table 4.

Table 4: All generated plasmids and their integrated insert.

Name	Insert	Reference

pJP4	*alcA(p)::YFPN::fphA, pyro*	(Purschwitz *et al.*, 2008)
pJP5	*alcA(p)::YFPC::fphA, pyrG*	(Purschwitz *et al.*, 2008)
pASK_FphA*syn*	*tet(p)::AnfphAsyn::strep-tag,* AmpR	(Brandt *et al.*, 2008)
pACYCDuet-1_bphO	*lac(p)::bphO* (*bphO* from *P. aeruginosa* (PA4116) in pACYCDuet-1); CmR	(Yu *et al.*, 2019)
pMCB17apx	*alcA(p)::gfp; pyr4; ampR*	(Veith *et al.*, 2005)
pET28a	T7(p)::*6xHis*::T7(t)	Novagen
pALBL9	*alcA(p)::YFPN::lreA, pyro*	(Blumhofer, 2024)
pALBL33	*alcA(p)::YFPN::atfA, pyro*	(Blumhofer, 2024)
pALBL34	*alcA(p)::YFPC::atfA, pyrG*	(Blumhofer, 2024)
pAUL3	*alcA(p)::YFPC::cryA, pyrG*	This work
pAUL4	*alcA(p)::YFPN::cryA, pyro*	This work
pAUL5	*alcA(p)::cryA::trpC(t), pyrG*	This work
pAUL6	*alcA(p)::GFP::cryA, pyrG*	This work
pAUL12	*∆cryA x pJEt1.2, pyrG*	This work
pAUL13	T7*(p)::6xHis-tag::cryA*::T7*(t),* Kanamycin	This work
pAUL15	*cryA(p)::cryA, pyrG*	This work
pAUL32	*alcA(p)::GFP::∆20NTE-cryA, pyrG*	This work
pAUL34	*alcA(p)::GFP::∆60NTE-cryA, pyrG*	This work
pAUL44	*alcA(p)::∆70NTE-cryA::trpC(t), pyrG*	This work
pAUL81	*alcA(p)::GFP::$^{\Delta 4\text{-}6(KRK)}$cryA, pyrG*	This work
pAUL82	*alcA(p)::GFP::$^{\Delta 77\text{-}82(VHWFR)}$cryA, pyrG*	This work
pAUL83	*alcA(p)::GFP::$^{\Delta 4\text{-}6(KRK),\Delta 77\text{-}82(VHWFR)}$cryA, pyrG*	This work

pAUL93	*alcA(p)::cryA^{C42A}::trpC(t), pyrG*	This work
pAUL103	*tet(p)::fphAsyn^{C195A}::strep-tag,* Ampicillin	This work
pAUL106	*alcA(p)::GFP::CPDphr, pyrG*	This work
pAUL107	*tet(p)::CPDphr::strep-tag,* Ampicillin	This work
pAUL108	*alcA(p)::GFP::CPDphr^{C50A}, pyrG*	This work
pAUL111	*tet(p)::CPDphr::strep-tag,* Ampicillin	This work

4.6 Oligonucleotides

All oligonucleotides used in this work are listed below in Table 5.

Table 5: The names of the relevant oligonucleotides, their sequences, and descriptions of their fields of usage.

Name	Sequence 5´ to 3´	Description
CryA YFPC Efi for	catgaaccacGGCGCGCCgATGCGGCAGAAGCGCAAAC	N-terminal YFPC fusion
CryA YFPN Efi for	CCATCGCCACGGCGCGCCGATGCGGC AGAAGCGCAAAC	N-terminal YFPN fusion
CryA GFP Efi for	GAACTATACAAAGGCGCGCCGATGCGGCAGAAGCGCAAAC	N-terminal GFP fusion
CryA GFP/YFP Efi rev	ctagaggatccTTAATTAATTATGCTCCCCGCGCAGC	N-terminal YFP/GFP fusion
CryA -GFP +trpC Efi for	CAGTTAATTAGGGCGCGCCgATGCGGCAGAAGCGCAAAC	Overexpression backbone
CryA -GFP +trpC Efi rev	gtaacgttaagtTTAATTAATTATGCTCCCCGCGCAGC	Overexpression backbone
CryA pET28a for	ggtgccgcgcggcagccatATGCGGCAGAAGCGCAAAC	Heterologous expression of CryA

CryA pET28a rev	gtggtggtggtggtgctcgaGTGCTCCCCGCGCAGCATCC	Heterologous expression of CryA
pyrG ΔcryA 2000 bp US for	AAACTTCGCAAGCTTGGAACGATCTTCATCATTCGTCGCTTTC	Homologous recombination of CryA
pyrG ΔcryA 2000 bp DS rev	TATGAACTGGACCTGTATATACTGCTTCCTCAACCTCTCGA	Homologous recombination of CryA
ΔcryA 2000 bp US for	GGCTCGAGTTTTTCAGCAAGATCTAGAACCATGTACGTGCTAAAAC	Homologous recombination of CryA
ΔcryA 2000 bp US rev	GTTCCAAGCTTGCGAAGTTTATTTG	Homologous recombination of CryA
ΔcryA 2000 bp DS for	TATATACAGGTCCAGTTCATATAACG	Homologous recombination of CryA
ΔcryA 2000 bp DS rev	AGGAGATCTTCTAGAAAGATGAAGGCCGCATGCCACCATCGCAT	Homologous recombination of CryA
ΔcryA PyrG Forward Primer Kontrolle	GAGCTCTCGTCAAGAGTGGAA	Test primer for Δ*cryA*
ΔcryA PyrG Reverse Primer Kontrolle	CATTTTGGGCCAAGGGTTTCTC	Test primer for Δ*cryA*
CryA N-trunc 20 GFP for	ATGGATGAACTATACAAAGGCGCGCCGCAAACGGCAGATTTCGGCATC	N-terminal fusion of GFP
CryA N-trunc 60 GFP for	CAT GGA TGA ACT ATA CAA AGG CGC GCC GTA CAC AGA GAC GAG CGC TCA	N-terminal fusion of GFP
atfA YFPC Efi for	AAC AGA AGG TCA TGA ACC ACG GCG CGC CGA TGT CTG CCG CCG TGG CT	N-terminal fusion of YFPC
atfA YFPN Efi for	TCA TGC GCT CCA TCG CCA CGG GCG CGC CGA TGT CTG CCG CCG TGG CT	N-terminal fusion of YFPN

atfA YFP Efi rev	GTC GAC TCT AGA GGA TCC TTA ATT AAT CAA GTG TAT GGA GGA TTC GGG	N-terminal fusion of YFPC/N/GFP
CryA ∆70 NTE cutoff OE for	GTT CTC TAC TCA GTT AAT TAG GGC GCG CCA ATG ACC GCG AAC GCG GCA	Overexpression of truncated CryA
CryA Del Cysteine in NTE to Ala for	GAA GCT TAC AAC AGC GGA ATC C	Deletion of cysteine to alanine
CryA Del Cysteine in NTE to Ala rev	ATTCCGCTGTTGTAAGCTTCGGCCC GCGCGTTGCTCATTTCTG	Deletion of cysteine to alanine
CryA native promoter in Efimov for	aaaacgacggccagtgaattGTGCAGGATG ATCGCATCGA	Recomplementation of *cryA*
CryA native promoter in Efimov rev	agttcttctcctttactcatGTTCCAAGCTTGC GAAGTTTATTTG	Recomplementation of *cryA*
CryA deletion NLS for	ATG GAT GAA CTA TAC AAA GGC G CG CCG ATGCGG CAG GCG GCC G CA CTC TCC AAT GGC GCTGAT GA	Deletion of NLS
CryA deletion MTS for	TCC GAT CTA CGT CTA CAC GAC	Deletion of MTS
CryA deletion MTS rev	CGT GTA GAC GTA GAT CGG ACG C CG CGG CTGCCG CCA CTG CCG C GT TCG CG	Deletion of MTS
FphA Deletion of C195 small fragment for	AAT GAA TAG TTC GAC AAA AAT CTA GAA ATA ATT TTG TTT AAC TTT AAG AAG GAG ATA TAC ATA TGA GCG AGC TGC CGA GC	Small fragment for deletion of cysteine
FphA Deletion of C195 small fragment rev	GGA ATA TGA ATC GGT TCA TCT TCG GCC GCT TTA AAG CTA TCC ACG GTA	Small fragment for deletion of cysteine
FphA Deletion of C195 big fragment for	GAA GAT GAA CCG ATT CAT ATT CCG	Big fragment for deletion of cysteine
FphA Deletion of C195 big fragment rev	CTC CAA GCG CTG AGA CCA TGG TCG CTA TGG GTA TAC GGG	Big fragment for deletion of cysteine

CPDphr GFP Efi for	TGG ATG AAC TAT ACA AAG GCG CGC CGA TGT CTG CAA ACA AGA ACA ATC TG	CPDphr fused to GFP
CPDphr GFP Efi rev	GAC TCT AGA GGA TCC TTA ATT AA C TAT ACAGAT ATC TTA GCA TTC A AA TT	CPDphr fused to GFP
CPDphr^{C50A} GFP for	GAG TTC AAC AAA AAG CGC	CPDphr cysteine deletion mutant fused to GFP
CPDphr^{C50A} GFP rev	AGG CGC TTT TTG TTG AAC TCG G CT CCC TGCGCT GCT CTG C	CPDphr cysteine deletion mutant fused to GFP
CPDphr heterologous expression for	ATG AAT AGT TCG ACA AAA ATC TA G AAA TAATTT TGT TTA ACT TTA AG A AGG AGA TAT ACATAT GTC TGC A AA CAA GAA CAA TCT GA	Heterologous expression of CPDphr
CPDphr heterologous expression rev	TCC AAG CGC TGA GAC CAT GGT C TA CAG ATATCT TAG CAT TCA AAT T AG GG	Heterologous expression of CPDphr
brlA_RT_Anid for	GGGACTTCCATACGGTAGCA	qRT-PCR
brlA_RT_Anid rev	TTCTGAGGGCATCCACAGTT	qRT-PCR
flbB_RT_Anid for	TGAGCGGAAGGAGCAATACA	qRT-PCR
flbB_RT_Anid rev	TTGGTGAACAGCAAGGTTCG	qRT-PCR
ccgA_RT_Anid for	CGCTTCCCTCACTTCTCGT	qRT-PCR
ccgA_RT_Anid rev	TTCTTAGCGGCCTCCTTGTG	qRT-PCR
ccgB_RT_Anid for	ATAACGCCGACCTGACTACG	qRT-PCR
ccgB_RT_Anid rev	TTGGCGGCTTCCTTGTAAAC	qRT-PCR
cryA_RT_Anid for	GCCGCATCATCAATCTCTGT	qRT-PCR
cryA_RT_Anid rev	TCGAATAAGCTTTGCCTCGC	qRT-PCR
AN11314_RT_Anid for	GCCTACTGAGTCGCAGACAA	qRT-PCR

AN11314_RT_Anid rev	GTAGATTGTATCGGCAGGGC	qRT-PCR
conJ_RT_Anid for	ACCAGAACCCCGGTAACTTC	qRT-PCR
conJ_RT_Anid rev	CAGAGTCCATACTGGCAAAGC	qRT-PCR
H2B_RT_Anid for	GAAGAAGCGCGGAAAGACC	qRT-PCR
H2B_RT_Anid rev	TAGACATAGCACGGGTGGAG	qRT-PCR
cetJ_RT_Anid for	TTC TAA ACC CAA CTC GCC CT	qRT-PCR
cetJ_RT_Anid rev	GAT GGG CGA CTG AGA GAT GA	qRT-PCR
AN8930_RT_Anid for	TTCGACCATCCTGAGCTGAA	qRT-PCR
AN8930_RT_Anid rev	GTTTGGCTAGCTCCTCGTTG	qRT-PCR
catA_RT_Anid for	TCG AAC TGA ACC GCA ACA TC	qRT-PCR
catA_RT_Anid rev	GGG TCG TCA GAG AAG TCG AT	qRT-PCR
catB_RT_Anid for	GTGGTGTTGACTTCACCGAG	qRT-PCR
catB_RT_Anid rev	TGGGCAACTGCTCAAAGTTC	qRT-PCR
glrA_RT_Anid for	TCACGTTCACAAGAAGCACC	qRT-PCR
glrA_RT_Anid rev	ATCTCCGAGCCATCGTTCAT	qRT-PCR
trxA_RT_Anid for	GCTAAACGCGCCTTTTCATC	qRT-PCR
trxA_RT_Anid rev	TGGAATTCGGCCTTAGAGGT	qRT-PCR
prxA_RT_Anid for	GTTATGCCATCGTCCTCGAC	qRT-PCR
prxA_RT_Anid rev	GTGCTTGATGACAGTCTCGG	qRT-PCR
ccgA_ChIP_Anid for	GTGGTAATGACAGGAAAGGCC	ChIP
ccgA_ChIP_Anid rev	GAGTTCGTCATAAGCATGGGCG	ChIP
actA_ChIP_Anid for	CTTCTCAACATCCAACTCCC	ChIP
actA_ChIP_Anid rev	GGTGGATTAGAATCGAACTAC	ChIP

4.7 Bioinformatical methods

UniProt (https://www.uniprot.org) and FungiDB (https://fungidb.org/fungidb/app) were used to obtain protein- and genomic sequences. InterPro (https://www.ebi.ac.uk/interpro/) and SUPERFAMILY (https://supfam.org) were used for protein domain predictions. Phylogenetic tree analysis and protein sequence alignments were carried out in Geneious Prime 2024 (https://www.geneious.com). Visualization of quantitative PCR results and statistical analysis was done with GraphPad Prism 9.0 (https://www.graphpad.com/features). Microscopic images were processed with ImageJ (https://imagej.net/ij/). Modification and design of DNA-vectors was performed with ApE (A plasmid editor). AlphaFold 3 (doi:org/10.1038/s41586-024-07487-w) was used to model protein structures (Date of access: 11th Sep 2024). Coloring and visualization of protein structures and chromophores from AlphaFold 3 were done with ChimeraX (https://www.cgl.ucsf.edu/chimerax/) (Meng *et al.*, 2023). AlphaFill was used together with the protein models generated with AlphaFold 3 to predict chromophores (https://alphafill.eu) (Date of access: 11th Sep 2024). DeepL Write was used for improving grammar and spelling (https://www.deepl.com/en/write). Unless specifically noted, each experiment was repeated three or more times independently. Most of the images, graphs and generated datasets used in this dissertation, as well as their descriptions, were created previously for and transferred from (Landmark *et al.*, 2026).

4.8 Microbiological methods

4.8.1 Organisms and cultivation techniques

Standard cloning techniques and standard transformation protocols for *A. nidulans* and *E. coli* were used (Yelton *et al.*, 1984; Pope & Kent, 1996). Q5 High-Fidelity DNA Polymerase from NEB was used for DNA amplification. Chemically competent *E. coli* Top10 was used for the amplification of plasmids and their preservation. Heterologous protein expression was carried out in *E. coli* BL21 (DE3). The organisms and their genotype are listed in Table 6.

Table 6: Used *E. coli* strains and their genotype.

Name	Genotype	Reference
Top10	*F- mcrA Δ(mrr-hsdRMSmcrBC) Φ80lacZΔM15 ΔlacX74 recA1 araD139 Δ(araleu)7697, galU galK rpsL (Str^R) endA1, nupG*	New England Biolabs
BL21 (DE3)	*F- ompT hsdSB (rB-, mB-) gal dcm (DE3)*	

For the cultivation of *A. nidulans* supplemented minimal media (MM) was used (Käfer, 1965). For incubation of transformed protoplasts supplemented *Aspergillus* minimal media (AMM) was used (Brakhage & Van den Brulle, 1995). For growth assays of *A. nidulans* supplemented complete media (CM) was used (Käfer, 1977). *E. coli* strains were cultivated in LB-media (lysogeny broth) at 37 °C and 180 rpm. Media composition and concentrations are listed in Table 7.

Table 7: List of the used media, their composition, and added supplements.

Media	Composition
LB	Tryptone 1 % (w/v)
	Yeast extract 0.5 % (w/v)
	NaCl 1 % (w/v)
	pH 7.5
Supplements	
Ampicillin	100 µg/ml
Chloramphenicol	30 µg/ml
Kanamycin	30 µg/ml
Sorbitol	100 mM
Betain	2.5 mM
Agar-Agar	(1.5 % (w/v)
Media	**Composition**
SOC	Tryptone/Peptone 2 % (w/v)
	Yeast extract 0.5 % (w/v)
	KCl 2.5 mM
	NaCl 10 mM
	$MgSO_4$ 10 mM
	$MgCl_2$ 10 mM

	Glucose 20 mM
MM	Salt solution 5 % (v/v)
	Trace elements 0.1 % (v/v)
	Glucose 20 g/l
	pH 6.5
	Agar-Agar 15 g/l
AMM	Salt solution 5 % (v/v)
	Trace elements 0.1 % (v/v)
	Glucose 20 g/l
	Sorbitol 181 g/l
	pH 6.5
	Agar-Agar 15 g/L (3g/L for AMM-Top)
Microscopy media	Salt solution 5 % (v/v)
	Trace elements 0.1 % (v/v)
	Vitamin solution 0.1 % (v/v)
	Threonine 2 % (v/v)
	pH 6.5
Salt solution	$NaNO_3$ 120 g/l
	KCl 10,4 g/l
	$MgSO_4$ x 7 H_2O 10,4 g/l
	KH_2PO_4 30,4 g/l
Trace elements	$ZnSO_4$ x 7 H_2O 22 g/l
	H_3BO_3 11 g/l
	$MnCl_2$ x 4 H_2O 5 g/l
	$FeSO_4$ x 7 H_2O 5 g/l
	$CoCl_2$ x 6 H_2O 1.6 g/l
	$CuSO_4$ x 5 H_2O 1.6 g/l
	$(NH_4)_6Mo_7O_{24}$ x 4 H_2O 1.1 g/l
	EDTA-Na_2 x 2 H_2O 50 g/l
	pH 6.5
Vitamin solution	Biotin 0.1 g/l
	Pyridoxine 0.1 g/l
	Thiamine 0.1 g/l
	Riboflavin 0.1 g/l

	p-Aminobenzoic acid 0.1 g/l
	Nicotinic acid 0.1 g/l
Supplements	
Uridine	1 g/ml
Threonine	20 g/l
Glycerol	20 g/l
Uracil	1 g/ml
Pyridoxine	1 g/ml

4.8.2 Growth assays

For the phenotypic analysis of *cryA* mutants 1,000 spores were inoculated on solid minimal media supplemented with 2 % glucose to repress promoter activity, 2 % threonine or 2 % glycerol to induce promoter activity. For each condition and strain, 8 replicates were used independently.

4.8.3 Determination of cell count

For the determination of cell count for microscopy and growth assays, a Neubauer cell counting chamber was used, following the manufacturer's instructions.

4.8.4 Generation and transformation of *A. nidulans* protoplasts

To generate protoplasts of *A. nidulans*, sufficient spores were removed from a Petri dish covered with MM medium and incubated in 100 ml of liquid medium with appropriate auxotrophy markers for 16 hours at 30 °C and 180 rpm. The resulting mycelium was then filtered through sterile Miracloth filters and washed with a cold 0.7 M NaCl solution. 2-3 g of mycelia are then transferred into a 50 ml Falcon tube and 15 ml 0.7 M NaCl solution, supplemented with 500 mg Glucanex (VinoTaste® Pro, Novozymes) and 50 mg kitalase (Fujifilm Wako), were added. Cell wall digestion was performed at 30 °C, 110 rpm for 90 min. After the incubation period, the solution was filtered through sterile Miracloth filters into a fresh 50 ml Falcon. The supernatant was centrifuged at 2430 rpm, 4 °C for 10 min. The supernatant was removed and the pelleted resuspended in 15 ml STC buffer and again centrifuged at 2430 rpm, 4 °C for

10 min. The supernatant was removed and the pellet resuspended in 1 ml STC buffer. For transformation, 100 µl of protoplast solution was prepared in a 50 ml Falcon. 5 µg of the target plasmid was added and incubated for 5 min at 4 °C. Afterwards, 1 ml of 40 % PEG 4000 in STC was added and the mixture was incubated for 20 min at RT. 30 ml of warm AMM Top media was added and transferred on an AMM plate with the respective auxotrophy marker. The plates were incubated at 37 °C for 3 days. Used buffers are listed in Table 8.

Table 8: Composition of the STC buffer used for *A. nidulans* protoplasts generation.

Name	Composition
STC	1.2 M Sorbitol
	10 mM $CaCl_2$
	10 mM Tris-HCl, pH 7.5

4.8.5 Isolation of genomic DNA from *A. nidulans*

To isolate genomic DNA from *A. nidulans*, spores were incubated overnight for 16 h in a Petri dish with MM medium and corresponding auxotrophy markers at 37 °C. After incubation, the fungal mycelium on the top (Kahmhaut) was removed with a spatula, dried, and lyophilized using liquid nitrogen. The frozen mycelium was crushed using a mortar and dissolved in 750 µl of gDNA extraction buffer (0.2 % SDS, 50 mM EDTA). The mycelium was then incubated at 68 °C for 45 min on a shaking heating block. 350 µl of a 3 M potassium acetate solution was added and the sample was centrifuged for 10 min at 4 °C and 13,000 rpm. 650 µl of the supernatant was removed and mixed with the same volume of cold 100 % isopropanol. The sample was then placed on ice for 30 min and subsequently centrifuged for 10 min at 4 °C and 13,000 rpm. The supernatant was discarded and the pellet was washed with 70 % ethanol for 3 min at 4 °C and 13,000 rpm. The remaining ethanol was discarded, and the pellet was dried at 68 °C and then resuspended in 50 µl dH_2O.

4.8.6 Transformation of chemically competent *E. coli* cells

For transformation, 1 µg of the corresponding plasmid was added to the *E. coli* cells. After an incubation period of 5 minutes on ice, the cells were incubated for 45 seconds at 42 °C (heat shock). After a subsequent two-minute phase on ice, 400 µl SOC

medium was added and then incubated for one hour at 37 °C and 180 rpm. Finally, 200 µl of the cell suspension was spread on agar plates with LB medium and corresponding antibiotics (ampicillin 100 µg/ml, kanamycin 50 µg/ml, chloramphenicol 50 µg/ml) and incubated overnight at 37 °C.

4.8.7 Microscopy

For microscopic examination of the fluorescence-labeled CryA protein, 5 x 10^4 spores were inoculated onto 500 µl MM medium with corresponding auxotrophy markers on 170 ± 5 µm Precision Coverslips (Roth). The samples were then incubated at 25 °C for 14 hours. For the overexpression of *cryA*, 2 % threonine was added to the MM medium instead of glucose, while for the de-repression of the *alcA* promoter, 2 % glycerol was added as a C-source to obtain balanced expression of the CryA protein fused with GFP. Fluorescence microscopy and differential interference contrast (DIC) images were taken at RT using a Zeiss Axio Imager Z1 microscope with a Plan-Apochromat 63x/1.4 Oil DIC objective and a Plan-Apochromat 10x objective.

4.9 Molecular biological methods

4.9.1 Plasmid construction

Plasmids were constructed using the Gibson Assembly method following the *NEBuilder® HiFi DNA Assembly* system (#E2621, New Englands Biolabs). The vector was linearized using a restriction digest and the DNA insert was generated using PCR. Gibson Assembly was performed using 50 ng of backbone vector and a 3:1 molar surplus of insert for a total reaction volume of 20 µl. The reaction was incubated for 30 min at 50 °C. The composition of the reaction mix is detailed in Table 9.

Table 9: Buffer composition and reaction mix for the Gibson Assembly method.

Buffer	Composition
5x ISO-Buffer	500 mM Tris/HCl pH 7.5
	50 mM $MgCl_2$
	1 mM dGTP
	1 mM dCTP
	1 mM dATP

	1 mM dTTP
	50 mM DTT
	25 % PEG 8000 (w/v)
	5 mM NAD
1.33x Reaction mix	
320 µl 5x ISO-Buffer	
0.64 µl T5 Exonuclease (10U/µl)	
20 µl Q5® DNA Polymerase (2 U/µl)	
160 µl Taq DNA Ligase (40 U/µl)	
699.36 µl ddH_2O	
Separate in 15 µl aliquots	

4.9.2 Plasmid extraction from *E. coli*

Transformed Top10 cells were incubated in 25 ml liquid LB medium with the appropriate antibiotic for 16 h at 37 °C and 180 rpm. For high purity and quality, extraction of the plasmid DNA was performed using the *NucleoSpin® Plasmid Easypure* Kit (Macherey-Nagel, Düren). The extraction was done according to the manufacturer's instructions. For verification of the success of transformation, 2 ml of transformed Top10 *E. coli* cells were centrifuged for 1 min at 13,000 rpm and 4 °C. The supernatant was removed and the pellet resuspended in 200 µl of cell suspension buffer. 200 µl of lysis buffer was added, mixed, and incubated for 2 min at RT. Afterwards, 200 µl of neutralization buffer was added, mixed, and centrifuged for 5 min at 4 °C and 13,000 rpm. 500 µl of the supernatant was mixed with 500 µl of 100 % cold isopropanol and centrifuged for 10 min at 4 °C and 13,000 rpm. The supernatant was discarded and the pellet washed with 70 % cold ethanol and centrifuged for 3 min at 4 °C and 13,000 rpm. The ethanol was completely removed by drying the pellet on a heat block at 68 °C resuspended in 50 µl dH_2O. The buffer compositions are listed in Table 10.

Table 10: Buffers used in plasmid extraction and the respective components and their concentrations.

Buffer	Composition
Cell suspension buffer	50 mM Tris-HCl pH 7.5
	10 mM EDTA
Lysis buffer	0.2 M NaOH
	1 % SDS (w/v)

Neutralization buffer	1 M potassium acetate pH 4.8

4.9.3 Analysis of DNA concentration

The DNA concentration of extracted plasmids was measured using the NP-80 (Implen) spectrophotometer with an absorption of 260 nm. The purity was confirmed by the ratios of A_{260}/A_{230} nm and A_{260}/A_{280} nm.

4.9.4 Polymerase chain reaction

The polymerase chain reaction (PCR) was used to amplify DNA fragments. Q5® High-Fidelity DNA Polymerase (#M0491, NEB) was used for PCR reactions according to the manufacturer's instructions. Reaction mixtures are usually composed for a volume of 25 µl and use a touchdown protocol of the thermocycler, which was adjusted depending on the length of the amplicon and increased the annealing temperature at the beginning of the PCR for improved specificity. An exemplary PCR protocol is listed in Table 11.

Table 11: Exemplary PCR protocol for amplification of DNA using the Q5 polymerase.

Step	Temperature	Time
Initial denaturation	95	5 min
Denaturation	95	30 s
Annealing	63	30 s
Elongation	72	20 s per kilobase (kb)
Repeat 5x at 1st denaturation		
Denaturation	95	30 s
Annealing	61	30 s
Elongation	72	20 s per kb
Repeat 5x at 2nd denaturation		
Denaturation	95	30 s
Annealing	59	30 s
Elongation	72	20 s per kb
Repeat 30x at 3rd denaturation		

4.9.5 Restriction enzyme digestion

Restriction enzymes were used according to the manufacturer's instructions (NEB, Frankfurt) to digest vectors and PCR products into specific patterns. An exemplary restriction enzyme digestion is usually prepared in a volume of 10 µl. Details about the components and the concentrations of a restriction enzyme digestion are listed in Table 12.

Table 12: Exemplary DNA digest in a 10 µl volume using restriction enzymes.

Components	Concentration
DNA	0.5-1 µg
CutSmart®-Puffer	1 µl
Restriction enzyme	0.5
dH_2O	Fill up to 10 µl

4.9.6 Gel electrophoresis

DNA fragments were separated by size using electrophoresis on a 1 % agarose gel in 0.5x TAE buffer (20 mM TRIS acetate pH 8.0, 1 mM EDTA). A 1 kb DNA ladder (#N3232; New England Biolabs) served as the molecular weight marker. DNA bands were visualized using Midori^{GREEN} Advance (Nippon Genetics) and 6x staining buffer. Gel electrophoresis was performed for 30 min at 135 V. Composition of the staining buffer is listed in Table 13.

Table 13: Composition of the 6x staining buffer.

Component	Concentration
Bromphenol blue	0.25 % (w/v)
Xylenecyanol FF	0.25 % (w/v)
Glycerin	30 % (v/v)

4.9.7 Sequencing

Sequencing of the generated plasmids was done with Eurofins Genomics. The sample preparation was done following manufacturer’s instructions.

4.9.8 Isolation of RNA

For the preparation of RNA, a spore suspension was generated by harvesting spores from two plates per strain in 10 ml of the appropriate medium and transferring them into a 50 ml Falcon tube for subsequent quantification. For each biological replicate, a small Petri dish was filled with 10 ml of medium and inoculated with $1.5x10^8$ spores, before being incubated overnight at 37 °C under static conditions. The following day, the quality of the Kahmhaut was assessed before it was removed from the dish, dried using Miracloth and paper towels, and transferred into a 1.5 ml microcentrifuge tube for flash-freezing in liquid nitrogen. The mass of the harvested mycelium was determined using a precision balance, using an empty tube as a reference, followed by the isolation of the RNA.

A mortar and pestle were pre-cooled with liquid nitrogen, and the frozen mycelium was ground twice before being transferred into a 15 ml centrifuge tube while still containing residual nitrogen. Once the liquid nitrogen had evaporated, 1 ml of Trizol was added per 100 mg of mycelium and the tube was vortexed to resuspend the sample. Subsequently, 15 mg of this mixture was moved to a new 1.5 ml tube and the volume was adjusted to 1 ml with Trizol. Following a five-minute incubation at room temperature, 200 µl of chloroform was added, the sample was vortexed, incubated for three minutes at room temperature, and then centrifuged at 13,000 rpm for 15 minutes at 4 °C. This centrifugation separated the mixture into three distinct phases: a lower pink chloroform-phenol phase containing proteins, an interphase containing DNA, and an upper aqueous phase containing the RNA. Exactly 400 µl of this upper aqueous phase was collected and transferred to a new 1.5 ml tube, where the RNA was precipitated by the addition of 500 µl of isopropanol, followed by incubation at 4 °C for 30 minutes. After centrifugation at 13,000 rpm and 4 °C for 10 min, the supernatant was discarded, and the precipitated RNA was washed with 1 ml of 70 % ethanol. The sample was centrifuged for five minutes at 13,000 rpm and 4 °C, after which 950 µl of the wash was removed and the sample was centrifuged again for an additional 5 minutes at the same settings. The remaining supernatant was discarded, and the RNA pellet was air-dried for 45 minutes at room temperature to allow any residual ethanol to evaporate before finally being dissolved in 50 µl of nuclease-free water.

To remove genomic DNA from the RNA samples, a DNase digestion was performed using the TURBO DNA-free™ Kit (ThermoFisher Scientific, Invitrogen). First, the concentration and quality of the RNA were verified via NanoDrop (Implen)

and subsequently diluted to 200 ng/µl in a total volume of 50 µl. For the digestion, 5 µl of DNase buffer and 1 µl of DNase were added, followed by incubation at 37 °C for 30 minutes. An additional 1 µl of DNase was then added and incubated for another 30 minutes to ensure the removal of any residual gDNA. To compensate for the double amount of enzyme used, the volume of the DNase Inactivation Reagent was adjusted from 5 µl to 10 µl. The samples were incubated for five minutes at room temperature with regular mixing, then centrifuged for 1.5 minutes at 10,000 rpm, after which 40 µl of the supernatant was collected. For downstream applications such as qPCR, the RNA concentration and quality were re-measured using the NanoDrop (Implen), and the samples were adjusted to a final volume of 50 µl before being stored at -80 °C.

4.9.9 qRT-PCR

For gene expression analysis via quantitative real-time PCR, the *Luna Universal One-Step RT-qPCR* Kit (NEB) was utilized according to the manufacturer's instructions, with reactions performed in a CFX Connect (Bio-Rad). The putative *histone 2b* (*h2b*) gene served as the housekeeping gene for expression analysis in *A. nidulans*. Relative expression levels were calculated using the ΔCT method (Schmittgen & Livak, 2008). All experiments, unless otherwise stated, were conducted in biological triplicates and technical duplicates. Statistical analysis was performed using an unpaired, parametric, two-sided t-test (*p-value<0.05).

4.9.10 cDNA synthesis

For the synthesis of complementary DNA (cDNA) from RNA, the *SuperScript Double-Stranded cDNA Synthesis* Kit (ThermoFisher Scientific) was used following the manufacturer's protocol.

4.9.11 Chromatin immunoprecipitation (ChIP)

To analyze chromatin modifications, four biological replicates each of the respective strains were prepared in 25 ml liquid cultures. Crosslinking via formaldehyde was performed using 1 % formaldehyde in a 50 ml culture for 15 minutes at 37 °C. Then, glycine was added to reach a final concentration of 125 mM, and the mixture was incubated for 5 minutes at room temperature. The mycelium was filtered through

Miracloth, dried on paper towels, flash frozen in liquid nitrogen, and ground with a mortar and pestle. The pulverized mycelium was transferred to a 2-ml Eppendorf tube containing 1 ml of sonication buffer.

Sonication was performed in Sylvia Erhardt's laboratory under Jasmin Böhm's supervision. 100 mg of the ground mycelium were sonicated using a Q800R3 sonicator (QSonica) with the following settings: The samples were sonicated in cycles on ice for two minutes (“on”) and then rested for one minute (“off”) at maximum power for a total treatment time of 60 minutes. Then, the samples were centrifuged for one minute at 13,000 rpm and 4 °C. The supernatant was transferred to a new tube, and 50 µL of Protein G Plus Agarose (Santa Cruz Biotechnology) was added. The solution was pre-cleared for 60 minutes on a spinning wheel (Thermo Fisher Scientific) at 4 °C. After centrifuging for one minute at 13,000 rpm and 4 °C, the supernatant was transferred, and the protein content was measured using a Qubit™ 4.0 (Invitrogen). The protein concentration was diluted to 200 µg in a final volume of 1 ml. 100 µl of the sample were removed as an input sample.

2 µg of the respective antibody (Anti-H3 antibody (Abcam), Anti-H3K9ac antibody (Merck Millipore) was added to 200 µg of protein, and the mixture was incubated overnight at 4 °C on a spinning wheel. Then, 50 µL of Protein G Plus Agarose was added, and the solution was rotated for 60 minutes at 4 °C. All subsequent steps were carried out on the spinning wheel at 4 °C for 5 minutes. The supernatant was removed, and the agarose was washed with the following buffers: 1) 1 mL of low salt washing buffer, 2) 1 mL of high salt wash buffer, 3) 1 mL of LiCl wash buffer, and 4) twice with 1 mL of TE buffer.

Next, the TE buffer was removed, and 50 µL of fresh resuspension buffer was added. The solution was then incubated for 15 minutes at 65 °C. Then, the sample was centrifuged for two minutes at 13,000 rpm and 4 °C, and the supernatant was transferred to a new tube. This step was repeated once more to reach a final volume of 100 µL. The following steps are carried out for the precipitated and reserved input samples. 4 µl of a 5 M NaCl solution were added, and the solution was incubated overnight at 65 °C. Then, the samples were incubated with 40 mM Tris-HCl (pH 6.5), 10 mM EDTA, and 20 µg of Proteinase K (Merck Millipore) for 60 minutes at 45 °C to reverse the cross-linking and remove protein contamination. DNA purification was performed using the ChIP Cleanup and Concentrator Kit (Zymo Research), following the manufacturer's instructions.

For quantitative RT-PCR, the input control was diluted 1:100 in dH_2O, and the precipitated sample was diluted 1:10. Technical duplicates were used for the qPCR, and the results were analyzed using the percent input method. Actin gene *actA* was used as a control. The used buffers are listed in Table 14.

Table 14: List of used ChIP buffers and their composition.

Buffer	Composition
Sonication buffer	50 mM HEPES-KOH pH 7.5 140 mM NaCl, 1 mM EDTA 1 % Triton X-100 0.1 % Na-deoxycholate 1 Pierce Protease Inhibitor Tablet (Thermo Fisher Scientific)
Low salt wash buffer	150 mM NaCl 0.2 % SDS 0.5 % Triton X-100 2 mM EDTA 20 mM Tris-HCl pH 8
High salt wash buffer	500 mM NaCl 0.2 % SDS 0.5 % Triton X-100 2 mM EDTA 20 mM Tris-HCl pH 8
LiCl salt wash buffer	0.25 mM LiCl 0.5 % Na-deoxycholate 1 mM EDTA 10 mM Tris-HCl pH 8 0.5 % NP-40
TE buffer	1 mM EDTA 10 mM Tris-HCl pH 8
Resuspension buffer	1 % SDS 0.1 M $NaHCO_3$

4.9.12 High performance liquid chromatography

For reverse phase high performance liquid chromatography (RP-HPLC) of CryA chromophores the Vanquish Core HPLC System together with a Hypersil Gold 150 mm x 4.6 mm, 3 µm C18 column (Thermo Fisher Scientific) was used. Buffer A1 (10 mM Na2HPO4 and 45 mM Citric acid, pH 2.4 in dH2O) and Buffer B1 (100 % methanol) were used for separation of chromophores. The equilibration and wash step was performed with 0.5 CV and 10 % methanol concentration; elution was performed with 2.5 CV and a continuously increasing methanol gradient to 100 %.

4.9.13 Secondary metabolite extraction

The extraction of metabolites from *A. nidulans* was carried out by cutting the mycelia from a seven-day-old agar plate of the respective strains in approximately 1.5 cm^2 pieces. These mycelia pieces were then crushed in a 50 ml falcon, and shaken with 10 mL ethyl acetate for three hours at 20 °C. The samples were centrifuged for 5-10 minutes at 13,000 rpm at RT and the supernatant, without any solid agar or mycelia pieces, was transferred into several new 2 ml reaction vessel. These were then evaporated at RT overnight or at 40-70 °C for several hours to concentrate the metabolites. Extracts from the same sample were then combined in a total volume of 50 µl

4.9.14 Thin layer chromatography

For the analysis of the extracted metabolites of *A. nidulans*, between 10 and 40 µL of the respective extract were applied at intervals of 1 cm from each other and from the lower edge onto a thin-layer chromatography plate. The stationary phase consisted of 0.25 mm silica gel 60. The carrier material was glass (LuxPlate TLC Silicagel 10 x 20 cm, Merck Millipore) A solvent mixture of toluene, ethyl acetate, and formic acid in a ratio of 5:4:1 served as the mobile phase. The loaded chromatography plate was placed in 15 mL of running buffer in the running chamber. The elution front reached the desired width in approximately 25 minutes, with a distance of 1 cm from the upper edge of the plate. After the eluent had evaporated at RT for 15 min, the DC plate was irradiated with UV light at 254 nm and 365 nm in order to observe the fluorescence/absorption of the samples.

4.10 Biochemical methods

4.10.1 Heterologous protein expression

For protein purification, the pET28a vector (Novagen) for CryA and the pASK-iba3plus vector (IBA Lifescience) for FphA were used. pET28a contains an Isopropyl ß-D-1-thiogalactopyranoside (IPTG) inducible T7 promoter and either a N- or C-terminal 6xHisTag for purification of the target protein. The pASK-iba3plus vectors contains an anhydrotetracycline (AHT) inducible *tet*-promoter and a C-terminal strep-tag for purification of the target protein. For the purification of FphA, the bacterial heme oxygenase BphO from *Pseudomonas aeruginosa* was assembled in a pACYC vector and co-transformed with FphA. To accomplish the expression of functional FphA, BphO is essential for degradation of heme to biliverdin, the chromophore of FphA.

For FphA, BL21 DE3 cultures were grown in 2 L liquid LB, supplemented with 100 mM sorbitol, 2.5 mM betaine and the respective antibiotics, and incubated shaking at 37 °C until OD_{600} of 0.6 was achieved. To activate expression of BphO, 0.5 mM IPTG was added and the culture grown for 60 min at 37 °C. After cooling the culture down to 15 °C, 0.2 µg/ml AHT was added to induce FphA expression. After 16 h at 15 °C and 180 rpm, the culture was centrifuged twice at 9000 rpm at 4 °C for 15 min. The supernatant was removed, and the pellet resuspended in 40 ml buffer A (50 mM Tris-HCl, 300 mM NaCl, 0.05 % Tween20, 10 % glycerol, 1 mM PMSF, 5 mM DTT, pH 7.8). The cell walls were disrupted by using a high-pressure homogenizer (Avestin Inc.) and the pellet was separated by centrifugation for 45 min at 18,000 rpm and 4 °C. 40 µg/ml Avidin was used for 15 min and 4 °C to bind free biotin. The ÄktaPure (Cytiva) was used for protein purification with a 5 ml StrepTrap XT column following the instructions provided by the manufacturer. For elution, buffer A supplemented with 100 mM Biotin was used. For BLI analysis, a size exclusion chromatography (SEC) was used to remove any aggregated FphA complexes and isolate the functional phytochrome dimer. A vivaspin ultrafiltration unit (Sartorius) with a 50,000 molecular weight cut off (MWCO) was used to concentrate protein samples. All steps were performed under green safelight or darkness.

For CryA, a similar expression protocol was used with the following changes: Induction of CryA was achieved by the addition of 0.5 mM IPTG after cooling down to 15 °C. Buffer A was supplemented with 90 mM Imidazole for wash-steps and 500 mM for elution instead of biotin with a pH of 7.4. For purification a 5 ml HisTrap HP was used following the manufacturer’s instructions. Buffer of eluted CryA was exchanged

using a PD-10 desalting column (Cytiva) according to the manufacturer's protocol. A vivaspin ultrafiltration unit with a 30,000 MWCO was used to concentrate protein samples. All steps were performed under red safety light or in the dark.

4.10.2 SDS-PAGE

The quality of the purified protein was analyzed using sodium dodecyl sulfate polyacrylamide gel electrophoresis (SDS-PAGE), using a 5 % collecting gel and a 10 % separating gel. The samples were dissolved in 5x SDS sample buffer and boiled in it for 10 min at 95 °C. The samples were then loaded onto the collecting gel together with the PageRuler^{TM} 180 kDa prestained protein ladder (Thermo Fisher Scientific) and collected in the collecting gel at room temperature for 15 min at 80 V. Separation in the separating gel was performed for two hours at 100 V. 5 µl of the protein ladder and 10 µl of the eluate (E) were used. Only the separation gel was used to stain the protein bands. It was covered with 30 ml of Coomassie Brilliant Blue G-250 dye (Thermo Fischer Scientific) and stained for 30 minutes at 60 rpm. Decolorization was performed with a decolorization solution and ddH_2O at 60 rpm until a satisfactory result was achieved. As a final step, the gel was documented using the GP-FAS-V gel documentation system (NIPPON Genetics). The buffer composition is listed in Table 15.

Table 15: Used solutions for SDS-PAGE, the respective components and concentrations.

Solution	Component	Volume in ml
5 % Collection Gel	dH_2O	3.4
	30 % Acrylic amide solution	0.83
	0,5 M Tris pH 6,8	0.63
	10 % SDS	0.05
	10 % APS	0.05
	Tetramethylethylendiamine (TEMED)	0.007
10 % Separation Gel	dH_2O	4
	30 % Acrylic amide solution	3.3

	1,5 M Tris pH 8,8	2.5
	10 % SDS	0.1
	10 % APS	0.1
	TEMED	0.01
Buffer	**Component**	**Concentration**
SDS-Running Buffer	Tris	25 mM
	Glycine	192 mM
	SDS	0.1 %
5x SDS-Sample Buffer	Tris-HCl pH 6,8	200 mM
	SDS	10 %
	40 % Glycerol	20 %
	Bromphenole blue	0.05 %
	DTT	10 mM
Coomassie Staining Solution	Methanol	45 %
	100 % Acetic Acid	10 %
	ddH_2O	45 %
	Coomassie *Brilliant Blue* G-250	0.1 %
Coomassie Destaining Solution	Methanol	40 %
	100 % Acetic Acid	10 %
	ddH_2O	50 %

4.10.3 Biolayer interferometry assay

The BLItz system (Sartorius) was used for biolayer interferometry assays. Nickel-nitrilotriacetic acid (NTA) coated biosensors were used to immobilize the target protein tagged with a 6xHis-tag made up in BLItz buffer (137 mM NaCl, 2.7 mM KCl, 10 mM Na_2HPO_4, 1 mM KH_2PO_4, 0,5 % BSA, and 0,04 % Tween20, pH 7.4) as bait. The second protein was used as analyte in various concentrations made up in BLItz buffer. For the experiment the following steps were selected: 30 s baseline in BLI buffer, 120 s loading of the bait to the tip, 45 s baseline step, 120 s association step, 120 s dissociation step (Sultana & Lee, 2015). For the calculation of the K_d-value, step corrections for the start of the association and dissociation, a global analysis, and a 1:1 binding model were selected. A control of 0 µM of the analyte was used as reference for normalization.

4.10.4 Size exclusion chromatography

The size exclusion chromatography (SEC) was utilized with the Superdex^{TM} 200 Increase 10/300 GL together with the ÄktaPure^{TM} system (Cytiva), following manufacturer's instructions. For size dependent separation of the proteins a flow rate of 0.05 ml/min was used. For determination of the size of the eluted protein samples, the Gel Filtration Markers Kit 29,000-700,000 Da (Merck Millipore) was used.

4.10.5 Determination of protein concentrations

Protein concentrations were determined with the Qubit^{TM} *Protein Broad Range Assay* Kit and the Qubit^{TM} 4.0 fluorometer (Thermo Fisher Scientific, Invitrogen), following manufacturer's instructions.

4.10.6 UV/Vis Spectroscopy

All UV/Vis spectra were generated using the NP-80 photometer (Implen) or the JASCO-V750 (JASCO GmbH) under green or red safety light. Illumination of the samples was performed with blue light (200 µmol photons m^{-2} s^{-1}) for 1 min. The baseline was generated using the sample buffer.

5. References

Aguida, B., Babo, J., Baouz, S., Jourdan, N., Procopio, M., El-Esawi, M. A., Engle, D., Mills, S., Wenkel, S., Huck, A., Berg-Sørensen, K., Kampranis, S. C., Link, J. & Ahmad, M. (2024). 'Seeing' the electromagnetic spectrum: spotlight on the cryptochrome photocycle. *Front. Plant Sci.* **15**: 1340304.

Ahmad, M. (2016). Photocycle and signaling mechanisms of plant cryptochromes. *Curr. Opin. Plant Biol.* **33**: 108-115.

Arthaut, L.-D., Jourdan, N., Mteyrek, A., Procopio, M., El-Esawi, M., d'Harlingue, A., Bouchet, P.-E., Witczak, J., Ritz, T., Klarsfeld, A., Birman, S., Usselman, R. J., Hoecker, U., Martino, C. F. & Ahmad, M. (2017). Blue-light induced accumulation of reactive oxygen species is a consequence of the *Drosophila* cryptochrome photocycle. *PloS One* **12**: e0171836.

Azuma, N., Kanamaru, K., Matsushika, A., Yamashino, T., Mizuno, T., Kato, M. & Kobayashi, T. (2007). In vitro analysis of His-Asp phosphorelays in *Aspergillus nidulans*: the first direct biochemical evidence for the existence of His-Asp phosphotransfer systems in filamentous fungi. *Biosci. Biotechnol. Biochem.* **71**: 2493-2502.

Bahn, Y. S., Kojima, K., Cox, G. M. & Heitman, J. (2006). A unique fungal two-component system regulates stress responses, drug sensitivity, sexual development, and virulence of *Cryptococcus neoformans*. *Mol. Biol. Cell* **17**: 3122-3135.

Baker, C. L., Loros, J. J. & Dunlap, J. C. (2012). The circadian clock of *Neurospora crassa*. *FEMS Microbiol. Rev.* **36**: 95-110.

Balázs, A., Pócsi, I., Hamari, Z., Leiter, E., Emri, T., Miskei, M., Oláh, J., Tóth, V., Hegedus, N., Prade, R. A., Molnár, M. & Pócsi, I. (2010). AtfA bZIP-type transcription factor regulates oxidative and osmotic stress responses in *Aspergillus nidulans*. *Mol. Genet. Genomics* **283**: 289-303.

Ballario, P., Talora, C., Galli, D., Linden, H. & Macino, G. (1998). Roles in dimerization and blue light photoresponse of the PAS and LOV domains of *Neurospora crassa* white collar proteins. *Mol. Microbiol.* **29**: 719-729.

Ballario, P., Vittorioso, P., Magrelli, A., Talora, C., Cabibbo, A. & Macino, G. (1996). White collar-1, a central regulator of blue light responses in *Neurospora*, is a zinc finger protein. *EMBO J.* **15**: 1650-1657.

Baltussen, T. J. H., Zoll, J., Verweij, P. E. & Melchers, W. J. G. (2020). Molecular mechanisms of conidial germination in *Aspergillus spp*. *Microbiol. Mol. Bio. Rev.* **84**: e00049-00019.

Bastakis, E., Gerke, J., Özkan, S., Harting, R., Lienard, T., Sasse, C., Xylakis, E. S., Aden, M., Strohdiek, A., Heinrich, G., Grosse, V. & Braus, G. H. (2025). Molecular circuit between *Aspergillus nidulans* transcription factors MsnA and VelB to coordinate fungal stress and developmental responses. *PLoS Genet.* **21**: e1011578.

Bastakis, E., Harting, R., Scheel, A., Lienard, T., Sasse, C., Aden, M., Heinrich, G., Grosse, V., Scheiter, N. & Braus, G. H. (2026). The *Aspergillus nidulans* transcription factor SclB governs the transition from vegetative to asexual development. *mBio* **0**: e03488-03425.

Bayram, Ö., Bayram, Ö. S., Ahmed, Y. L., Maruyama, J.-i., Valerius, O., Rizzoli, S. O., Ficner, R., Irniger, S. & Braus, G. H. (2012). The *Aspergillus nidulans* MAPK module AnSte11-Ste50-Ste7-Fus3 controls development and secondary metabolism. *PLoS Genet.* **8**: e1002816.

Bayram, O., Biesemann, C., Krappmann, S., Galland, P. & Braus, G. H. (2008a). More than a repair enzyme: *Aspergillus nidulans* photolyase-like CryA is a regulator of sexual development. *Mol. Biol. Cell* **19**: 3254-3262.

Bayram, O., Braus, G. H., Fischer, R. & Rodriguez-Romero, J. (2010). Spotlight on *Aspergillus nidulans* photosensory systems. *Fungal Genet. Biol.* **47**: 900-908.

Bayram, Ö., Feussner, K., Dumkow, M., Herrfurth, C., Feussner, I. & Braus, G. H. (2016). Changes of global gene expression and secondary metabolite accumulation during light-dependent *Aspergillus nidulans* development. *Fungal Genet. Biol.* **87**: 30-53.

Bayram, O., Krappmann, S., Ni, M., Bok, J. W., Helmstaedt, K., Valerius, O., Braus-Stromeyer, S., Kwon, N. J., Keller, N. P., Yu, J. H. & Braus, G. H. (2008b). VelB/VeA/LaeA complex coordinates light signal with fungal development and secondary metabolism. *Science* **320**: 1504-1506.

Bayram, Ö. S. & Bayram, Ö. (2023). An anatomy of fungal eye: Fungal photoreceptors and signalling mechanisms. *J. Fungi* **9**: 591.

Beekman, C. N. & Ene, I. V. (2020). Short-term evolution strategies for host adaptation and drug escape in human fungal pathogens. *PLoS Pathog.* **16**: e1008519.

Beel, B., Prager, K., Spexard, M., Sasso, S., Weiss, D., Müller, N., Heinnickel, M., Dewez, D., Ikoma, D., Grossman, A. R., Kottke, T. & Mittag, M. (2012). A

flavin binding cryptochrome photoreceptor responds to both blue and red light in *Chlamydomonas reinhardtii*. *Plant Cell* **24**: 2992-3008.

Berrocal-Tito, G. M., Esquivel-Naranjo, E. U., Horwitz, B. A. & Herrera-Estrella, A. (2007). *Trichoderma atroviride* PHR1, a fungal photolyase responsible for DNA repair, autoregulates its own photoinduction. *Eukaryot. Cell* **6**: 1682-1692.

Binder, U., Oberparleiter, C., Meyer, V. & Marx, F. (2010). The antifungal protein PAF interferes with PKC/MPK and cAMP/PKA signalling of *Aspergillus nidulans*. *Mol. Microbiol.* **75**: 294-307.

Bluhm, B. H. & Dunkle, L. D. (2008). PHL1 of *Cercospora zeae-maydis* encodes a member of the photolyase/cryptochrome family involved in UV protection and fungal development. *Fungal Genet. Biol.* **45**: 1364-1372.

Blumenstein, A., Vienken, K., Tasler, R., Purschwitz, J., Veith, D., Frankenberg-Dinkel, N. & Fischer, R. (2005). The *Aspergillus nidulans* phytochrome FphA represses sexual development in red light. *Curr. Biol.* **15**: 1833-1838.

Blumhofer, A. (2024). Investigation of the function of HoxB in the oxidative stress response of *Aspergillus nidulans*.

Brakhage, A. A. & Van den Brulle, J. (1995). Use of reporter genes to identify recessive trans-acting mutations specifically involved in the regulation of *Aspergillus nidulans* penicillin biosynthesis genes. *J. Bacteriol.* **177**: 2781-2788.

Brandt, S., von Stetten, D., Günther, M., Hildebrandt, P. & Frankenberg-Dinkel, N. (2008). The fungal phytochrome FphA from *Aspergillus nidulans*. *J. Biol. Chem.* **283**: 34605-34614.

Breitenbach, M., Weber, M., Rinnerthaler, M., Karl, T. & Breitenbach-Koller, L. (2015). Oxidative stress in fungi: Its function in signal transduction, interaction with plant hosts, and lignocellulose degradation. *Biomol.* **5**: 318-342.

Brown, L. S. (2004). Fungal rhodopsins and opsin-related proteins: eukaryotic homologues of bacteriorhodopsin with unknown functions. *Photochem. Photobiol. Sci.* **3**: 555-565.

Brudler, R., Hitomi, K., Daiyasu, H., Toh, H., Kucho, K., Ishiura, M., Kanehisa, M., Roberts, V. A., Todo, T., Tainer, J. A. & Getzoff, E. D. (2003). Identification of a new cryptochrome class. Structure, function, and evolution. *Mol. Cell* **11**: 59-67.

Cáp, M., Váchová, L. & Palková, Z. (2012). Reactive oxygen species in the signaling and adaptation of multicellular microbial communities. *Oxid. Med. Cell Longev.* **2012**: 976753.

Carrasco-Navarro, U. & Aguirre, J. (2021). H_2O_2 induces major phosphorylation changes in critical regulators of signal transduction, gene expression, metabolism and developmental networks in *Aspergillus nidulans*. *J. Fungi* **7**: 624.

Casal, J. J. (2000). Phytochromes, cryptochromes, phototropin: photoreceptor interactions in plants. *Photochem. Photobiol. Sci.* **71**: 1-11.

Castello, P. R., Drechsel, D. A. & Patel, M. (2007). Mitochondria are a major source of paraquat-induced reactive oxygen species production in the brain. *J. Biol. Chem.* **282**: 14186-14193.

Castrillo, M., García-Martínez, J. & Avalos, J. (2013). Light-dependent functions of the *Fusarium fujikuroi* CryD DASH cryptochrome in development and secondary metabolism. *Appl. Environ. Microbiol.* **79**: 2777-2788.

Chaves, I., Yagita, K., Barnhoorn, S., Okamura, H., van der Horst, G. T. & Tamanini, F. (2006). Functional evolution of the photolyase/cryptochrome protein family: importance of the C terminus of mammalian CRY1 for circadian core oscillator performance. *Mol. Biol. Cell* **26**: 1743-1753.

Cheng, P., Yang, Y. & Liu, Y. (2001). Interlocked feedback loops contribute to the robustness of the *Neurospora* circadian clock. *PNAS* **98**: 7408-7413.

Coesel, S., Mangogna, M., Ishikawa, T., Heijde, M., Rogato, A., Finazzi, G., Todo, T., Bowler, C. & Falciatore, A. (2009). Diatom PtCPF1 is a new cryptochrome/photolyase family member with DNA repair and transcription regulation activity. *EMBO Rep.* **10**: 655-661.

Cohrs, K. C. & Schumacher, J. (2017). The two cryptochrome/photolyase family proteins fulfill distinct roles in DNA photorepair and regulation of conidiation in the gray mold fungus *Botrytis cinerea*. *Appl. Environ. Microbiol.* **83**: e00812-00817.

Corrochano, L. M., Corrochano-Luque, M., Franco-Cano, A., Gutiérrez, G. & Cánovas, D. (2025). Light sensing in fungi. *Curr. Biol.* **35**: R1134-R1138.

Corrochano, L. M., Lauter, F. R., Ebbole, D. J. & Yanofsky, C. (1995). Light and developmental regulation of the gene con-10 of *Neurospora crassa*. *Dev. Biol.* **167**: 190-200.

Dasgupta, A., Chen, C.-H., Lee, C., Gladfelter, A. S., Dunlap, J. C. & Loros, J. J. (2015). Biological significance of photoreceptor photocycle length: VIVID photocycle governs the dynamic VIVID-white collar complex pool mediating photo-adaptation and response to changes in light intensity. *PLoS Genet.* **11**: e1005215.

Delaunay, A., Isnard, A. D. & Toledano, M. B. (2000). H_2O_2 sensing through oxidation of the Yap1 transcription factor. *EMBO J.* **19**: 5157-5166.

Deppisch, P., Helfrich-Förster, C. & Senthilan, P. R. (2022). The gain and loss of cryptochrome/photolyase family members during evolution. *Genes (Basel)* **13**: 1613.

Doan, A. G., Schafer, J. E., Douglas, C. M., Quintanilla, M. S., Morse, M. E., Edwards, H., Huso, W. D., Gray, K. J., Lee, J., Dayie, J. K., Harris, S. D. & Marten, M. R. (2025). Protein kinases MpkA and SepH transduce crosstalk between CWI and SIN pathways to activate protective hyphal septation under echinocandin cell wall stress. *mSphere* **10**: e00641-00624.

Du, G., Zheng, K., Sun, C., Sun, M., Pan, J., Meng, D., Guan, W. & Zhao, H. (2025). The relationship mammalian p38 with human health and its homolog Hog1 in response to environmental stresses in *Saccharomyces cerevisiae*. *Front. Cell Dev. Biol.* **13**: 1522294.

Duran, R., Cary, J. W. & Calvo, A. M. (2010). Role of the osmotic stress regulatory pathway in morphogenesis and secondary metabolism in filamentous fungi. *Toxins (Basel)* **2**: 367-381.

Eagan, J. L. & Keller, N. P. (2025). Fungal secondary metabolism. *Curr. Biol.* **35**: R503-R508.

El-Esawi, M., Arthaut, L.-D., Jourdan, N., d'Harlingue, A., Link, J., Martino, C. F. & Ahmad, M. (2017). Blue-light induced biosynthesis of ROS contributes to the signaling mechanism of *Arabidopsis* cryptochrome. *Sci. Rep.* **7**: 13875.

Ercolini, A. & Berti, R. (1975). Light sensitivity experiments and morphology studies of the blind phreatic fish *Phreatichthys andruzzii* from Somalaia. *Mon. Zool. Ita. Suppl.* **6**: 29-43.

Ercolini, A., Berti, R., Chelazzi, L. & Messana, G. (1982). Researches on the phreatobic fishes of Somalia: Achievements and prospects. *Mon. Zool. Ita.* **17**: 219-241.

Evans, E., Dodson, C., Maeda, K., Biskup, T., Wedge, C. & Timmel, C. (2013). Magnetic field effects in flavoproteins and related systems. *Interface focus* **3**: 20130037.

Evans, R., O'Neill, M., Pritzel, A., Antropova, N., Senior, A., Green, T., Žídek, A., Bates, R., Blackwell, S., Yim, J., Ronneberger, O., Bodenstein, S., Zielinski, M., Bridgland, A., Potapenko, A., Cowie, A., Tunyasuvunakool, K., Jain, R., Clancy, E., Kohli, P., Jumper, J. & Hassabis, D. (2021). Protein complex prediction with AlphaFold-Multimer. *bioRxiv*.

Fellas, A., Pidoux, A. L., Tong, P., Hewes, H. H., Wallace, E. C. & Allshire, R. C. (2026). Heterochromatin epimutations impose mitochondrial dysfunction to confer antifungal resistance. *EMBO J.* **45**: 417-448.

Fischer, R., Aguirre, J., Herrera-Estrella, A. & Corrochano, L. M. (2016). The complexity of fungal vision. *Microbiol. Spectr.* **4**: 1128.

Fischer, T., Xu, Q., Zhao, K.-H., Gärtner, W., Slavov, C. & Wachtveitl, J. (2020). Effect of the PHY domain on the photoisomerization step of the forward Pr→Pfr conversion of a knotless phytochrome. *Chem. Eur. J.* **26**: 17261-17266.

Frawley, D., Karahoda, B., Sarikaya Bayram, Ö. & Bayram, Ö. (2018). The HamE scaffold positively regulates MpkB phosphorylation to promote development and secondary metabolism in *Aspergillus nidulans*. *Sci. Rep.* **8**: 16588.

Frawley, D., Stroe, M. C., Oakley, B. R., Heinekamp, T., Straßburger, M., Fleming, A. B., Brakhage, A. A. & Bayram, Ö. (2020). The pheromone module SteC-MkkB-MpkB-SteD-HamE regulates development, stress responses and secondary metabolism in *Aspergillus fumigatus*. *Front. Microbiol.* **11**: 811.

Frenzel, D. & Willbold, D. (2014). Kinetic titration series with biolayer interferometry. *PLoS One* **9**: e106882.

Froehlich, A. C., Chen, C.-H., Belden, W. J., Madeti, C., Roenneberg, T., Merrow, M., Loros, J. J. & Dunlap, J. C. (2010). Genetic and molecular characterization of a cryptochrome from the filamentous fungus *Neurospora crassa*. *Eukaryot. Cell* **9**: 738-750.

Froehlich, A. C., Loros, J. J. & Dunlap, J. C. (2003). Rhythmic binding of a WHITE COLLAR-containing complex to the frequency promoter is inhibited by FREQUENCY. *PNAS* **100**: 5914-5919.

Fuchs, B. B. & Mylonakis, E. (2009). Our paths might cross: the role of the fungal cell wall integrity pathway in stress response and cross talk with other stress response pathways. *Eukaryot. Cell* **8**: 1616-1625.

Fujioka, T., Mizutani, O., Furukawa, K., Sato, N., Yoshimi, A., Yamagata, Y., Nakajima, T. & Abe, K. (2007). MpkA-Dependent and -independent cell wall integrity signaling in *Aspergillus nidulans*. *Eukaryot. Cell* **6**: 1497-1510.

Fuller, K. K., Cramer, R. A., Zegans, M. E., Dunlap, J. C. & Loros, J. J. (2016). *Aspergillus fumigatus* photobiology illuminates the marked heterogeneity between isolates. *mBio* **7**: e01517-01516.

Fuller, K. K., Ringelberg, C. S., Loros, J. J. & Dunlap, J. C. (2013). The fungal pathogen *Aspergillus fumigatus* regulates growth, metabolism, and stress resistance in response to light. *mBio* **4**: e00142-00113.

Futagami, T. & Goto, M. (2012). Putative cell wall integrity sensor proteins in *Aspergillus nidulans*. *Commun. Integr. Biol.* **5**: 206-208.

Galland, P., Palit, A. & Lipson, E. D. (1985). Phycomyces: Phototropism and light-growth response to pulse stimuli. *Planta* **165**: 538-547.

García-Esquivel, M., Esquivel-Naranjo, E. U., Hernández-Oñate, M. A., Ibarra-Laclette, E. & Herrera-Estrella, A. (2016). The *Trichoderma atroviride* cryptochrome/photolyase genes regulate the expression of blr1-independent genes both in red and blue light. *Fungal Biol.* **120**: 500-512.

García-Martínez, J., Brunk, M., Avalos, J. & Terpitz, U. (2015). The CarO rhodopsin of the fungus *Fusarium fujikuroi* is a light-driven proton pump that retards spore germination. *Sci. Rep.* **5**: 7798.

Garrido-Bazán, V., Jaimes-Arroyo, R., Sánchez, O., Lara-Rojas, F. & Aguirre, J. (2018). SakA and MpkC stress MAPKs show opposite and common functions during stress responses and development in *Aspergillus nidulans*. *Front. Microbiol.* **9**: 2518.

Genoud, T., Schweizer, F., Tscheuschler, A., Debrieux, D., Casal, J. J., Schäfer, E., Hiltbrunner, A. & Fankhauser, C. (2008). FHY1 mediates nuclear import of the light-activated phytochrome A photoreceptor. *PLoS Genet.* **4**: e1000143.

Gerke, J. & Braus, G. H. (2014). Manipulation of fungal development as source of novel secondary metabolites for biotechnology. *Appl. Environ. Microbiol.* **98**: 8443-8455.

Gin, E., Diernfellner, A. C., Brunner, M. & Höfer, T. (2013). The *Neurospora* photoreceptor VIVID exerts negative and positive control on light sensing to achieve adaptation. *Mol. Syst. Biol.* **9**: 667.

Goffart, S., Tikkanen, P., Michell, C., Wilson, T. & Pohjoismäki, J. L. O. (2021). The Type and Source of Reactive Oxygen Species Influences the Outcome of Oxidative Stress in Cultured Cells. *Cells* **10**: 1075.

Griffin, E. A., Staknis, D. & Weitz, C. J. (1999). Light-independent role of CRY1 and CRY2 in the mammalian circadian clock. *Science* **286**: 768-771.

Hagiwara, D., Asano, Y., Marui, J., Yoshimi, A., Mizuno, T. & Abe, K. (2009a). Transcriptional profiling for *Aspergillus nidulans* HogA MAPK signaling pathway in response to fludioxonil and osmotic stress. *Fungal Genet. Biol.* **46**: 868-878.

Hagiwara, D., Mizuno, T. & Abe, K. (2009b). Characterization of NikA histidine kinase and two response regulators with special reference to osmotic adaptation and asexual development in *Aspergillus nidulans*. *Biosci. Biotechnol. Biochem.* **73**: 1566-1571.

Hagiwara, D., Sakamoto, K., Abe, K. & Gomi, K. (2016). Signaling pathways for stress responses and adaptation in *Aspergillus* species: stress biology in the post-genomic era. *Biosci. Biotechnol. Biochem.* **80**: 1667-1680.

Han, K. H. & Prade, R. A. (2002). Osmotic stress-coupled maintenance of polar growth in *Aspergillus nidulans*. *Mol. Microbiol.* **43**: 1065-1078.

Hedtke, M., Rauscher, S., Röhrig, J., Rodríguez-Romero, J., Yu, Z. & Fischer, R. (2015). Light-dependent gene activation in *Aspergillus nidulans* is strictly dependent on phytochrome and involves the interplay of phytochrome and white collar-regulated histone H3 acetylation. *Mol. Microbiol.* **97**: 733-745.

Henríquez-Urrutia, M., Spanner, R., Olivares-Yánez, C., Seguel-Avello, A., Pérez-Lara, R., Guillén-Alonso, H., Winkler, R., Herrera-Estrella, A., Canessa, P. & Larrondo, L. F. (2022). Circadian oscillations in *Trichoderma atroviride* and the role of core clock components in secondary metabolism, development, and mycoparasitism against the phytopathogen Botrytis cinerea. *eLife* **11**: e71358.

Hughes, R. M., Vrana, J. D., Song, J. & Tucker, C. L. (2012). Light-dependent, dark-promoted interaction between *Arabidopsis* cryptochrome 1 and phytochrome B proteins. *J. Biol. Chem.* **287**: 22165-22172.

Hunt, S. M., Thompson, S., Elvin, M. & Heintzen, C. (2010). VIVID interacts with the WHITE COLLAR complex and FREQUENCY-interacting RNA helicase to alter light and clock responses in *Neurospora*. *PNAS* **107**: 16709-16714.

Idnurm, A. (2013). Light sensing in *Aspergillus fumigatus* highlights the case for establishing new models for fungal photobiology. *mBio* **4**: e00260-00213.

Idnurm, A. & Bahn, Y. S. (2016). Fungal physiology: Red light plugs into MAPK pathway. *Nat. Microbiol.* **1**: 16052.

Jia, K., Jia, Y., Zeng, Q., Yan, Z. & Wang, S. (2024). Regulation of conidiation and aflatoxin B1 biosynthesis by a blue light sensor LreA in *Aspergillus flavus*. *J. Fungi* **10**: 650.

Johnson, J. L., Hamm-Alvarez, S., Payne, G., Sancar, G. B., Rajagopalan, K. V. & Sancar, A. (1988). Identification of the second chromophore of *Escherichia coli* and yeast DNA photolyases as 5,10-methenyltetrahydrofolate. *PNAS* **85**: 2046-2050.

Jug, A., Bratkovič, T. & Ilaš, J. (2024). Biolayer interferometry and its applications in drug discovery and development. *Trends Anal. Chem.* **176**: 117741.

Käfer, E. (1965). Origins of translocations in *Aspergillus nidulans*. *Genet.* **52**: 217.

Käfer, E. (1977). Meiotic and mitotic recombination in *Aspergillus* and its chromosomal aberrations. *Adv. Genet.* **19**: 33-131.

Kamat, V. & Rafique, A. (2017). Designing binding kinetic assay on the bio-layer interferometry (BLI) biosensor to characterize antibody-antigen interactions. *Anal. Biochem.* **536**: 16-31.

Kawasaki, L. & Aguirre, J. (2001). Multiple catalase genes are differentially regulated in *Aspergillus nidulans*. *J. Bacteriol.* **183**: 1434-1440.

Kawasaki, L., Wysong, D., Diamond, R. & Aguirre, J. (1997). Two divergent catalase genes are differentially regulated during *Aspergillus nidulans* development and oxidative stress. *J. Bacteriol.* **179**: 3284-3292.

Keller, N. P., Turner, G. & Bennett, J. W. (2005). Fungal secondary metabolism — from biochemistry to genomics. *Nat. Rev. Microbiol.* **3**: 937-947.

Kim, G., Weiss, S. J. & Levine, R. L. (2014). Methionine oxidation and reduction in proteins. *Biochim. Biophys. Acta.* **1840**: 901-905.

Kiontke, S., Geisselbrecht, Y., Pokorny, R., Carell, T., Batschauer, A. & Essen, L. O. (2011). Crystal structures of an archaeal class II DNA photolyase and its complex with UV-damaged duplex DNA. *EMBO J.* **30**: 4437-4449.

Kiontke, S., Göbel, T., Brych, A. & Batschauer, A. (2020). DASH-type cryptochromes - solved and open questions. *Biol. Chem.* **401**: 1487-1493.

Klar, T., Kaiser, G., Hennecke, U., Carell, T., Batschauer, A. & Essen, L. O. (2006). Natural and non-natural antenna chromophores in the DNA photolyase from *Thermus thermophilus*. *Chem. Biochem.* **7**: 1798-1806.

Kleine, T., Lockhart, P. & Batschauer, A. (2003). An *Arabidopsis* protein closely related to *Synechocystis* cryptochrome is targeted to organelles. *Plant J.* **35**: 93-103.

Kleiner, O., Kircher, S., Harter, K. & Batschauer, A. (1999). Nuclear localization of the *Arabidopsis* blue light receptor cryptochrome 2. *Plant J.* **19**: 289-296.

Kocsis, B., Lee, M. K., Antal, K., Yu, J. H., Pócsi, I., Leiter, É. & Emri, T. (2023). Genome-wide gene expression analyses of the AtfA/AtfB-mediated menadione stress response in *Aspergillus nidulans*. *Cells* **12**: 463.

König, S., Juhas, M., Jäger, S., Kottke, T. & Büchel, C. (2017). The cryptochrome—photolyase protein family in diatoms. *J. Plant Physiol.* **217**: 15-19.

Kottke, T., Oldemeyer, S., Wenzel, S., Zou, Y. & Mittag, M. (2017). Cryptochrome photoreceptors in green algae: Unexpected versatility of mechanisms and functions. *J. Plant Physiol.* **217**: 4-14.

Krysan, P. J. & Colcombet, J. (2018). Cellular complexity in MAPK signaling in plants: Questions and emerging tools to answer them. *Front. Plant Sci.* **9**: 1674.

Kumar, A. (2020). *Aspergillus nidulans*: A potential resource of the production of the native and heterologous enzymes for industrial applications. *Int. J. Microbiol.* **2020**: 8894215.

Lai, H.-T. & Chiang, C.-M. (2013). Bimolecular fluorescence complementation (BiFC) assay for direct visualization of protein-protein interaction *in vivo*. *Bio-protocol* **3**: e935.

Lamparter, T., Michael, N., Mittmann, F. & Esteban, B. (2002). Phytochrome from *Agrobacterium tumefaciens* has unusual spectral properties and reveals an N-terminal chromophore attachment site. *PNAS* **99**: 11628-11633.

Lamparter, T., Mittmann, F., Gärtner, W., Börner, T., Hartmann, E. & Hughes, J. (1997). Characterization of recombinant phytochrome from the cyanobacterium *Synechocystis*. *PNAS* **94**: 11792-11797.

Landmark, A. (2022). Analysis of the biochemical and biological properties of cryptochrome CryA in connection with other light receptors in *Aspergillus nidulans*.

Landmark, A., Rudolf, T., Hundshammer, K., Böhm, J., Leister, K., Erhardt, S. & Fischer, R. (2026). The photolyase/cryptochrome of *Aspergillus nidulans* senses oxidative stress and shuttles from nuclei to mitochondria. *Nat. Commun.* **17**: 1483.

Lara-Rojas, F., Sánchez, O., Kawasaki, L. & Aguirre, J. (2011). *Aspergillus nidulans* transcription factor AtfA interacts with the MAPK SakA to regulate general stress responses, development and spore functions. *Mol. Microbiol.* **80**: 436-454.

Laurindo, F. R., Araujo, T. L. & Abrahão, T. B. (2014). Nox NADPH oxidases and the endoplasmic reticulum. *ARS* **20**: 2755-2775.

Laz, E. V., Lee, J. & Levin, D. E. (2020). Crosstalk between *Saccharomyces cerevisiae* SAPKs Hog1 and Mpk1 is mediated by glycerol accumulation. *Fungal Biol.* **124**: 361-367.

Leister, K., Dong, Y., Landmark, A., Ma, Y., Schreckenberger, B., Yu, Z., Lu, L. & Fischer, R. (2025). Distinct roles of phytochromes A and B in *Aspergillus fumigatus* in environmental sensing and pathogenicity. *mBio* **16**: e0220425.

Li, H., Scheitle, C., Di Mauro, G., Fuselli, S., Fritsch-Decker, S., Todo, T., Weiss, C., Vallone, D., Lamparter, T., Bertolucci, C. & Foulkes, N. S. (2025a). Conservation of dark CPD photolyase function in blind cavefish. *Nat. Commun.* **16**: 7377.

Li, H., Scheitle, C., Hu, X., Kaiber, J. J., Todo, T., Vallone, D., Fischer, R. & Foulkes, N. S. (2025b). 6-4 photolyase differentially modulates transcription in the vertebrate circadian clock. *PLoS Genet.* **21**: e1011971.

Li, J., Li, G., Wang, H. & Wang Deng, X. (2011). Phytochrome signaling mechanisms. *Arabidopsis Book* **9**: e0148.

Li, Q., Zhang, M., Wei, B., Lan, W., Wang, Q., Chen, C., Zhao, H., Liu, D. & Gadd, G. M. (2024). Fungal biomineralization of toxic metals accelerates organic pollutant removal. *Curr. Biol.* **34**: 2077-2084.e2073.

Liao, B., Ye, X., Chen, X., Zhou, Y., Cheng, L., Zhou, X. & Ren, B. (2021). The two-component signal transduction system and its regulation in *Candida albicans*. *Virulence* **12**: 1884-1899.

Lim, J. M., Kim, G. & Levine, R. L. (2019). Methionine in proteins: It's not just for protein initiation anymore. *Neurochem. Res.* **44**: 247-257.

Linden, H. & Macino, G. (1997). White collar 2, a partner in blue-light signal transduction, controlling expression of light-regulated genes in *Neurospora crassa*. *EMBO J.* **16**: 98-109.

Liu, F., Guo, L., Luo, Y., Li, J., Zhou, Y., Wang, J., Huang, X., Tan, X., Fu, M., Yu, B., Gao, Y., Liu, R., Takaya, N. & Zhou, S. (2025). Peroxiredoxin PrxA and thioredoxin TrxA mediate the redox signal to the transcription factor NapA in the fungus *Aspergillus nidulans*. *Int. J. Biol. Macromol.* **310**: 143434.

Lloyd, E., Olive, C., Stahl, B. A., Jaggard, J. B., Amaral, P., Duboué, E. R. & Keene, A. C. (2018). Evolutionary shift towards lateral line dependent prey capture behavior in the blind Mexican cavefish. *Dev. Biol.* **441**: 328-337.

Lokhandwala, J., Hopkins, H. C., Rodriguez-Iglesias, A., Dattenböck, C., Schmoll, M. & Zoltowski, B. D. (2015). Structural biochemistry of a fungal LOV domain photoreceptor reveals an evolutionarily conserved pathway integrating light and oxidative stress. *Structure* **23**: 116-125.

Loor, G., Kondapalli, J., Schriewer, J. M., Chandel, N. S., Vanden Hoek, T. L. & Schumacker, P. T. (2010). Menadione triggers cell death through ROS-dependent mechanisms involving PARP activation without requiring apoptosis. *Free Radic. Biol. Med.* **49**: 1925-1936.

Lopez, L., Fasano, C., Perrella, G. & Facella, P. (2021). Cryptochromes and the circadian clock: The story of a very complex relationship in a spinning world. *Genes (Basel)* **12**: 672.

Lyu, X., Shen, C., Fu, Y., Xie, J., Jiang, D., Li, G. & Cheng, J. (2016). The microbial opsin homolog Sop1 is involved in *Sclerotinia sclerotiorum* development and environmental stress response. *Front. Microbiol.* **6**: 1504.

Más, P., Devlin, P. F., Panda, S. & Kay, S. A. (2000). Functional interaction of phytochrome B and cryptochrome 2. *Nature* **408**: 207-211.

Masuda, S., Hasegawa, K., Ishii, A. & Ono, T. A. (2004). Light-induced structural changes in a putative blue-light receptor with a novel FAD binding fold sensor of blue-light using FAD (BLUF). *Biochem.* **43**: 5304-5313.

Mattila, H., Österman-Udd, J., Mali, T. & Lundell, T. (2022). Basidiomycota fungi and ROS: genomic perspective on key enzymes involved in generation and mitigation of reactive oxygen species. *Front. Fungal Biol.* **3**: 837605.

Mattison, C. P. & Ota, I. M. (2000). Two protein tyrosine phosphatases, Ptp2 and Ptp3, modulate the subcellular localization of the Hog1 MAP kinase in yeast. *Genes Dev.* **14**: 1229-1235.

McClung, C. R. (2006). Plant circadian rhythms. *Plant Cell* **18**: 792-803.

Mejia, R. (2011). Cave-Dwelling Fish Provide Clues to the Circadian Cycle. *PLoS Biol.* **9**: e1001141.

Mendoza-Martínez, A. E., Lara-Rojas, F., Sánchez, O. & Aguirre, J. (2017). NapA mediates a redox regulation of the antioxidant response, carbon utilization and development in *Aspergillus nidulans*. *Front. Microbiol.* **8**: 516.

Meng, E. C., Goddard, T. D., Pettersen, E. F., Couch, G. S., Pearson, Z. J., Morris, J. H. & Ferrin, T. E. (2023). UCSF ChimeraX: Tools for structure building and analysis. *Protein Sci.* **32**: e4792.

Michael, A. K., Fribourgh, J. L., Van Gelder, R. N. & Partch, C. L. (2017). Animal cryptochromes: Divergent roles in light perception, circadian timekeeping and beyond. *Photochem. Photobiol. Sci.* **93**: 128-140.

Miki, H. & Funato, Y. (2012). Regulation of intracellular signalling through cysteine oxidation by reactive oxygen species. *J. Biochem* **151**: 255-261.

Miller, K. Y., Wu, J. & Miller, B. L. (1992). StuA is required for cell pattern formation in *Aspergillus*. *Genes Dev.* **6**: 1770-1782.

Miskei, M., Ibragimova, S., Kocsis, B., Nagy, T., Park, H.-S., Emri, T., Yu, J.-H., Leiter, É. & Pócsi, I. (2025). Genome-wide mapping reveals an extensive AtfA regulatory influence on development, metabolism, and stress preparedness in *Aspergillus nidulans*. *Cells* **14**: 1965.

Mulford, K. E. & Fassler, J. S. (2011). Association of the Skn7 and Yap1 transcription factors in the *Saccharomyces cerevisiae* oxidative stress response. *Eukaryot. Cell* **10**: 761-769.

Navarro, E., Niemann, N., Kock, D., Dadaeva, T., Gutiérrez, G., Engelsdorf, T., Kiontke, S., Corrochano, L. M., Batschauer, A. & Garre, V. (2020). The DASH-type cryptochrome from the fungus *Mucor circinelloides* Is a canonical CPD-photolyase. *Curr. Biol.* **30**: 4483-4490.e4484.

Navarro, R., Stringer, M., Hansberg, W., Timberlake, W. & Aguirre, J. (1996). *catA,* a new *Aspergillus nidulans* gene encoding a developmentally regulated catalase. *Curr. Genet.* **29**: 352-359.

Ninfa, A. J. & Magasanik, B. (1986). Covalent modification of the glnG product, NRI, by the glnL product, NRII, regulates the transcription of the glnALG operon in *Escherichia coli*. *PNAS* **83**: 5909-5913.

Nsa, I. Y., Karunarathna, N., Liu, X., Huang, H., Boetteger, B. & Bell-Pedersen, D. (2014). A novel cryptochrome-dependent oscillator in *Neurospora crassa*. *Genet.* **199**: 233-245.

Oiki, S., Nasuno, R., Urayama, S. I., Takagi, H. & Hagiwara, D. (2022). Intracellular production of reactive oxygen species and a DAF-FM-related compound in *Aspergillus fumigatus* in response to antifungal agent exposure. *Sci. Rep.* **12**: 13516.

Oldemeyer, S., Haddad, A. Z. & Fleming, G. R. (2020). Interconnection of the antenna pigment 8-HDF and flavin facilitates red-Light reception in a bifunctional animal-like cryptochrome. *Biochem.* **59**: 594-604.

Olmedo, M., Ruger-Herreros, C., Luque, E. M. & Corrochano, L. M. (2010). A complex photoreceptor system mediates the regulation by light of the conidiation genes con-10 and con-6 in *Neurospora crassa*. *Fungal Genet. Biol.* **47**: 352-363.

Olmedo, M., Ruger-Herreros, C., Luque, E. M. & Corrochano, L. M. (2013). Regulation of transcription by light in *Neurospora crassa*: A model for fungal photobiology? *Fungal Biol. Rev.* **27**: 10-18.

Palayam, M., Ganapathy, J., Guercio, A. M., Tal, L., Deck, S. L. & Shabek, N. (2021). Structural insights into photoactivation of plant Cryptochrome-2. *Commun. Biol.* **4**: 28.

Panzer, S., Brych, A., Batschauer, A. & Terpitz, U. (2019). Opsin 1 and Opsin 2 of the corn smut fungus *Ustilago maydis* are green light-driven proton pumps. *Front. Microbiol.* **10**: 735.

Papon, N. & Stock, A. M. (2019). Two-component systems. *Curr. Biol.* **29**: R724-R725.

Park, S. Y. & Tame, J. R. H. (2017). Seeing the light with BLUF proteins. *Biophys. Rev.* **9**: 169-176.

Pedmale, U. V., Huang, S. C., Zander, M., Cole, B. J., Hetzel, J., Ljung, K., Reis, P. A. B., Sridevi, P., Nito, K., Nery, J. R., Ecker, J. R. & Chory, J. (2016). Cryptochromes interact directly with PIFs to control plant growth in limiting blue light. *Cell* **164**: 233-245.

Pinheiro, Â., Piontkivska, D., Sequeira, P., Martins, T. M. & Silva Pereira, C. (2023). *Aspergillus nidulans*. *Trends in Microbiol* **31**: 212-213.

Pontecorvo, G., Roper, J. A., Hemmons, L. M., Macdonald, K. D. & Bufton, A. W. (1953). The genetics of *Aspergillus nidulans*. *Adv. Genet.* **5**: 141-238.

Pope, B. & Kent, H. M. (1996). High efficiency 5 min transformation of *Escherichia coli*. *Nucleic Acids Res.* **24**: 536-537.

Purschwitz, J., Müller, S. & Fischer, R. (2009). Mapping the interaction sites of *Aspergillus nidulans* phytochrome FphA with the global regulator VeA and the White Collar protein LreB. *Mol. Genet. Genomics* **281**: 35-42.

Purschwitz, J., Müller, S., Kastner, C. & Fischer, R. (2006). Seeing the rainbow: light sensing in fungi. *Curr. Opin. Microbiol.* **9**: 566-571.

Purschwitz, J., Müller, S., Kastner, C., Schöser, M., Haas, H., Espeso, E. A., Atoui, A., Calvo, A. M. & Fischer, R. (2008). Functional and physical interaction of blue- and red-light sensors in *Aspergillus nidulans*. *Curr. Biol.* **18**: 255-259.

Rana, A. & Thakur, A. (2025). Translation regulation promotes stress adaptation in the human fungal pathogen *Candida glabrata*. *Genet.* **231**: 134.

Rodriguez-Romero, J., Hedtke, M., Kastner, C., Müller, S. & Fischer, R. (2010). Fungi, hidden in soil or up in the air: light makes a difference. *Annu. Rev. Microbiol.* **64**: 585-610.

Röhrig, J., Kastner, C. & Fischer, R. (2013). Light inhibits spore germination through phytochrome in *Aspergillus nidulans*. *Curr. Genet.* **59**: 55-62.

Romero, B., Turner, G., Olivas, I., Laborda, F. & Ramón De Lucas, J. (2003). The *Aspergillus nidulans alcA* promoter drives tightly regulated conditional gene expression in *Aspergillus fumigatus* permitting validation of essential genes in this human pathogen. *Fungal Genet. Biol.* **40**: 103-114.

Rozenberg, A., Inoue, K., Kandori, H. & Béjà, O. (2021). Microbial rhodopsins: The last two decades. *Annu. Rev. Microbiol.* **75**: 427-447.

Ruger-Herreros, C., Rodríguez-Romero, J., Fernández-Barranco, R., Olmedo, M., Fischer, R., Corrochano, L. M. & Canovas, D. (2011). Regulation of conidiation by light in *Aspergillus nidulans*. *Genet.* **188**: 809-822.

Sancar, A. (2003). Structure and function of DNA photolyase and cryptochrome blue-light photoreceptors. *Chem. Rev.* **103**: 2203-2238.

Sanchez, R. E. A., Kalume, F. & de la Iglesia, H. O. (2022). Sleep timing and the circadian clock in mammals: Past, present and the road ahead. *Semin. Cell Dev. Biol.* **126**: 3-14.

Sang, Y., Li, Q. H., Rubio, V., Zhang, Y. C., Mao, J., Deng, X. W. & Yang, H. Q. (2005). N-terminal domain-mediated homodimerization is required for photoreceptor activity of *Arabidopsis* CRYPTOCHROME 1. *Plant Cell* **17**: 1569-1584.

Sato, I., Shimizu, M., Hoshino, T. & Takaya, N. (2009). The glutathione system of *Aspergillus nidulans* involves a fungus-specific glutathione S-transferase. *J. Biol. Chem.* **284**: 8042-8053.

Schafmeier, T., Haase, A., Káldi, K., Scholz, J., Fuchs, M. & Brunner, M. (2005). Transcriptional feedback of *Neurospora* circadian clock gene by phosphorylation-dependent inactivation of its transcription factor. *Cell* **122**: 235-246.

Schmittgen, T. D. & Livak, K. J. (2008). Analyzing real-time PCR data by the comparative C(T) method. *Nat. Protoc.* **3**: 1101-1108.

Schmoll, M. (2018). Light, stress, sex and carbon - The photoreceptor ENVOY as a central checkpoint in the physiology of *Trichoderma reesei*. *Fungal Biol.* **122**: 479-486.

Schmoll, M., Esquivel-Naranjo, E. U. & Herrera-Estrella, A. (2010). *Trichoderma* in the light of day--physiology and development. *Fungal Genet. Biol.* **47**: 909-916.

Schrader, M. & Fahimi, H. D. (2006). Peroxisomes and oxidative stress. *Biochim. Biophys. Acta - Gen. Subj* **1763**: 1755-1766.

Schuhmacher, L., Heck, S., Pitz, M., Mathey, E., Lamparter, T., Blumhofer, A., Leister, K. & Fischer, R. (2024). The LOV-domain blue-light receptor LreA of the fungus *Alternaria alternata* binds predominantly FAD as chromophore and acts as a light and temperature sensor. *J. Biol. Chem.* **300**: 107238.

Schumacher, J. (2017). How light affects the life of Botrytis. *Fungal Genet. Biol.* **106**: 26-41.

Segal, L. M. & Wilson, R. A. (2018). Reactive oxygen species metabolism and plant-fungal interactions. *Fungal Genet. Biol.* **110**: 1-9.

Seo, J. A., Han, K. H. & Yu, J. H. (2004). The gprA and gprB genes encode putative G protein-coupled receptors required for self-fertilization in *Aspergillus nidulans*. *Mol. Microbiol.* **53**: 1611-1623.

Sheerin, D. J., Menon, C., zur Oven-Krockhaus, S., Enderle, B., Zhu, L., Johnen, P., Schleifenbaum, F., Stierhof, Y. D., Huq, E. & Hiltbrunner, A. (2015). Light-activated phytochrome A and B interact with members of the SPA family to promote photomorphogenesis in *Arabidopsis* by reorganizing the COP1/SPA complex. *Plant Cell* **27**: 189-201.

Song, C., Psakis, G., Lang, C., Mailliet, J., Gärtner, W., Hughes, J. & Matysik, J. (2011). Two ground state isoforms and a chromophore D-ring photoflip triggering extensive intramolecular changes in a canonical phytochrome. *PNAS* **108**: 3842-3847.

Strohdiek, A., Köhler, A. M., Harting, R., Stupperich, H., Gerke, J., Bastakis, E., Neumann, P., Ahmed, Y. L., Ficner, R. & Braus, G. H. (2025). The *Aspergillus nidulans* velvet domain containing transcription factor VeA is shuttled from cytoplasm into nucleus during vegetative growth and stays there for sexual development, but has to return into cytoplasm for asexual development. *PLoS Genet.* **21**: e1011687.

Sultana, A. & Lee, J. E. (2015). Measuring protein-protein and protein-nucleic Acid interactions by biolayer interferometry. *Curr. Protoc. Protein Sci.* **79**: 19.25.11-19.25.26.

Tagua, V. G., Pausch, M., Eckel, M., Gutiérrez, G., Miralles-Durán, A., Sanz, C., Eslava, A. P., Pokorny, R., Corrochano, L. M. & Batschauer, A. (2015). Fungal cryptochrome with DNA repair activity reveals an early stage in cryptochrome evolution. *PNAS* **112**: 15130-15135.

Takahashi, M., Teranishi, M., Ishida, H., Kawasaki, J., Takeuchi, A., Yamaya, T., Watanabe, M., Makino, A. & Hidema, J. (2011). Cyclobutane pyrimidine dimer (CPD) photolyase repairs ultraviolet-B-induced CPDs in rice chloroplast and mitochondrial DNA. *Plant J.* **66**: 433-442.

Takahashi, S., Teranishi, M., Izumi, M., Takahashi, M., Takahashi, F. & Hidema, J. (2014). Transport of rice cyclobutane pyrimidine dimer photolyase into mitochondria relies on a targeting sequence located in its C-terminal internal region. *Plant J.* **79**: 951-963.

Takala, H., Edlund, P., Ihalainen, J. & Westenhoff, S. (2020). Tips and turns of bacteriophytochrome photoactivation. *Photochem. Photobiol. Sci.* **19**: 1488-1510.

Thieme, K. G., Gerke, J., Sasse, C., Valerius, O., Thieme, S., Karimi, R., Heinrich, A. K., Finkernagel, F., Smith, K., Bode, H. B., Freitag, M., Ram, A. F. J. & Braus, G. H. (2018). Velvet domain protein VosA represses the zinc cluster transcription factor SclB regulatory network for *Aspergillus nidulans* asexual

development, oxidative stress response and secondary metabolism. *PLoS Genet.* **14**: e1007511.

Tisch, D. & Schmoll, M. (2010). Light regulation of metabolic pathways in fungi. *Appl. Environ. Microbiol.* **85**: 1259-1277.

Tisch, D., Schuster, A. & Schmoll, M. (2014). Crossroads between light response and nutrient signalling: ENV1 and PhLP1 act as mutual regulatory pair in *Trichoderma reesei*. *BMC Genomics* **15**: 425.

Toews, M. W., Warmbold, J., Konzack, S., Rischitor, P., Veith, D., Vienken, K., Vinuesa, C., Wei, H. & Fischer, R. (2004). Establishment of mRFP1 as a fluorescent marker in *Aspergillus nidulans* and construction of expression vectors for high-throughput protein tagging using recombination in vitro (GATEWAY). *Curr. Genet.* **45**: 383-389.

Tripathi, S., Hoang, Q. T. N., Han, Y.-J. & Kim, J.-I. (2019). Regulation of photomorphogenic development by plant phytochromes. *Int. J. Mol. Sci.* **20**: 6165.

Trott, A. J. & Menet, J. S. (2018). Regulation of circadian clock transcriptional output by CLOCK:BMAL1. *PLoS Genet.* **14**: e1007156.

Vargas-Pérez, I., Sánchez, O., Kawasaki, L., Georgellis, D. & Aguirre, J. (2007). Response regulators SrrA and SskA are central components of a phosphorelay system involved in stress signal transduction and asexual sporulation in *Aspergillus nidulans*. *Eukaryot. Cell* **6**: 1570-1583.

Vazquez, J. A. & Sobel, J. D. (2006). Anidulafungin: a novel echinocandin. *Clin. Infect. Dis.* **43**: 215-222.

Veith, D., Scherr, N., Efimov, V. P. & Fischer, R. (2005). Role of the spindle-pole-body protein ApsB and the cortex protein ApsA in microtubule organization and nuclear migration in *Aspergillus nidulans*. *J. Cell Sci.* **118**: 3705-3716.

Walker, W. H., 2nd, Walton, J. C., DeVries, A. C. & Nelson, R. J. (2020). Circadian rhythm disruption and mental health. *Transl. Psychiatry* **10**: 28.

Wang, F., Han, T. & Jeffrey Chen, Z. (2024). Circadian and photoperiodic regulation of the vegetative to reproductive transition in plants. *Commun. Biol.* **7**: 579.

Wang, J., Du, X., Pan, W., Wang, X. & Wu, W. (2015). Photoactivation of the cryptochrome/photolyase superfamily. *J. Photochem. Photobiol. C.* **22**: 84-102.

Wang, Q. & Lin, C. (2020a). Mechanisms of cryptochrome-mediated photoresponses in plants. *Annu. Rev. Plant Biol.* **71**: 103-129.

Wang, Q. & Lin, C. (2020b). A structural view of plant CRY2 photoactivation and inactivation. *Nat. Struct. Mol. Biol.* **27**: 401-403.

Wang, Q., Liu, Q., Wang, X., Zuo, Z., Oka, Y. & Lin, C. (2018a). New insights into the mechanisms of phytochrome–cryptochrome coaction. *New Phytol.* **217**: 547-551.

Wang, Z., Wang, J., Li, N., Li, J., Trail, F., Dunlap, J. C. & Townsend, J. P. (2018b). Light sensing by opsins and fungal ecology: NOP-1 modulates entry into sexual reproduction in response to environmental cues. *Mol. Ecol.* **27**: 216-232.

Wemmie, J. A., Steggerda, S. M. & Moye-Rowley, W. S. (1997). The *Saccharomyces cerevisiae* AP-1 protein discriminates between oxidative stress elicited by the oxidants H2O2 and diamide. *J. Biol. Chem.* **272**: 7908-7914.

Wieser, J. & Adams, T. H. (1995). flbD encodes a Myb-like DNA-binding protein that coordinates initiation of *Aspergillus nidulans* conidiophore development. *Genes Dev.* **9**: 491-502.

Winkelströter, L. K., Bom, V. L. P., de Castro, P. A., Ramalho, L. N. Z., Goldman, M. H. S., Brown, N. A., Rajendran, R., Ramage, G., Bovier, E., dos Reis, T. F., Savoldi, M., Hagiwara, D. & Goldman, G. H. (2015). High osmolarity glycerol response PtcB phosphatase is important for *Aspergillus fumigatus* virulence. *Mol. Microbiol.* **96**: 42-54.

Wurgler-Murphy, S. M., Maeda, T., Witten, E. A. & Saito, H. (1997). Regulation of the *Saccharomyces cerevisiae* HOG1 mitogen-activated protein kinase by the PTP2 and PTP3 protein tyrosine phosphatases. *Mol. Cell Biol.* **17**: 1289-1297.

Yaakoub, H., Sanchez, N. S., Ongay-Larios, L., Courdavault, V., Calenda, A., Bouchara, J. P., Coria, R. & Papon, N. (2022). The high osmolarity glycerol (HOG) pathway in fungi. *Crit. Rev. Microbiol.* **48**: 657-695.

Yang, H. Q., Wu, Y. J., Tang, R. H., Liu, D., Liu, Y. & Cashmore, A. R. (2000). The C termini of *Arabidopsis* cryptochromes mediate a constitutive light response. *Cell* **103**: 815-827.

Yasui, A., Yajima, H., Kobayashi, T., Eker, A. P. & Oikawa, A. (1992). Mitochondrial DNA repair by photolyase. *Mutat. Res.* **273**: 231-236.

Yelton, M. M., Hamer, J. E. & Timberlake, W. E. (1984). Transformation of *Aspergillus nidulans* by using a *trpC* plasmid. *PNAS* **81**: 1470-1474.

Yu, Z., Ali, A., Igbalajobi, O. A., Streng, C., Leister, K., Krauß, N., Lamparter, T. & Fischer, R. (2019). Two hybrid histidine kinases, TcsB and the phytochrome FphA, are involved in temperature sensing in *Aspergillus nidulans*. *Mol. Microbiol.* **112**: 1814-1830.

Yu, Z., Armant, O. & Fischer, R. (2016). Fungi use the SakA (HogA) pathway for phytochrome-dependent light signalling. *Nat. Microbiol.* **1**: 16019.

Yu, Z. & Fischer, R. (2019). Light sensing and responses in fungi. *Nat. Rev. Microbiol.* **17**: 25-36.

Yu, Z., Hübner, J., Herrero, S., Gourain, V. & Fischer, R. (2020). On the role of the global regulator RlcA in red-light sensing in *Aspergillus nidulans*. *Fungal Biol.* **124**: 447-457.

Yu, Z., Streng, C., Seibeld, R. F., Igbalajobi, O. A., Leister, K., Ingelfinger, J. & Fischer, R. (2021). Genome-wide analyses of light-regulated genes in *Aspergillus nidulans* reveal a complex interplay between different photoreceptors and novel photoreceptor functions. *PLoS Genet.* **17**: e1009845.

Zeng, D., Lv, J., Li, X. & Liu, H. (2025). The *Arabidopsis* blue-light photoreceptor CRY2 is active in darkness to inhibit root growth. *Cell* **188**: 60-76.e20.

Zhang, X., St Leger, R. J. & Fang, W. (2017). Pyruvate accumulation is the first line of cell defense against heat stress in a fungus. *mBio* **8**: e01284-01217.

Zhang, Z., Chen, Y., Li, B., Chen, T. & Tian, S. (2020). Reactive oxygen species: A generalist in regulating development and pathogenicity of phytopathogenic fungi. *Comput. Struct. Biotechnol. J.* **18**: 3344-3349.

Zheng, X., Chen, D., Zoltowski, B. & Sehgal, A. (2024). Mitochondrial inhibitors reveal roles of specific respiratory chain complexes in CRY-dependent degradation of TIM. *Sci. Rep.* **14**: 26051.

Zhu, P. & Idnurm, A. (2018). The contribution of the White Collar complex to *Cryptococcus neoformans* virulence is independent of its light-sensing capabilities. *Fungal Genet. Biol.* **121**: 56-64.

Ziegler, T. & Möglich, A. (2015). Photoreceptor engineering. *Front. Mol. Biosci.* **2**: 30.

6. Appendix

Table 16: Table of the analyzed CPF members used in the phylogenetic tree in Fig. 7 with their respective organisms, the correspondent CPD subfamily, and the UniProt ID.

Name	Organism	CPD subfamily	UniProt ID (Last accessed: 31 Oct 2024)
A. alt Phr1	*Alternaria alternata*	CPD photolyases	A0A177DDI4
A. cla CPD Phr1	*Aspergillus clavatus*	CPD photolyases	A1CSD2
A. cla Cry2	*Aspergillus clavatus*	Animal cryptochrome (ACRY)	A1CJL8
A. fab PhrA	*Agrobacterium fabrum*	Plant cryptochrome (PCRY)	A9CJC9
A. fla CPD Pho	*Aspergillus flavus*	CPD photolyases	A0A364LX54
A. fum CPD Pho	*Aspergillus fumigatus*	CPD photolyases	A0A9P8NN75
A. nid CryA	*Aspergillus nidulans*	CPD photolyases	Q5BGE3
A. nig Cry2	*Aspergillus niger*	Animal cryptochrome (ACRY)	A0A9W5ZSF5
A. nig CPD	*Aspergillus niger*	CPD photolyases	A0A9W5ZU83
A. tha Cry1	*Arabidopsis thaliana*	Plant cryptochrome (PCRY)	Q43125
A. tha Cry2	*Arabidopsis thaliana*	Plant cryptochrome (PCRY)	Q96524
A. tha Cry3	*Arabidopsis thaliana*	CRY-DASH	Q84KJ5
A. tha PHR	*Arabidopsis thaliana*	CPD photolyases	Q9SB00
B. cin Cry1	*Botrytis cinerea*	CPD photolyases	A0A384JIP4

B. cin Cry2	*Botrytis cinerea*	CRY-DASH	A0A384JRT3
C. rei Cph1	*Chlamydomonas reinhardtii*	Plant cryptochrome (PCRY)	Q42696
D. mel CPD	*Drosophila melanogaster*	CPD photolyases	P00914
D. mel Cry1	*Drosophila melanogaster*	Animal cryptochrome (ACRY)	O77059
E. col PHR	*Escherichia coli*	CPD photolyases	Q16526
H. sap Cry1	*Homo sapiens*	Animal cryptochrome (ACRY)	S2K8G5
M. cir CryA	*Mucor circinelloides*	CRY-DASH	A0A4P7N0U2
N. cra CRY	*Neurospora crassa*	CRY-DASH	Q7SI68
N. cra PHR	*Neurospora crassa*	CPD photolyases	A1Z757
S. cer PHR	*Saccharomyces cerevisiae*	CPD photolyases	P05066
S. scl Cry1	*Sclerotinia slerotiorum*	CRY-DASH	A7F2C9
Syn. sp CryD	*Synechocystes sp.*	CRY-DASH	P77967
Syn. sp PHR	*Synechocystes sp.*	CPD photolyases	P05327
T. the PHR	*Thermus thermophilus*	CPD photolyases	P61497
U. may CRY-DASH	*Ustilago maydis*	CRY-DASH	A0A0D1DUB1
X. lae CRY-DASH	*Xenopus laevis*	CRY-DASH	Q75WS4

Table 17: Table of the analyzed photolyases used in the phylogenetic tree in Fig. 33 with their respective organisms, the correspondent CPD subfamily, and the UniProt ID.

Name	Organism	CPD subfamily	UniProt ID (Last accessed: 03 March 2026)
A. cla CPD Phr1	*Aspergillus clavatus*	CPD I photolyase	A1CSD2
A. cla Cry2	*Aspergillus clavatus*	6-4 photolyase	A1CJL8
A. nig CPD	*Aspergillus niger*	CPD I photolyase	A0A9W5ZU83
A. nig Cry2	*Aspergillus niger*	6-4 photolyase	A0A9W5ZSF5
A. nid CryA	*Aspergillus nidulans*	CPD I photolyase	Q5BGE3
A. tha PHR	*Arabidopsis thaliana*	CPD II photolyase	Q9SB00
C. car PHR1	*Carassius auratus*	CPD II photolyase	P34205
D. mel CPD Pho	*Drosophila melanogaster*	CPD II photolyase	P00914
D. rer CPD	*Danio rerio*	CPD II photolyase	Q7SYI9
E. col PHR	*Escherichia coli*	CPD III photolyase	Q16526
F. het CPD	*Fundulus heteroclitus*	CPD II photolyase	A0A3Q2PPE9
N. cra PHR	*Neurospora crassa*	CPD I photolyase	A1Z757
O. lat 6-4phr	*Oryzias latipes*	6-4 photolyase	H2MAP7
P. and CPDphr	*Phreatichthys andruzzii*	CPD II photolyase	A0A3G2JQM2
S. pur CPD	*Strongylcentrotus purpuratus*	CPD II photolyase	A0A7M7NN77
T. atr PHR1	*Trichoderma atroviride*	CPD I photolyase	G9PA82
T. rub CPD	*Takifugu rubripes*	CPD II photolyase	A0A674NA37

Danksagung

Vielen, vielen Leuten muss gedankt werden, dafür dass diese Arbeit hier zustande gekommen ist.

Zuallererst danke ich Reinhard Fischer für die hervorragende Betreuung und für die Möglichkeit, viele Konferenzen besuchen zu können. Auch möchte ich dafür danken dass man immer kommen konnte, um über Probleme oder Fragen zu sprechen und gerade die Hilfe beim Schreiben des Papers war wirklich unerlässlich.

I also want to thank Nick Foulkes for being my co-referee. Talking to you about cryptochromes and hearing the enthusiasm for the project and future ideas was great, so thanks a lot.

Ich möchte auch den ganzen Leuten aus dem Fischer Lab danken. Zuerst kommt da Kevin Thompson, ohne dich würde dieses Werk hier nicht stehen, danke für deine ganze Zusammenarbeit und deine Art, war wirklich großartig, dich als Azubi zu haben.

Elke, vielen, vielen Dank für die ganzen Tipps und Unterstützung, nicht nur im Laboralltag, sondern auch bei alltäglichen Problemen und manchen Charakterschwächen. Nochmals sorry für die Bananenschale. Auch dir Anna will ich danken, es war großartig mit dir Witze hin und her zu schießen und über deine kümmerlichen Versuche zu lachen, Dinge im oberen Schrank zu erreichen. Danke auch an die beiden neuen Azubis Feli und Emily, auch wenn wir nicht viel miteinander zu tun hatten, ihr seid beide echt super und passt gut rein. Natürlich auch ein Dank an Julia Ungefug für die Hilfe am Ende beim Paper, es war immer sehr unterhaltsam mit dir.

Als nächstes will ich danach Lars Schuhmacher danken, du, zusammen mit Kevin, hast wohl das Projekt mehr oder minder mitgestaltet und dich einfach zu wirklich allem Fragen zu können hat so viel erleichtert und besser gemacht. Danke für die fast 5 Jahre zusammen.

Natürlich muss ich den Magicbuben danken, also dem Großen, dem Kahle, dem Babbler und unserem Prinzen, Adetoye Wolfgang Adeyemo. Danke für die ganze Zeit zusammen gerade beim Magic zocken, danke für die ganzen Jokes und Lacher und die wirklich gute Zeit im Labor. Auch dafür danke, dass wenn ich manchmal mich nicht

von meiner besten Seite gezeigt habe (gerade bei dir Johannes), dass das sich schnell erledigt hat. Natürlich auch danke für das Korrekturlesen der Arbeit.

Ebenso gebührt auch dem Rest des Fischerlabs großer Dank, mit spezieller Erwähnung von Satur, Violetta und Marius, danke für die Hilfe bei den ein oder anderen Experimenten.

Auch ein Dank an die Sekretärinnen Fabienne Cochard-Rein, Angela Pendl und Blanca Garzón Bautista, danke dass ihr bei meinen verwirrten Fragen Durchblick hattet und mir immer bei allen organisatorischen Problemen zur Seite standet.

Ich möchten noch den ehemaligen Doktoranden danken, vor allem Kai Leister, der mich in der Masterarbeit betreut hat und so sehr für das Thema Proteine und Licht begeistern konnten und einfach ein toller Mensch ist. Auch Michael Pitz will ich danken für seine hilfreichen Lehren und den ein oder anderen (ich hoffe) gut gemeinten Spruch. Durch dich wurde diese Arbeit wahrscheinlich auch erst so richtig möglich. Dank gebührt auch Henrik Schweder, du wirst das hier nie lesen, aber danke, dass du das Leben im Labor einfacher gemacht hast.

Natürlich möchte ich auch Jasmin Böhm danken, einmal für die Hilfe bei der ChIP natürlich aber auch für den Tratsch und die Zeit beim Kaffee trinken, war immer sehr erfreut über deine Anwesenheit.

An alle anderen die nicht namentlich genannt sind, natürlich auch ein Dank für die Zeit im Labor und bei Kaffee und Kuchen sowie an meine Freunde außerhalb des Labors, danke an euch Daniel, Fabian, Lugge, Tobi, Julia und Jonas.

Großer Dank gebührt meiner Familie, vor allem meiner Oma Gertrud, meinem Stiefvater Josef, meiner Schwester Simone und meiner Mutter Gudrun, welche mich in der ganzen Zeit unterstützt hat, und mich einfach hat gewähren lassen. Es wurd was Mutter, kein Stress.

Schlussendlich will ich meiner Freundin Lara danken für alles, was wir bisher zusammen erlebt haben. Vielen Dank dafür, dass es dich gibt und dass du bei der ganzen Reise bei mir geblieben bist und immer meinen Rücken hattest.